Rapid-Response Surveillance System Design and Aerodynamic Modeling

by

David Iranzo-Greus

B.S.E. Mechanical and Aerospace Engineering
Princeton University, 1996

Submitted to the Department of Aeronautics and Astronautics in Partial Fulfillment of the Requirements for the Degree of

Master of Engineering in Aeronautics and Astronautics

at the

MASSACHUSETTS INSTITUTE OF TECHNOLOGY

June 1997

Author .....
Department of Aeronautics and Astronautics
May 9, 1997

Certified by .....
Charles Boppe
Senior Lecturer, Department of Aeronautics and Astronautics
Thesis Supervisor

Certified by .....
Mark Drela
Associate Professor of Aeronautics and Astronautics
Thesis Supervisor

Accepted by .....
Jaime Peraire
Chairman, Departmental Graduate Committee

Rapid-Response Surveillance System Design and Aerodynamic Modeling

by
David Iranzo Greus

Submitted to the Department of Aeronautics and Astronautics
on May 9, 1997, in partial fulfillment of the requirements for the degree of
Master of Engineering in Aeronautics and Astronautics

Abstract

The Rapid-Response Surveillance System (also known as WASP or Wide Area Surveillance Projectile) was developed within the context of the MIT/Draper Technology Development Partnership Project, which had as its aims the development of a first-of-a-kind system within a time-frame of two years and the development of an entrepreneurial spirit in the participating engineering students at MIT. After some studies, the final concept consisted of a integrated shell-flier system, known as the Super-Shell. After being launched from a standard Army or Navy gun, the shell would deploy a parachute during the ballistic trajectory, to de-spin and slow down. Aerodynamic surfaces (wings and tails) would deploy out of the shell, and the flier would conduct a 15-minute surveillance mission, recording images with a visual sensor, and sending them back to a ground station.

In the aerodynamic analysis and modeling, this report shows the trade studies performed in selecting the best aerodynamic configuration in terms of performance and stability. The propulsion system selection is an integral part of the aerodynamic performance, and a propeller driven by an electric motor was selected. In the static and dynamic stability analysis, the aerodynamic configuration was modeled and analyzed using existing software, to provide sufficient control for a flexible mission.

Thesis Supervisor: Charles Boppe
Title: Senior Lecturer, Department of Aeronautics and Astronautics

Thesis Supervisor: Mark Drela
Title: Associate Professor of Aeronautics and Astronautics

Acknowledgments

I would like to thank the MIT/Draper project team for a great year and all their help and support, including Professor Charlie Boppe and Professor John Deyst. Special thanks to Professor Mark Drela, for all his knowledge and guidance.

I would also like to thank the Charles Stark Draper Laboratory for giving me the opportunity to participate in such an exciting venture.

I would like to thank my family, who have made this possible. "Gracias, papá y mamá, por darme la oportunidad de llegar hasta aquí, y gracias a mis hermanos Vicente, José y María por todo vuestro apoyo."

"Gracias MJ por todo tu cariño, verte todos los días me ayudó a llegar al final."

Table of Contents

List of Figures

List of Tables

Chapter 1 Introduction

1.1 The MIT/Draper Technology Development Partnership Project

The MIT/Draper Technology Development Partnership Project was created to develop a first-of-a-kind system important to the needs of the United States. A second objective of the project was to develop an entrepreneurial and innovative spirit in current engineering students at the Institute. The project proposal, submitted to Draper Laboratories in June of 1996 is shown in Appendix A.

The project aimed at combining the resources available at the Charles Stark Draper Laboratories, the Massachusetts Institute of Technology and Lincoln Laboratories. Within a time frame of two years, the partnership project team was tasked with developing a prototype of a working system, or alternatively demonstrating the key technologies for operating an innovative system.

Within the MIT team, the Aeronautics and Astronautics Department provided most of the participants for the first part of the project. The participants included five Master of Engineering students (Joshua Bernstein, Matt Burba, Ted Conklin, Cory Hallam, and the author), two Master of Science students (Vladislav Gavrilets and Tan Trinh) and three undergraduate students (Bernard Asare, Margarita Brito and Staci Jenkins). Moreover, two faculty members (Charles Boppe and John Deyst) were full-time participants in the project, while other professors were included in the team at different stages of the project.

1.2 Opportunity Identification and Concept Development

Unlike the traditional academic environment, where research takes place and applications are sought after this research is concluded, the MIT/Draper project had at its starting point the search for the needs of the nation. Once these needs had been identified, the project would proceed to determine the possible technological requirements needed to meet this deficiency.

During the initial stages of the project, various categories of national needs were identified by literature research and contacts with government, academia and industry. The needs were divided and categorized according to a National Critical Technologies List

produced by the White House in 1995. This list, shown in appendix B, addresses the technological requirements for national security and economic prosperity. The major seven categories are:

- Energy Efficiency and Independence.
- Environmental Quality.
- Information Access and Communication Effectiveness.
- Health Care and Agricultural Efficiency.
- Advanced Manufacturing.
- Improved Materials.
- Advanced Transportation.

Each of these categories had a series of sub-categories, as shown in appendix B.

Simultaneously, the team participants assessed the capabilities of the participating organizations, in order to determine the best match between the national needs and these existing product development resources. The engineering departments at MIT and Draper and Lincoln Laboratories were investigated, to determine the current projects taking place and the resources available in terms of laboratories and faculty.

After this preliminary research, several brainstorming sessions took place, where the team members came up with opportunity areas. These opportunity areas would meet the requirements of being compatible with the given national needs as well as the available resources. Moreover, the areas would have broad application and potential, and it would be difficult for competitors to match.

A list of initial opportunity areas was developed following these guidelines. The areas were reviewed and grouped into Low, Medium and High priorities, depending on the alignment with the various circumstances that define an opportunity area. The initial list was reduced to four opportunity areas: innovative projectile systems, advanced aircraft navigation, inexpensive space capabilities, and intelligent cooperative systems.

The innovative projectile systems opportunity area included applications of existing shells to the deployment of sensors and other smart systems for surveillance or assistance missions. The advanced aircraft navigation opportunity area included various approaches to solving the problem of modernizing air traffic control. The inexpensive space capability opportunity area included the development of innovative launch systems and small satellite

technology. The intelligent cooperative systems opportunity area ranged from UAV's for various applications to intelligent transportation systems.

Once again, a brainstorming of ideas took place, this time within the framework of the opportunity areas outlined above, and with the goal of developing concepts that could be pursued. Numerous concepts surfaced in each of the areas. In order to reduce the number of concepts for the team to be able to conduct a deeper study into each of them, a Project Selection Matrix was produced. Appendix C shows this matrix together with the projects that were left after an initial selection. The matrix shows the considerations that were taken into account when selecting the project.

After a first attempt at doing preliminary engineering calculations on some of the concepts, some of the projects were rejected on the basis of the matrix criteria. The team was divided into five groups, each of which picked what they considered to be the most innovative project. Given the constraints of the project, the following five concepts were picked for further development and to be submitted to a market assessment:

- Hybrid Launch System.
- Tail-Sitter UAV.
- Advanced Search And Rescue System (ASARS).
- Innovative Projectile System.
- Solar Sail Demonstrator.

Space access has become increasingly expensive in the past. A Hybrid Launch System was developed as an attempt to reduce launch costs for space missions. Using a high altitude balloon to reach over 100,000 feet, the energy requirements for the rocket launcher would be significantly lower. Alternatively, a larger payload could be carried into orbit with the same rocket launcher.

The Tail-Sitter UAV attempted to incorporate two current trends in aircraft. On the one hand, the vehicle would try to incorporate acceptable cruise performance with vertical takeoff and landing. On the other hand, the vehicle would be unmanned and could be used in dangerous situations without endangering any human lives.

In an attempt to develop an intelligent cooperative system, an Advanced Search and Rescue System (ASARS) was conceived, which consisted of an integrated network of air,

water and underwater vehicles. This autonomous system would substitute human search in dangerous situations and would be able to search and integrate data from the various vehicles.

As an application of existing gun technology, the Innovative Projectile System was originally conceived to launch projectiles containing non-lethal equipment. This system could be equipped with sensors for surveillance or launched into an area that required monitoring. Data would be relayed autonomously to a ground station.

Another aspect of space access that increases its cost is the propulsion for long-term missions. The Solar Sail Demonstrator was conceived to demonstrate the feasibility of space propulsion via solar pressure. The author worked on this concept, and Appendix D describes in more detail the idea, as well as the results of the preliminary engineering analysis and the market assessment.

1.3 Market Assessment

One of the most important goals of the MIT/Draper Technology Development Partnership Project was to foster an entrepreneurial spirit among young engineers at MIT and to develop a product that could be marketed by Draper Laboratories.

The market assessment was a key component of this process, where each of the teams contacted outside organizations and potential customers to determine the feasibility of the chosen concepts and their marketability. Also, each of the sub-teams performed preliminary engineering calculations to ensure that the projects were feasible, to first order. All this data was contrasted with the capabilities of the participating organizations and the time and budget constraints of the project. In the end, a document was produced for each of the concepts.

The author, together with Joshua Bernstein, conducted the market assessment for the Solar Sail Demonstrator. The report is shown in Appendix D.

1.4 Concept Selection

Based on the market assessment conducted by the five teams, the student team, and later the Draper Laboratory team, chose what they considered to be the most innovative project within the framework of the project constraints. In the ranking from the students,

the Solar Sail Demonstrator was clearly at the top, and the Advanced Search and Rescue System was clearly at the bottom. The remaining projects (Tail-Sitter, Hybrid Launch, and Innovative Projectile System) where all in the middle of the range.

On the other hand, Draper Laboratory considered that this ranking did not match the capabilities and the business of the company. Therefore, the team was tasked with looking at the possible military surveillance missions that could be done with the tail-sitter concept and with the innovative projectile system. Considering that the surveillance projectile would be a better systems design, the team chose to pursue this project.

Chapter 2 Rapid-Response Surveillance System

2.1 Requirements Definition

An initial system requirements document for the Low-Cost Instrumented Surveillance Projectile (LISP), as it was originally called, was developed by Draper Laboratories in conjunction with members of the MIT team. This document is shown in appendix E, together with the logo for the project, which was renamed to Wide Area Surveillance Projectile (WASP).

The initial requirements called for a non-lethal rapid-response projectile that would provide reconnaissance information to military commanders. The main requirements for the projectile would be:

- Compatible with Army 155 mm and Navy 5 in. guns.
- 70-200 mile range.
- 1-8 hour mission time, 2 hour operational time.
- Imaging camera sensor.
- Near-real-time information relay to the ground station.
- Some degree of autonomous operation (to be determined).
- Cost between $20,000-$30,000 per vehicle.
- Self destruct mechanism to limit the size of any debris to no larger than an 8 oz. can of cat food.

Based on this initial document, the team started conducting a more intensive customer research and market assessment, to determine the possible modifications to these requirements. Both the Army and the Navy were contacted, as possible primary customers.

The team also considered the various possible missions that the surveillance system could perform. The missions range in complexity, range and loiter time required. These possible missions are shown in table 1 (from reference 2). For a more detailed description of the mission scenarios, see reference 2.

TABLE 1: MISSION SCENARIOS

Mission	Range	Loiter	Oper. Time	Resp. Time	Surv. Area	Customer Cost Limits
Company Recon	~75 km.	<30 min	<30 min	minutes	1-2 sq. km.	≤$10,000
Damage Assessment	75+ km.	<30 min	<30 min	minutes-hours	1-10 sq. km	$20-$30,000
Signals Intel.	75+ km.	>4 hrs	>4 hrs	hours	1-10 sq. km	$20-$30,000
Comm. Relay	75+ km.	>4 hrs	>4 hrs	hours	1-10 sq. km	$20-$30,000
Route Recon	100+ km.	N/A	= dist + speed	hours	= flt. dist.	$20,000
Scud Hunting	150-200 km.	<30 min	<30 min	hours	1-2 sq. km	$20,000
Hunter/ Killer	100+ km.	>4 hrs	>4 hrs	hours	1-10 sq. km	$20-$30,000
Area Surv.	75+ km.	>4 hrs.	2+ hrs.	hours	≤140+ sq. km.	$20-$30,000
Long Endurance	100+ km.	>4 hrs.	>4 hrs	hours	≤140+ sq. km.	$30,000

With these missions in mind, and after talking to the customer, the requirements were modified. The following changes were made to the initial set of requirements (reference 2):

- Range: Defined as the distance from the point of launch to the area to be reconnoitered. The range for WASP was set equal to the range provided by the ballistic trajectory of the projectile (about 15 to 20 kilometers without Rocket Assist). WASP would not be required to cruise beyond this point to the target area.
- Loiter Time: Goal of an hour, but required to be at least 20 to 30 minutes.
- Operational Time: Equal to the loiter time.
- Image Resolution: About 1 m. The ability of the team to meet this requirement would be highly dependent upon finding a suitable sensor.
- Information Timing: One image every few minutes, but no longer than 10 minutes between images (from interview with the Defense Airborne Reconnaissance Office, see reference 2 for more details).
- Cost: A new goal of $2,000-$3,000 per vehicle was established. As a goal, however, it was considered very tradable. The cost was capped, however, at $20,000 to $30,000 per vehicle, the original requirement.

2.2 Quality Function Deployment (QFD) Matrix

In order to conduct trade studies in the conceptual design phase of the project, a set of ranked technical requirements is needed. These technical requirements can be obtained and ranked from the customer needs using a Quality Function Deployment (QFD) requirements matrix, also known as a House of Quality.

The initial set of customer needs was obtained from the System Requirements document described in the previous section. Each of the needs was given a relative weight from 1 to 10, reflecting the degree of importance that the requirement would have for the success of the mission carried out by the system. These weights were based on the judgment of the team, and incorporated the voice of the customer (Army and Navy) as well as some Draper engineers. The following table shows the initial set of needs and their corresponding weights:

TABLE 2: CUSTOMER NEED WEIGHTING

Customer Needs	Relative Importance (1-10)
Long Range	5
Long Loiter	10
Long Operational Time	10
Maximum Field of View	8
Maximum Image Resolution	8
Accurate Image Position Determination	9
Minimum Self-Destruct Debris	4
Low Cost	10
Near Real-Time Information Processing	9
High Degree of Autonomy	8
Long Shelf Life	4
Strong Stealth Characteristics	5
Ease of Operations	10
Ease of Maintainability	9
High Reliability	8
High Extensibility	5
Short Launch Time	3
Very Safe	10

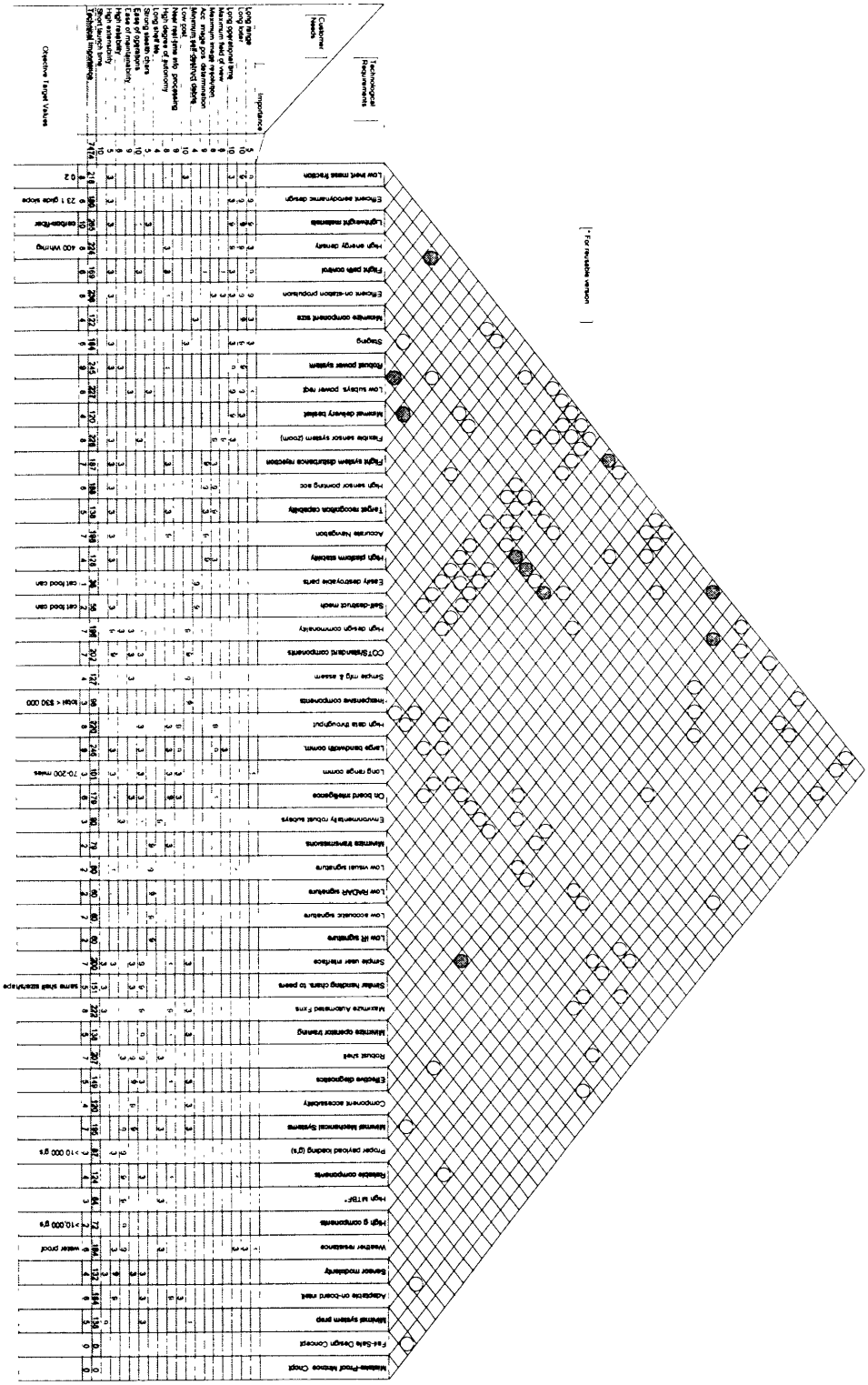

FIGURE 1: QUALITY FUNCTION DEPLOYMENT REQUIREMENTS MATRIX (COMPOSITION BY MATT BURBA)

The team developed a list of technical requirements needed to meet the given customer needs. This list is shown in Figure 1 above, in the top part of the QFD requirements matrix. By assigning a weight to the technical requirements for each of the customer needs, a ranking of the requirements is created. In this way, if a technical requirement is very important to meet a customer need, a weight of 9 is assigned, and correspondingly 3 and 1 are given to moderately and low importance technical requirements. Overall technical importance is then calculated by adding all the technical requirement weights times the weight of the customer need they meet.

Also shown at the bottom of the QFD matrix are target values for some of the technical requirements, as performance guidelines. Finally, the "roof" of the House of Quality shows the conflicts between the technical requirements. These conflicts have to be addressed, specially if the technical requirements that conflict are among the ones with the highest relative importance.

Based on the QFD matrix, table 3 shows the top technical requirements, with the relative importance levels:

TABLE 3: TECHNICAL REQUIREMENTS RANKING

Technical Requirements	Relative Importance (1-10)
Flight System Disturbance Rejection	10
Lightweight Materials	10
Large Bandwidth Communication	9
Robust Power System	9
Robust Shell	9
Efficient On-Station Propulsion	9
Flight Sensor System	9
Low Subsystem Power Requirement	9
High Energy Density	8
High Data Throughput	8
Low Inert Mass Fraction	8
On-Board Intelligence	8
Maximize Automated Functions	8
Accurate Navigation	8
High Design Commonality	7
COTS / Standard Components	7
Minimal Mechanical Systems	7

As mentioned above, the original list of requirements was modified after the team received some input from the Army's Picatinny Arsenal, from Draper, and from the Defense Airborne Reconnaissance Office (DARO). The DARO recommended that the team should

focus the design on a vehicle that had just the range of the gun, and would stay on station for a short time. Moreover, they recommended that the sensors and the vehicle should be day and night capable (and all-weather if possible) and transmission of images should take place every few minutes. A resolution in the order of one meter was considered sufficient.

2.3 Functional Flow Diagram (FFD)

The Functional Flow Diagram (FFD) shows the functions performed by the surveillance system, in a sequential manner. The FFD also indicates the tasks that are performed in parallel and those that are possible alternatives, by using the logic AND , OR symbols.

Variants of the design can be produced from a baseline FFD. In the baseline configuration, the shell would get launched from the gun and cruise to its deployment point after confirming that the systems are operating. After the deployment, the system would perform its surveillance mission and self-destruct. The FFD for the baseline configuration is shown in figure 2, in the following page.

2.4 Top-Level Architecture and Concept Generation

Given the final requirements and the FFD, the team was divided into two teams to generate top level architectures for the possible concepts. The resulting ideas are described from a top-level view in the following subsections. The team was then divided into subsystem teams, to analyze the designs and come up with common values of merit that could be used to compare the designs. The author was tasked with doing the aerodynamic analysis of the deployed fliers for each of the concepts. This analysis is shown in detail in the following chapter.

At this point, the team found out that there were existing patents on similar projectile systems. All these systems provided fast-response surveillance, so the team had to focus its design on some characteristics that would offer an advantage over the existing systems.

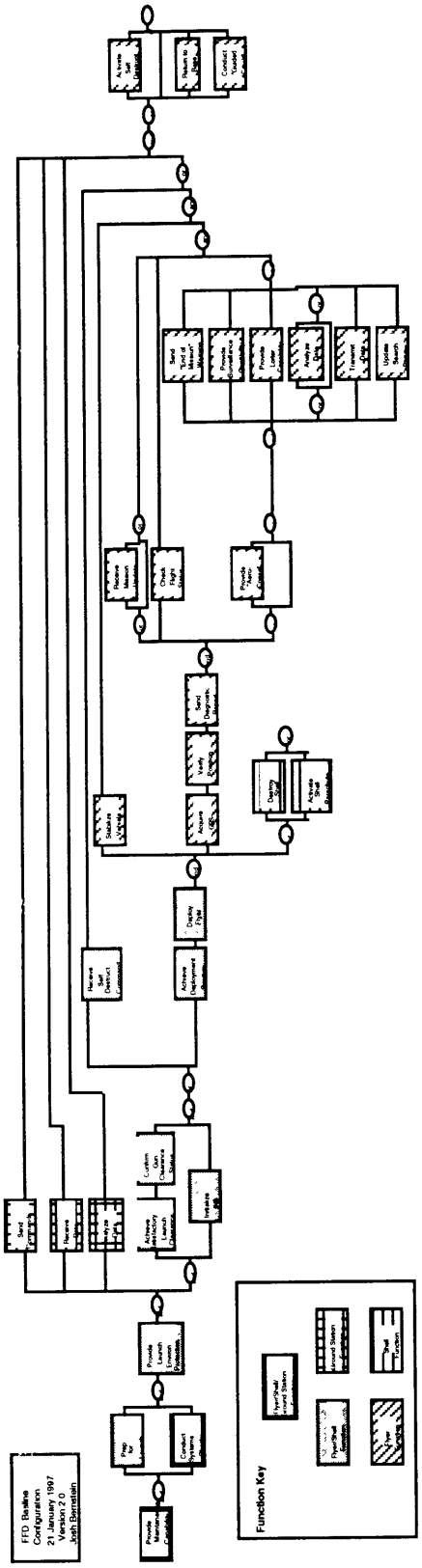

FIGURE 2: BASELINE FUNCTIONAL FLOW DIAGRAM (COMPOSITION BY JOSHUA BERNSTEIN).

2.4.1 "Super-Shell"

The Super-Shell was conceived to avoid disposing of the shell when the flyer is deployed. In its first version, the wings are deployed from the sides of the shell and are initially used to de-spin the shell and to pitch up and slow down the shell. Once the shell has slowed down, the wings are deployed completely, as are the tail surfaces and the propeller. After analyzing the pull-up maneuver, it was not clear if it would be advantageous. On the one hand, it did not yield a large gain in altitude, due to aerodynamic loses. On the other hand, it used components (the wings) that were already in the vehicle for other functions. An alternative option to performing the pull-up maneuver was to use of a parachute to de-spin and slow down the shell. Eventually, the shell would hang down from the parachute, at which point, the aerodynamic surfaces and the propeller would deploy. Figures 3(a) and 3(b) show the solid model of the vehicle and the typical mission being considered, respectively.

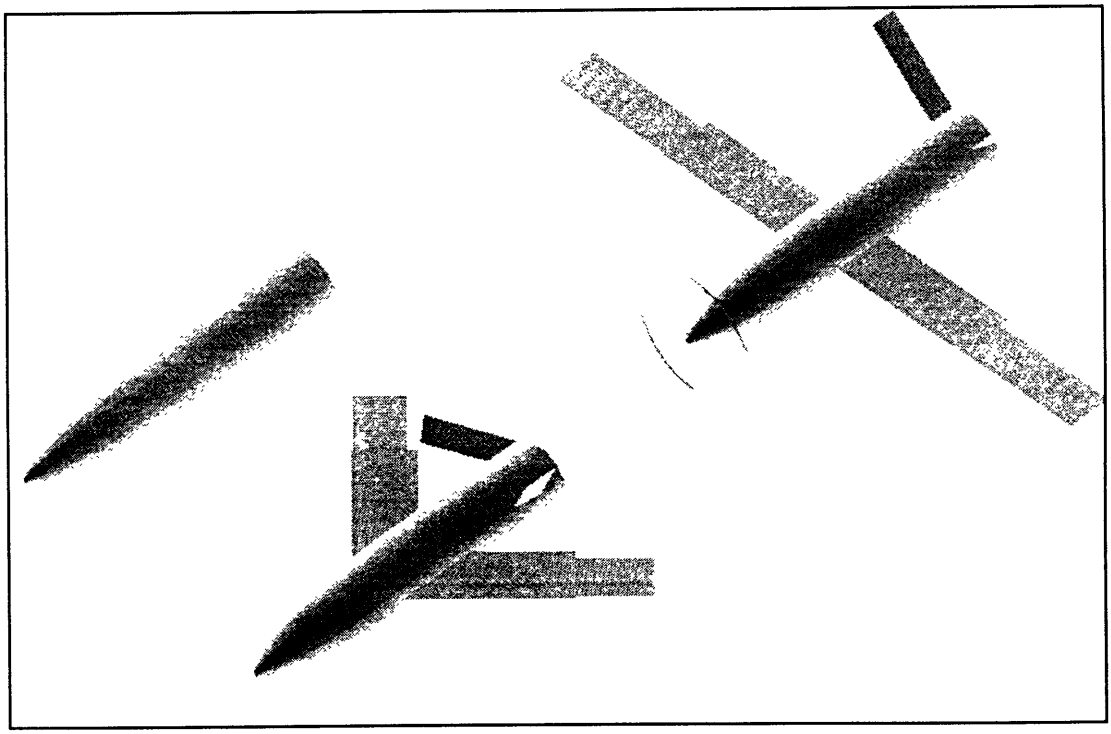

FIGURE 3(A): 3-D MODEL OF THE SUPER-SHELL (BY TAN TRINH).

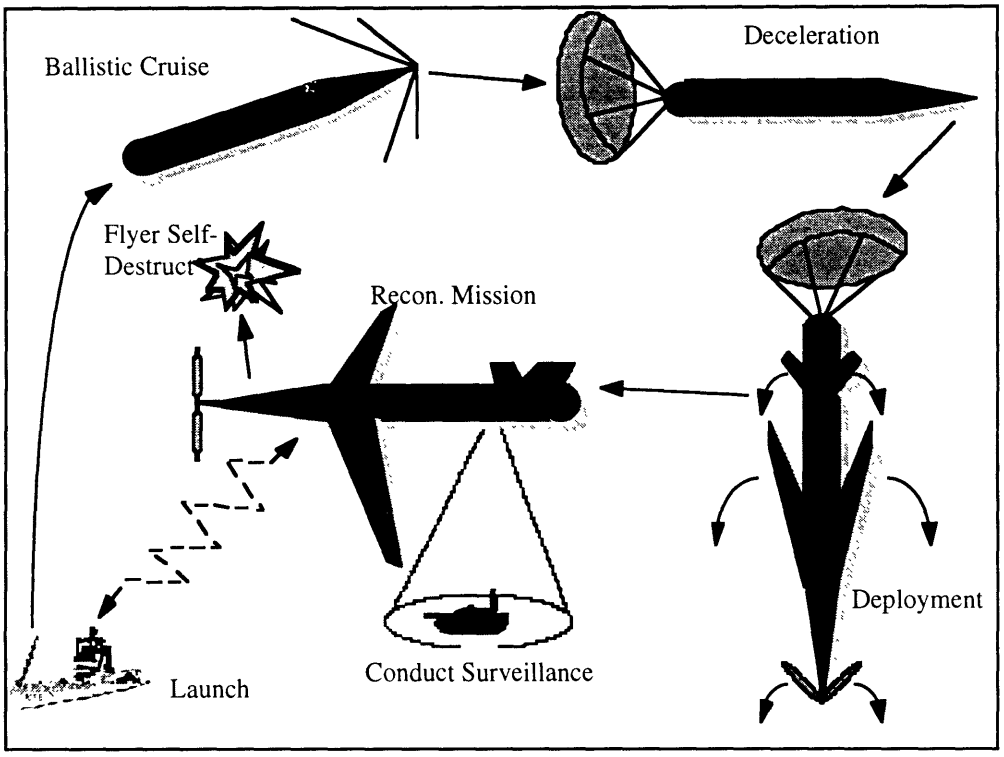

FIGURE 3(B): SUPER-SHELL MISSION

2.4.2 "Silent Eyes"

The Silent Eyes concept was the unpowered alternative to the Super-Shell. However, to achieve a better glide slope, the projectile casing was discarded after the flyer was ejected from inside, hence reducing the weight. This concept had packaging problems, since some of the equipment could not fit inside and existing shell. Figures 4(a) and 4(b) shows this concept.

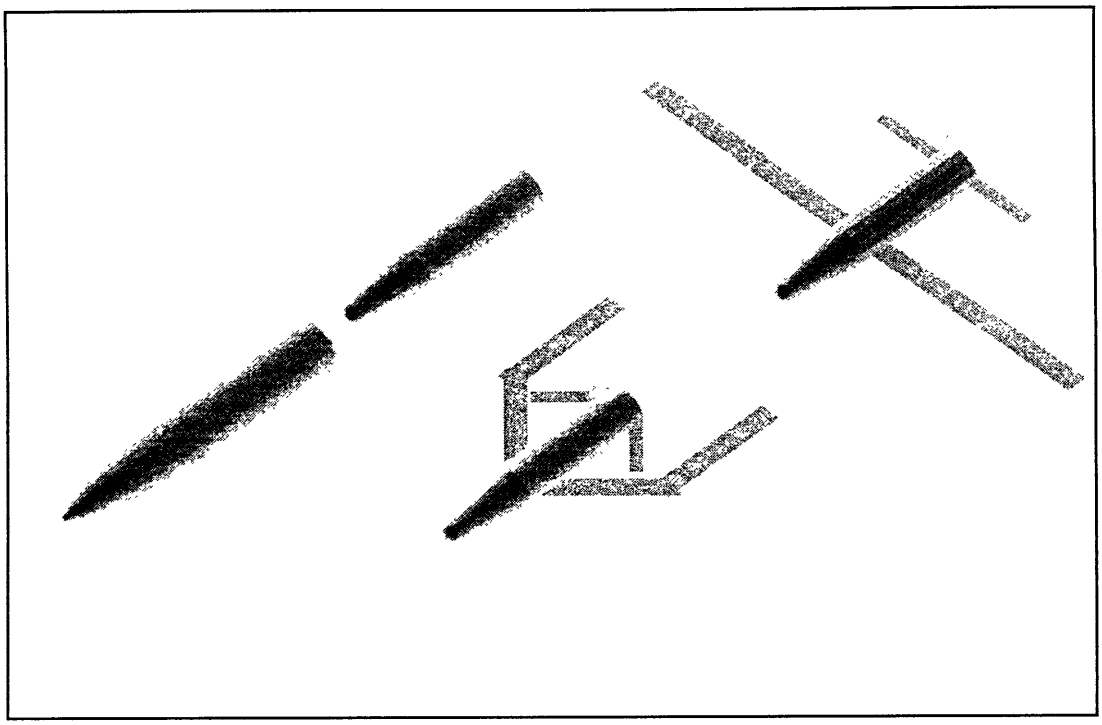

FIGURE 4(A): 3-D MODEL OF SILENT EYES (BY TAN TRINH).

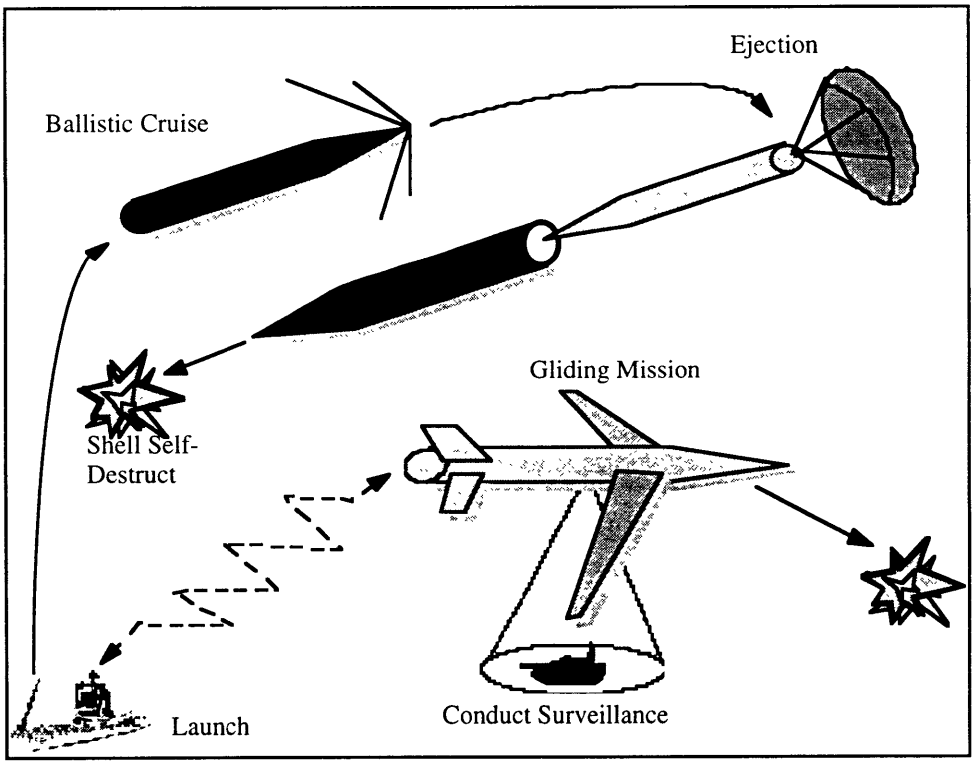

FIGURE 4(B): SILENT EYES MISSION.

2.4.3 "Flying Wing"

In the Flying Wing concept, a wing would be stored spanwise along the length of the shell. This wing would be ejected from the projectile casing at the desired location and conduct the desired mission. The advantage of such configuration was that all the components could be placed spanwise in the vehicle, making better use of the limited volume. Also, the aerodynamic efficiency would be better given the higher L/D ratio. In a conventional configuration, both fuselage and wings contribute to drag, and only the wings contribute to the lift, while in this configuration only the wing produces drag. However, this concept had to be discarded due to volume constraints, since all the equipment necessary could not be packaged into the wing.

2.4.4 "Pinky-and-Brain"

This concept was developed after the Flying Wing was rejected as unfeasible due to volume constraints. The idea of this concept was to split the projectile into two flyers, one of which would carry just the sensors and the required supporting equipment, while the other would fly higher and serve as the communications relay as well as the commander and "brain" for directing the first flyer. Figures 5(a) and 5(b) show the concept.

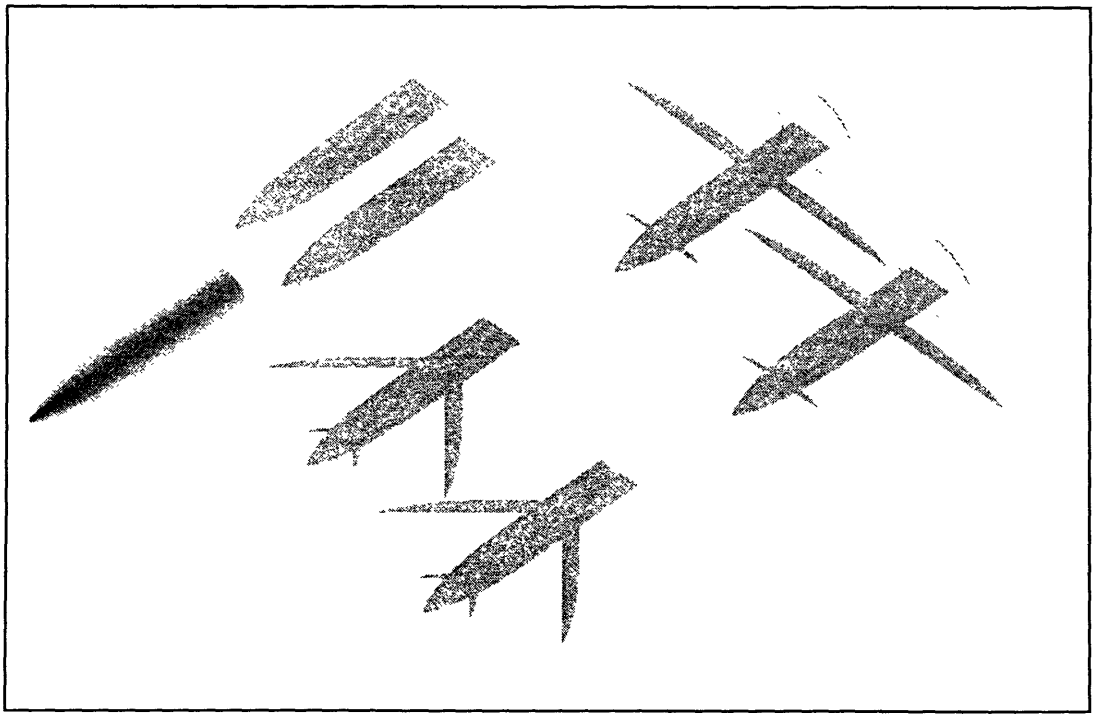

FIGURE 5(A): 3-D MODEL OF PINKY-AND-BRAIN (BY TAN TRINH).

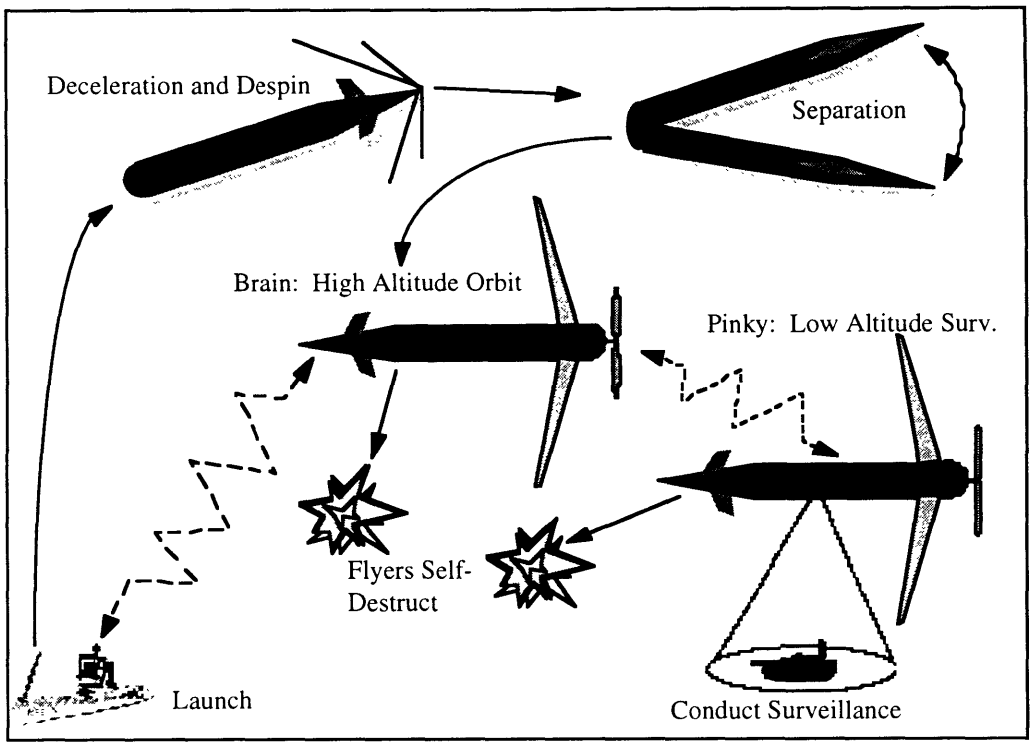

FIGURE 5(B): PINKY-AND-BRAIN MISSION.

2.5 Inboard Layout and Subsystem Interfaces

For each of the concepts, an inboard layout had to be produced, placing all the required components within the highly constrained volume. Figure 6 shows the initial inboard subsystem distribution for the Super-Shell.

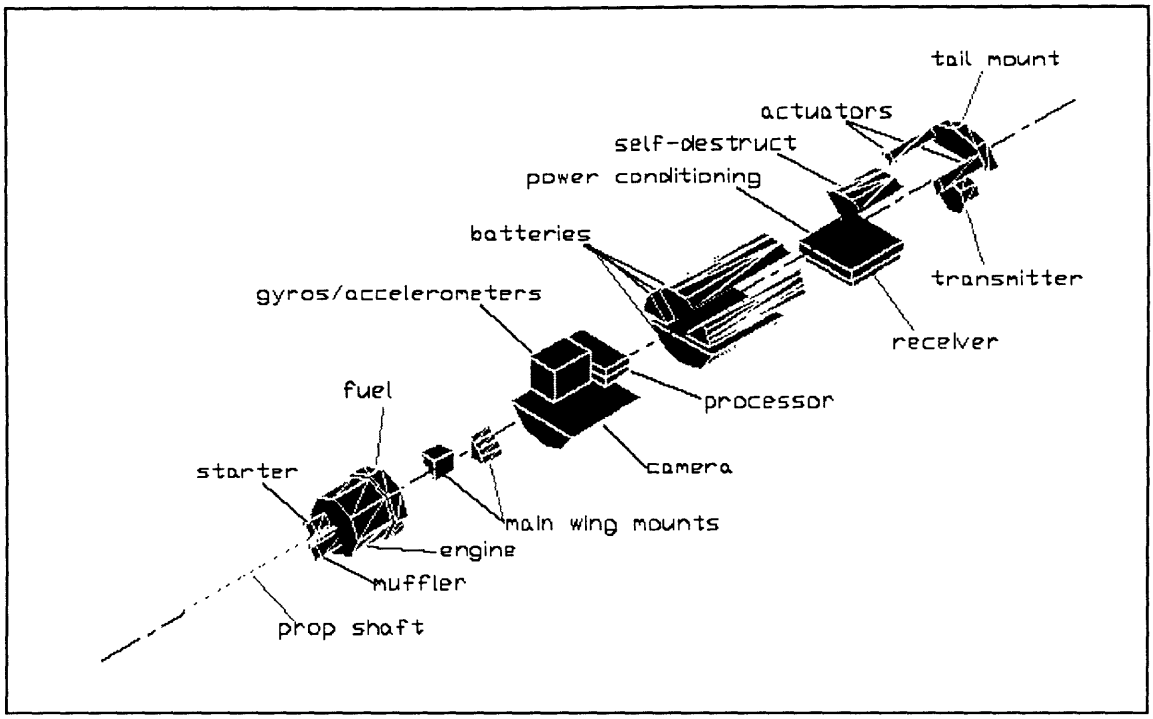

FIGURE 6: INBOARD LAYOUT (BY TAN TRINH).

Also, all the subsystems had to be connected by mechanical, digital or electrical connections. To facilitate the design, an N^2 diagram was created by Hallam (see reference 7 for more information). This initial diagram, shown in appendix F, shows the interfaces between the various subsystems. The diagram reflects a one-way communication system, and should be improved in the future to account for the two-way data link.

The design of the propulsion system can be found in reference 5 by Conklin. The design of the communications system can be found in reference 4 by Burba.

2.6 Project Management

As the assistant manager for the project, the author had the chance to work with Joshua Bernstein, the project manager and the faculty members in coordinating team efforts. The relatively large number of people involved made management a non-trivial task, as was seen several times during the year.

An example of a team schedule is shown in Appendix G and some conclusions and recommendations are given in section 5.2.

Chapter 3 Aerodynamic Modeling: Preliminary Analysis

3.1 Ballistic Trajectory and Deployment Scheme

The mission begins with the launching of a 155-mm or 5-in projectile. This projectile goes into a simple ballistic trajectory that takes it to the point of maximum altitude of the mission. The characteristics of this initial phase where modeled to determine several important performance characteristics: ballistic range, altitude and velocity at the apex of the trajectory, and time to reach this point of maximum altitude.

The equations of motion for this initial phase are given by:

$$\ddot{x} = -\frac{\rho S C_D}{2m} V^2 \cos\theta = -\frac{\rho S C_D}{2m} \dot{x}\sqrt{\dot{x}^2 + \dot{y}^2}$$

$$\ddot{y} = -g - \frac{\rho S C_D}{2m} V^2 \sin\theta = -9.81 - \frac{\rho S C_D}{2m} \dot{y}\sqrt{\dot{x}^2 + \dot{y}^2}$$

where ρ is the local density, which has an exponential dependence on altitude (y); S is the reference area (in this case the cross-sectional area of the projectile); m is the mass; and C_D is the drag coefficient which is a function of the Mach number, and hence of altitude and speed.

The drag coefficient versus Mach number dependence is shown in the Figure 7. This drag coefficient was obtained from reference 12 and represents the contributions of skin friction, pressure drag and wave drag.

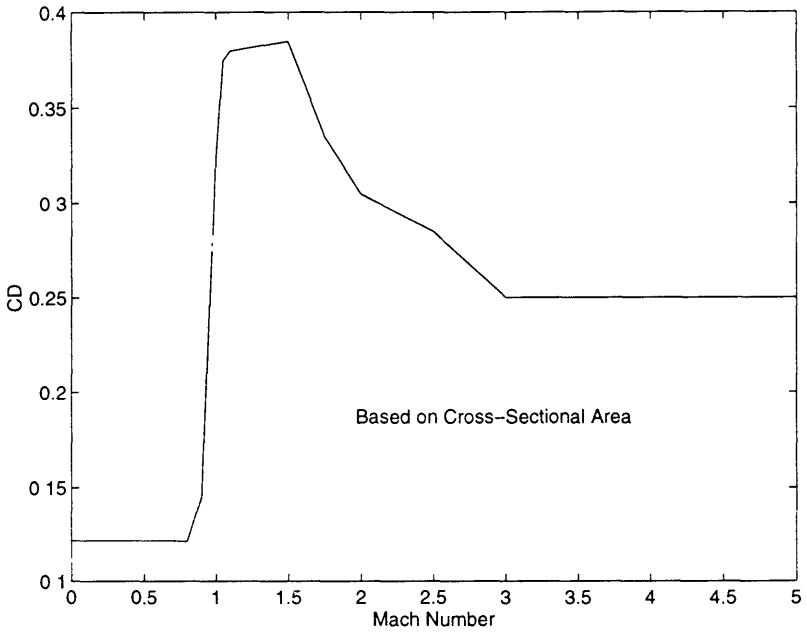

FIGURE 7: DRAG COEFFICIENT DEPENDENCE ON MACH NUMBER.

Using this model, and numerically integrating the equations of motion shown in the previous page, the trajectory can be generated for various masses. The initial firing of the shell is done at a 45-degree angle, for a performance slightly lower than optimal, and assuming a 10-Mega-Joule gun. From this imparted energy, the initial velocity can be calculated. This gun rating of 10 MJ refers to the kinetic energy delivered, and not to the overall chemical energy, which is almost twice as high. About 50% of the energy is converted into heat and sound (reference 14). The next generation of guns is projected to be in the 15 to 18 megajoule range, which would improve the range performance of the projectile.

The equations of motion were integrated using the MATLAB file aero.m, shown in appendix I, and the resulting trajectories are shown in Figure 8. This work was done in collaboration with Cory Hallam.

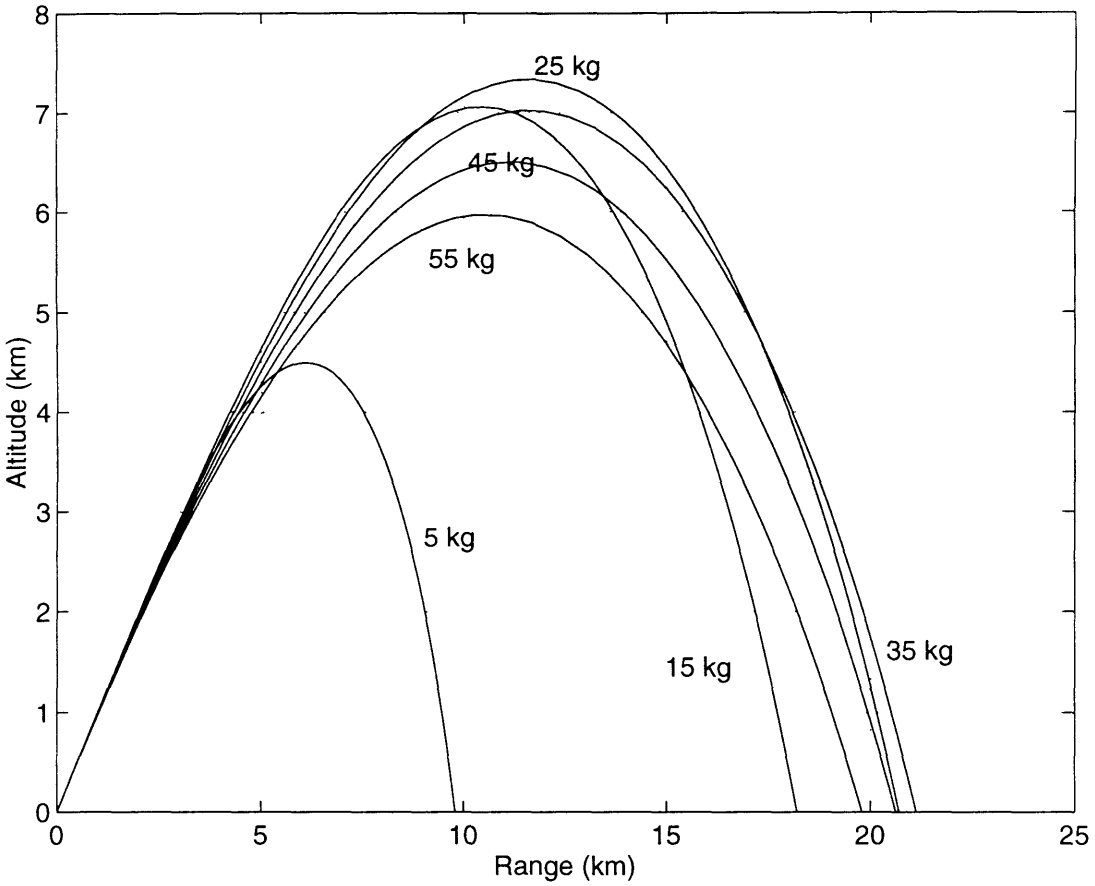

FIGURE 8: PROJECTILE TRAJECTORIES.

The following table shows the resulting performance characteristics for the various masses:

TABLE 4: TRAJECTORY CHARACTERISTICS

MASS (kg)	TOTAL RANGE (km)	APEX RANGE (km)	APEX ALTITUDE (km)	APEX VELOCITY (mph)	APEX MACH NUMBER
5	9.9	6.1	4.5	342	1.2
15	18.2	10.4	7.1	514	1.8
25	20.8	11.7	7.3	579	2.0
35	21.2	11.4	7.0	614	2.1
45	20.8	11.3	6.5	624	2.1
55	20.0	10.3	6.0	631	2.1

Once the projectile has reached the apex of the trajectory, or the desired location, the deployment sequence will begin. For each of the configurations, the deployment mechanism will be different. However, in all cases, the deployment will involve the use of either drag parachutes or a supersonic pull-up maneuver.

In the supersonic pull-up, the wings of the vehicle are deployed partially at the apex of the trajectory. The resulting aircraft has a delta-wing configuration, and due to the aerodynamic forces, the spinning of the shell is reduced substantially, and eventually stopped.

At this point, the aerodynamic control surfaces are deflected to put the vehicle into a high-load pull-up maneuver. In this fashion, the aircraft trades its kinetic energy for potential energy. As the velocity is reduced down to zero, the wings are deployed and unfolded to its low-speed configuration, and the vehicle begins its low-speed glide down to the operating altitude for the mission.

Another possible deployment scheme is the use of drag parachutes. An initial drag parachute would be deployed while the shell is traveling at supersonic speeds, and would de-spin the projectile and slow it down to high subsonic speeds. After some time it would be hanging from the parachute, and would eventually reach zero horizontal speed. In this position, the wing and tail surfaces would deploy and the parachute would detach and fall to the ground, as the flier started its gliding flight.

The possible deployment schemes are covered in detail in Reference 7 by Hallam.

3.2 Low-Speed Loiter: Glider

Once the flyer is deployed, the vehicle will begin a gliding descent down to the operational altitude of the mission. This operational altitude is determined from the sensor characteristics, such as the camera focal length and resolution.

For the gliding descent, the equations of motion are:

$$\ddot{x} = -\frac{\rho S C_D}{2m} V^2 \cos\theta - \frac{\rho S C_L}{2m} V^2 \sin\theta$$

$$= -\frac{\rho S C_D}{2m} \dot{x}\sqrt{\dot{x}^2 + \dot{y}^2} - \frac{\rho S C_L}{2m} \dot{y}\sqrt{\dot{x}^2 + \dot{y}^2}$$

$$\ddot{y} = -g - \frac{\rho S C_D}{2m} V^2 \sin\theta + \frac{\rho S C_L}{2m} V^2 \cos\theta$$

$$= -9.81 - \frac{\rho S C_D}{2m} \dot{y}\sqrt{\dot{x}^2 + \dot{y}^2} + \frac{\rho S C_L}{2m} \dot{x}\sqrt{\dot{x}^2 + \dot{y}^2}$$

where S in this case is the wing planform area, and the drag and lift coefficients, C_D and C_L, have been assumed constant (which is possible using the control surfaces to maintain a constant angle-of-attack).

As before, the equations of motion were integrated using the MATLAB file aero.m, shown in appendix I. This time the initial conditions are given by the altitude and range of the apex of the trajectory (or the desired deployment point), and the velocity after deployment. This velocity can be assumed to be close to zero. Figure 9 shows the resulting gliding trajectories. The initial oscillations in the trajectories are due to the presence of the phugoid. Under constant lift and profile drag coefficients, the vehicle oscillates in a rollercoaster-like motion, increasing the lift as the velocity increases, and decreasing the lift as the velocity decreases.

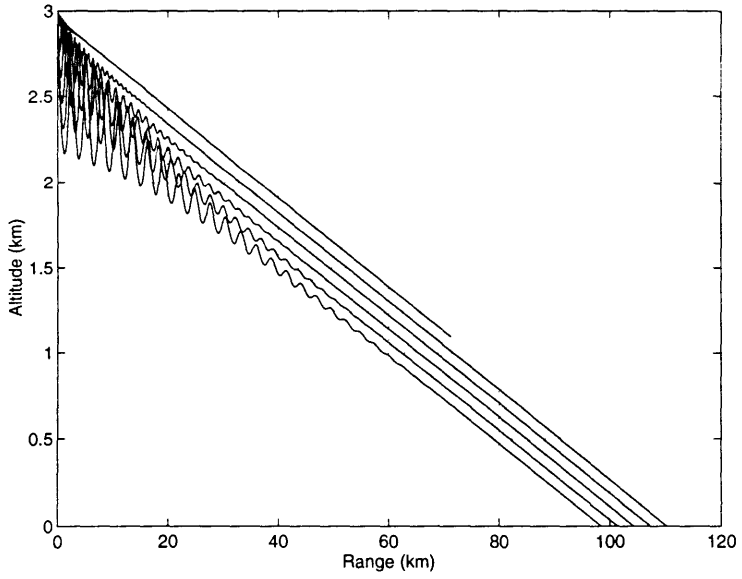

FIGURE 9: GLIDING TRAJECTORIES.

In Figure 9, the deployment of the flier has been assumed to happen at 3,000 meters from the ground. It can be seen from the trajectories that the flyer descends at a constant angle after the initial stabilization period. In fact, it can be seen that this angle θ is approximately equal to:

$$tan\theta = \frac{C_D}{C_L}$$

Therefore, the loiter and range gliding performance of a design can be determined by its drag to lift ratio. In order to maximize the gliding range, the maximum L/D must be achieved. This corresponds to requiring the minimum thrust for level flight, as follows.

In order to maintain steady level flight, the forces must balance. Therefore taking the components parallel and perpendicular to the flight velocity:

$$F_{prop} = D = \frac{1}{2}\rho V^2 S\left(C_{Do} + \frac{C_L^2}{\pi Ae}\right)$$

$$L = mg = \frac{1}{2}\rho V^2 S C_L$$

where F_{prop} is the thrust provided by the propulsion system, which is just the power provided by the engine divided by the flight velocity, A is the wing aspect ratio, e is the Oswald efficiency factor for finite wings, and C_{Do} is the zero-lift drag coefficient.

Hence, if these two equations are divided, the result shows that the thrust-to-weight ratio is equal to the inverse of the lift-to-drag ratio:

$$\frac{F_{prop}}{W} = \frac{1}{L/D} = \frac{qC_{Do}}{(W/S)} + \left(\frac{W}{S}\right)\frac{1}{q\pi Ae}$$

Hence, in order to obtain the maximum L/D for a given vehicle weight, the minimum F/W is required (and therefore the minimum engine thrust):

$$\frac{\partial P_{prop}}{\partial V} = \frac{3}{2}\rho V^2 S C_{Do} - \frac{(mg)^2}{1/2\,\rho V^2 S \pi A e} = 0$$

$$\Rightarrow V_{min} = \sqrt{\frac{2mg}{\rho S}}\sqrt{\frac{1}{3\pi A e C_{Do}}} \quad \text{and} \quad C_{Lmin} = \sqrt{3\pi A e C_{Do}}$$

In order to maximize the loiter time, the vertical velocity, or sink rate, must be minimized. The sink rate is equal to:

$$V_v = V\sin\theta = \sin\theta\sqrt{\frac{mg}{S}\frac{2\cos\theta}{\rho C_L}} = \sqrt{\frac{mg}{S}\frac{2\cos^3\theta C_D^2}{\rho C_L^3}} \cong \sqrt{\frac{mg}{S}\frac{2}{\rho(C_L^3/C_D^2)}}$$

And once again, the minimum can be obtained by differentiating with respect to the lift coefficient. This yields:

$$C_{L\,min} = \sqrt{3\pi A e C_{Do}} \quad \text{and} \quad V_{min} = \sqrt{\frac{2mg}{\rho S}}\sqrt{\frac{1}{3\pi A e C_{Do}}}$$

In the case of the surveillance projectile, the optimal lift coefficients could not be achieved due to the constraints in the velocity. In order to be able to take pictures of the desired area, a limit in the speed of the flier was imposed, which demanded a higher C_L to maintain level flight.

3.3 Low-Speed Loiter: Propelled Flight

When the vehicle reaches the desired operational altitude, the mission requires that the flyer stay at approximately constant altitude, which requires a propulsive force to maintain constant velocity (and hence constant lift). The equations of motion for propelled flight are similar to the equations for gliding flight, with the addition of a propulsion term. Moreover, due to the burning of fuel, the mass of the vehicle changes with time:

$$\ddot{x} = -\frac{\rho S C_D}{2m} V^2 \cos\theta - \frac{\rho S C_L}{2m} V^2 sin\theta + \frac{F_{prop}}{m}\cos\theta$$

$$= -\frac{\rho S C_D}{2m} \dot{x}\sqrt{\dot{x}^2 + \dot{y}^2} - \frac{\rho S C_L}{2m} \dot{y}\sqrt{\dot{x}^2 + \dot{y}^2} + \frac{P_{prop}}{m}\frac{\dot{x}}{\dot{x}^2 + \dot{y}^2}$$

$$\ddot{y} = -g - \frac{\rho S C_D}{2m} V^2 sin\theta + \frac{\rho S C_L}{2m} V^2 \cos\theta + \frac{F_{prop}}{m} sin\theta$$

$$= -9.81 - \frac{\rho S C_D}{2m} \dot{y}\sqrt{\dot{x}^2 + \dot{y}^2} + \frac{\rho S C_L}{2m} \dot{x}\sqrt{\dot{x}^2 + \dot{y}^2} + \frac{P_{prop}}{m}\frac{\dot{y}}{\dot{x}^2 + \dot{y}^2}$$

$$\dot{m} = -\frac{SFC \times P_{prop}}{g}$$

where the SFC is the engine specific fuel consumption, which will determine the rate at which fuel is burned.

Once again, the equations of motion were integrated using the MATLAB file aero.m, shown in appendix I. The flier was assumed to perform a gliding descent from the initial deployment altitude (3,000 meters) to 1,000 meters, at which point the engine was turned on for 10 minutes. After this, the flier continued its gliding descent until the time of self-destruct. Figure 10 shows the resulting trajectories. As in the previous figure, the oscillations are due to the phugoid mode of the aircraft.

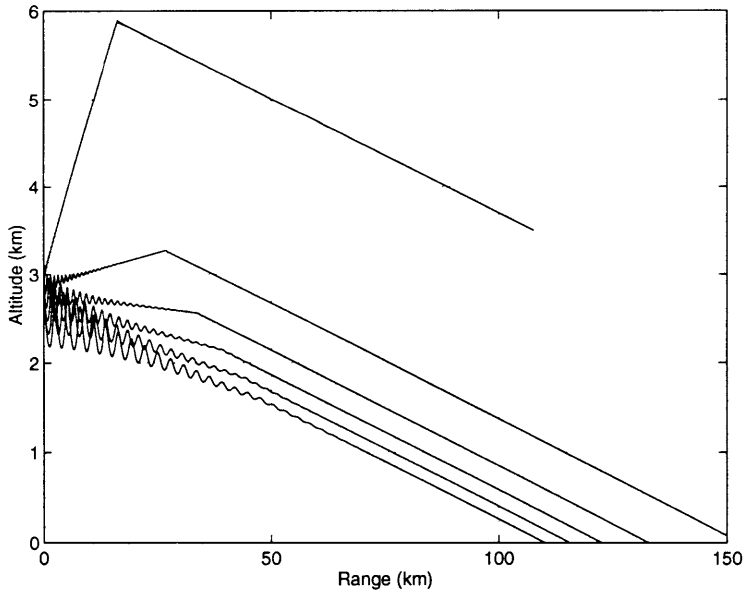

FIGURE 10: FLIER TRAJECTORIES (GLIDING AND WITH PROPULSION).

From the equations of motion, it can be seen that the amount of fuel is directly proportional to the power required from the propulsion system. Using the equations for level flight given in the previous section, this power is equal to:

$$P_{prop} = DV = \frac{1}{2}\rho V^3 S\left(C_{Do} + \frac{C_L^2}{\pi Ae}\right) = \frac{1}{2}\rho V^3 S C_{Do} + \frac{(mg)^2}{1/2\,\rho V S \pi Ae}$$

And therefore, it can be minimized:

$$\frac{\partial P_{prop}}{\partial V} = \frac{3}{2}\rho V^2 S C_{Do} - \frac{(mg)^2}{1/2\,\rho V^2 S \pi Ae} = 0$$

$$\Rightarrow V_{min} = \sqrt{\frac{2mg}{\rho S}}\sqrt{\frac{1}{3\pi Ae C_{Do}}} \quad \text{and} \quad C_{Lmin} = \sqrt{3\pi Ae C_{Do}}$$

It can be noted that this lift coefficient is the same as the optimum for minimum sink rate in gliding flight. In general, the limiting factor to achieving this optimum flight is the lift coefficient. Given the lift coefficient that can be provided, the C_{Do} is too large, or conversely, for a given zero-lift drag coefficient, the aircraft cannot provide enough lift to achieve optimum flight.

There were several propulsion options considered for the vehicle, including a two-stroke internal combustion engine, a Wankel engine, and an electric motor. The two-stroke internal combustion engine offers the best specific fuel consumption but also the highest mechanical complexity. The electric motor is the simplest option, mechanically, but has the requirement of having to carry heavy battery power. The Wankel engine is a compromise between both, offering the possibility of burning fuel (with a worse SFC than the two-stroke engine) with a low level of mechanical complexity. Reference 5 by Conklin offers a more comprehensive description of the power and propulsion system.

For the internal combustion engines, the range (R), loiter (T) and flight velocity (V) to maintain level flight can be calculated for a given vehicle weight.

$$R = \frac{\eta_p}{SFC}\frac{L}{D}\ln\left[g\left(1+\frac{m_f}{m_e}\right)\right] \quad \text{and} \quad T = \frac{1}{V}\frac{\eta_p}{SFC}\frac{L}{D}\ln\left[g\left(1+\frac{m_f}{m_e}\right)\right]$$

$$V = \sqrt{\frac{2mg}{\rho S C_L}}$$

where η_p is the propeller efficiency, m_f is the mass of fuel, and m_e is the vehicle empty weight. Similarly, for the electric motor:

$$R = \frac{\eta}{mg}\frac{L}{D}E \quad \text{and} \quad T = \frac{1}{V}\frac{\eta}{mg}\frac{L}{D}E$$

$$V = \sqrt{\frac{2mg}{\rho S C_L}}$$

where η is the overall power conversion efficiency (motor and propeller), and E is the battery energy content available for propulsion.

Figures 11(a) and 11(b) show the range, loiter and flight velocities for both propulsion options:

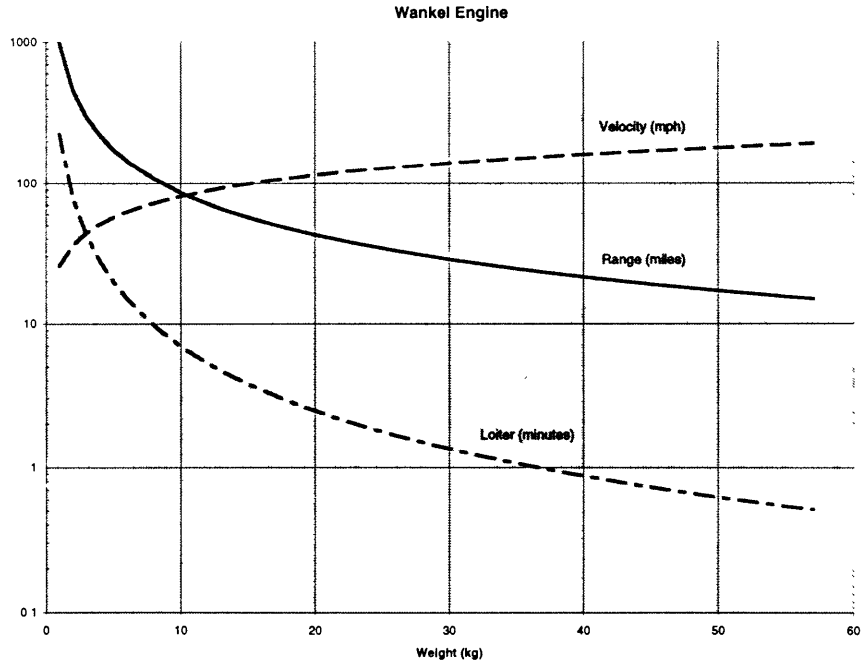

FIGURE 11(A): WANKEL ENGINE PERFORMANCE.

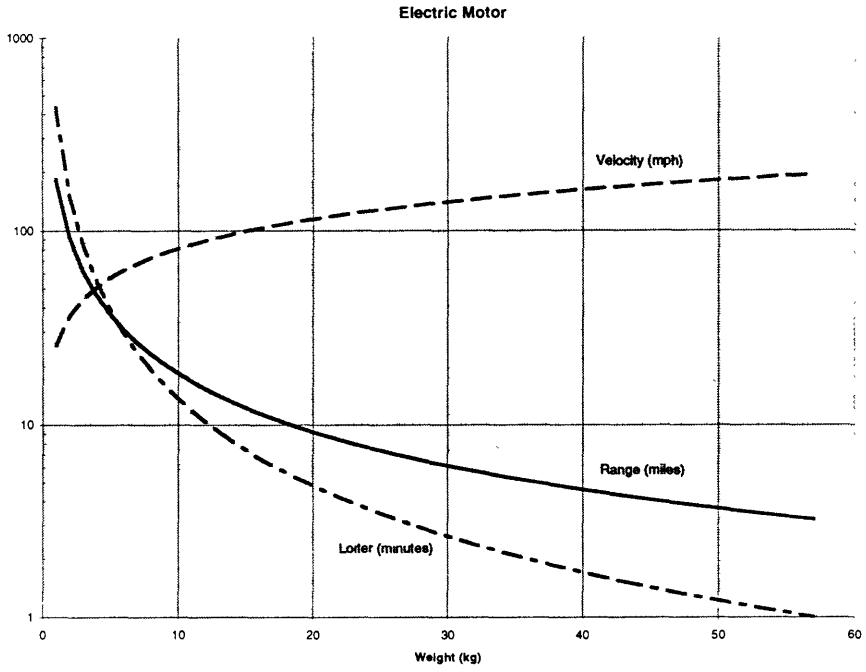

FIGURE 11(B): ELECTRIC MOTOR PERFORMANCE.

It can be seen from these figures that the internal combustion engine offers better performance. On the other hand, the electric motor is less complex, allowing for an easier g-hardening scheme. In the final concept, it was decided that the better performance of the internal combustion engine was worth the increase in complexity. This decision will be reviewed after planned centrifuge testing.

3.4 Vehicle Configuration Trade Studies and Concept Selection

The configurations described in Chapter 2 were assessed in trade studies to determine which configuration was better for the desired mission. First, a set of criteria was created to compare the design. These figures of merit were calculated, and compared by weighting them according to the results of the QFD analysis.

Having calculated the numerical values of each of the criteria, a relative score was calculated. The Silent Eyes concept was chosen as the baseline and given a score of unity. The other concepts were given a score by comparison to this concept.

The following list (from reference 2, see this reference for a more detailed description) shows the figure of merit and their relative weights:

- *Cost:* A mid-range cost estimate for each vehicle was calculated and compared. Lower cost was considered better, therefore it was weighted as -10 (the greater the cost, the more negative the cost score, and the lower the total score).

- *System Complexity:* A subjective measure of the overall complexity of the flyer and its systems. The system complexity multiplier was -10.

- *Loiter Time:* The estimated loiter time in seconds for the operational vehicle. Note that for analysis purposes, the loiter time was calculated between the altitudes of 1000m down to ground impact. This altitude range was used because this was the range of altitudes that were estimated to allow the camera to supply tactically useful information. Loiter time was weighted as 10 (longer times were better).

- *Inert Mass Fraction:* Used as a measure of the flier's ability to carry a payload. This value was calculated as the ratio of structural mass (excluding payload and fuel) to total mass. The IMF was weighted as -8, i.e., the lower it was the better the design.

- *Surveillance Area:* Total surface area (in square kilometers) viewed by the sensor between the operational altitudes of 1,000 m to ground impact. This was weighted as an 8.

- *Component Technology Availability:* This was a subjective measure used to judge whether or not all of the components needed for the flyer were existing presently or not. A higher score implied all of the necessary technology was available, a lower score implied development work would be required. The multiplication factor for this measure was an 8.

- *Deployment Scheme Complexity*: a subjective measure of the complexity of the deployment scheme for the flyer. Weighted as -7.

- *Electrical Power Volume Available*: This value was used to measure how much volume would be available for the flyer to carry batteries, and, therefore, it gave some indication

of how long the flyer's systems would be able to operate. This value was measured in cubic centimeters, and was weighted as 7.

- *Lift-to-Drag Ratio*: A classical measure of the aerodynamic efficiency of a flying vehicle. This value's multiplication factor was 6.

- *Flyer Range*: The linear distance traveled by the flier from 1,000 m altitude until it would crash into the ground. Measured in kilometers, the weighting factor for the value was 5.

From the point of view of the aerodynamic/propulsive analysis, the following results were obtained. The loiter time was significantly higher, around 20 minutes, for Super-Shell and for Pinky-and-Brain (with the latter being slightly higher). Even though Silent Eyes offered the best lift to drag ratio, the use of a propulsion system made the other two options come out ahead in terms of range and surveillance area covered.

The resulting comparison matrix is shown in Appendix H. Several conclusions were reached that determined the final selection:

- Pinky-and-Brain did not fit all the required components in the available volume, and was considered with the possibility of using a longer shell.

- The comparison tables lacked an adequate reflection of the level of complexity of each of the concepts.

- Pinky-and-Brain was rejected on the basis of its high degree of complexity and lack of operational advantage. The original idea of having a "brainless Pinky" proved unfeasible, since a lot of components would still be required in Pinky only to receive commands from Brain.

- Super-Shell offered a more flexible design in terms of downstream modifications. If the size of the components was significantly reduced in the future, the Super-Shell could turn into a Silent Eyes-like design. On the other hand, if the components was slightly bigger than expected, Silent Eyes would not be able to fit everything. Similarly, the propulsion system could always be dropped from the Super-Shell, but not added to Silent Eyes.

- Silent Eyes did not meet all of the initial customer requirements, since it did not have a mechanism to destroy the shell after deployment.

- Super-Shell offers a more innovative concept, innovation being one of the requirements of the MIT/Draper Technology Development Partnership project.

Based on all of these criteria and the selection matrices, Super-Shell was chosen as the concept to be pursued. A test plan and detail design schedule was then put together, to be able to meet the timeline of the project.

Chapter 4 Low-Speed Loiter: Aerodynamic Design

The detailed aerodynamic design of the selected concept began with a plotting of the final trajectory that the vehicle would undergo. The shell would be launched with a mass in the back, to provide enough stability during the ballistic flight, and would then release this mass (possibly using a parachute to avoid danger over friendly territory), reducing its mass down to 15 kg.

Figure 12 shows the overall trajectories of the vehicle, from launch of the shell from the gun until the final destruction of the vehicle, based on the aerodynamic coefficients and sizing of the preliminary analysis. It can be seen that the flier actually climbs with the engine at full power, and then begins descent once the engine has been turned off. In order to improve mission flexibility, the engine could be turned on and off several times to improve the loiter time, or as new target areas were desired.

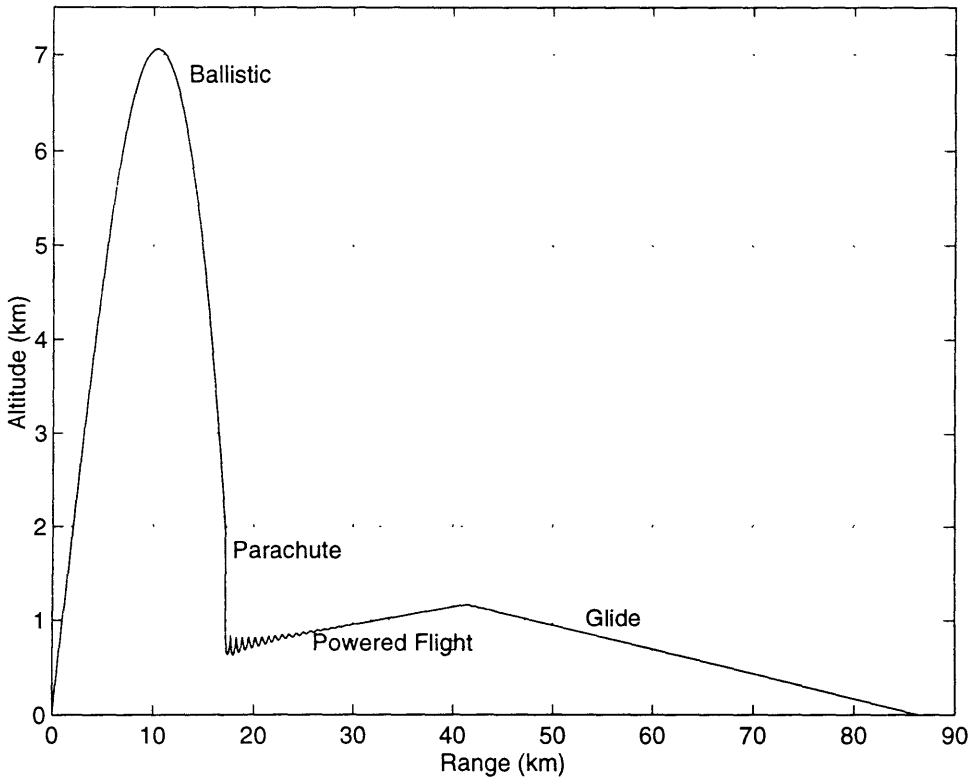

FIGURE 12: OVERALL TRAJECTORIES

After obtaining this initial performance estimate, a more detailed analysis was performed, where several parameters where changed. In changing this parameters, stability considerations had to be taken into account. Hence, the location of the wings as well as their sweep angle would influence the stability of the vehicle.

Figures 13 and 14 were produced by the MATLAB file loit.m, shown in appendix I. These are carpet plots of the loiter performance of Super-Shell for various wing surface areas, wing sweep angles and perpendicular (to the wing) lift coefficients. The performance is shown for both powered and unpowered versions. The surface area of the wing was reduced by reducing its span and moving its attachment point back, to improve its stability.

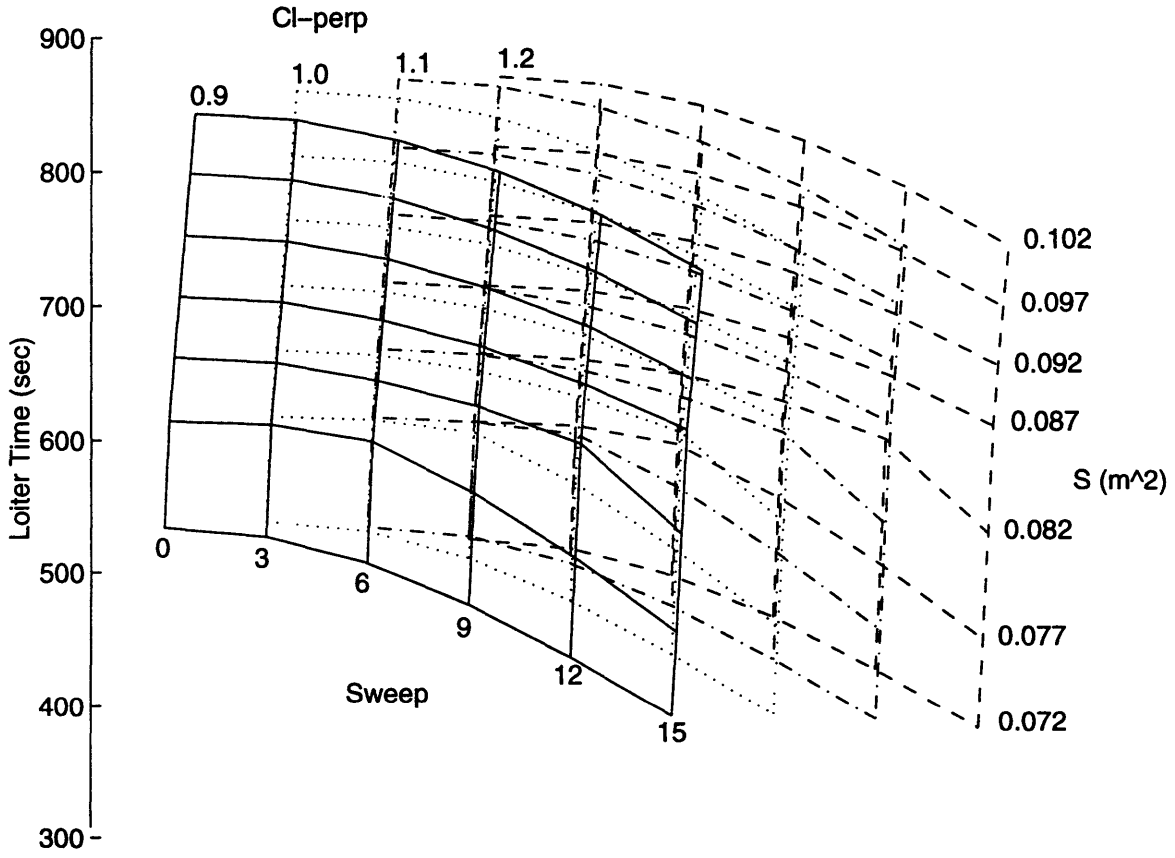

FIGURE 13: LOITER TIME PERFORMANCE (WITH PROPULSION).

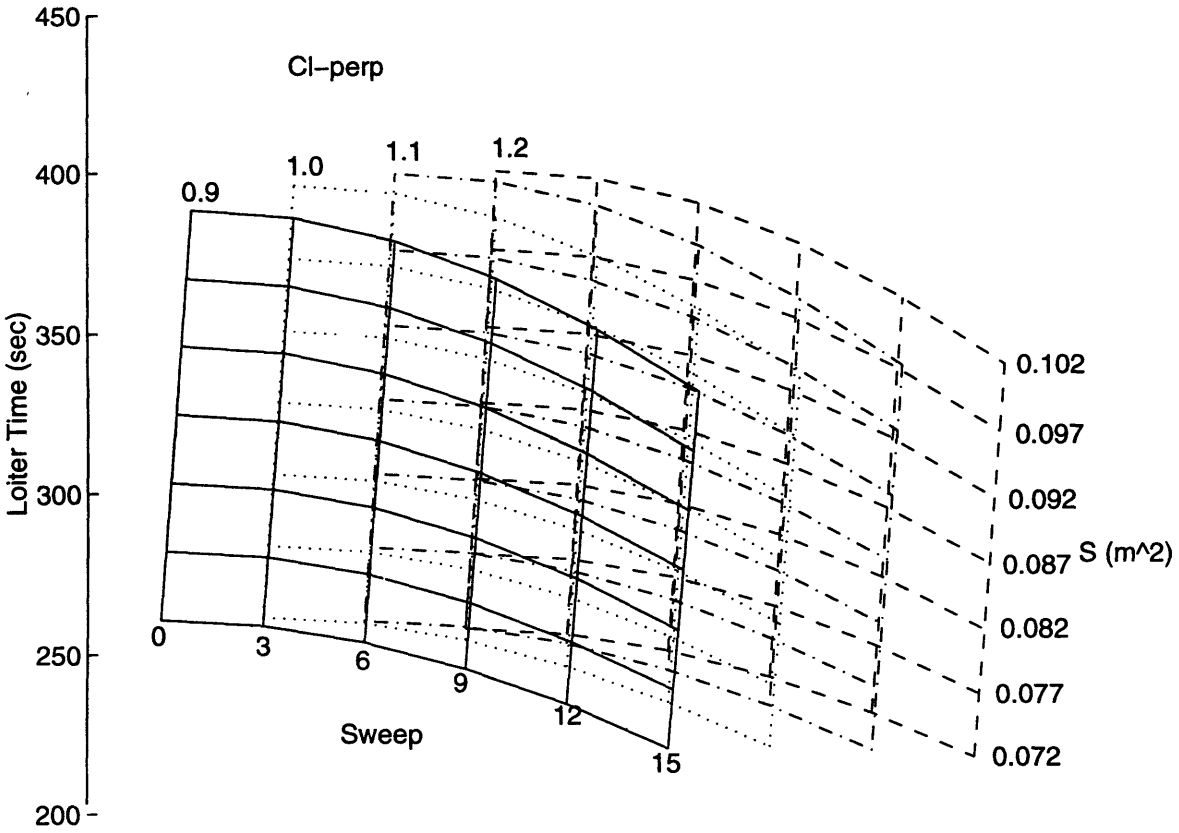

FIGURE 14: LOITER TIME PERFORMANCE (WITHOUT PROPULSION).

It can be seen from this figures that propulsion provides a significant increase to the loiter time performance of the vehicle. With this performance characteristics in mind, the design work continued to ensure a stable vehicle.

4.1 Aerodynamic Surface Modeling and Design

The aerodynamic configuration of the vehicle will determine its loiter and range performance. Besides the wing and tail surfaces, the flier body itself acts as an aerodynamic surface, providing a component of the overall lift. Moreover, the relative location of the aerodynamic center of the configuration and the center-of-gravity will determine the stability.

4.1.1 Airfoil Selection

The mission requirements were the basis for developing a suitable airfoil selection. The vehicle has to have optimal loiter performance at one speed (except for a short period after deployment), in the low subsonic regime. Therefore, this dictates a highly cambered airfoil. From reference 6, a cambered airfoil will have a higher maximum lift coefficient and a higher lift to drag ratio. On the downside, the ratio of maximum to minimum C_L will decrease. In this case, this is not an important concern, since the flyer will perform its mission at almost constant conditions.

The selected airfoil was the ND02 (see appendix I for the airfoil coordinates), which is a typical airfoil used on endurance-type model aircraft. Figures 15(a) and 15(b) show the pressure distributions for the airfoil at different angles of attach, in the flight regime that will occur during the missions. The pictures were produced by the software program XFOIL.

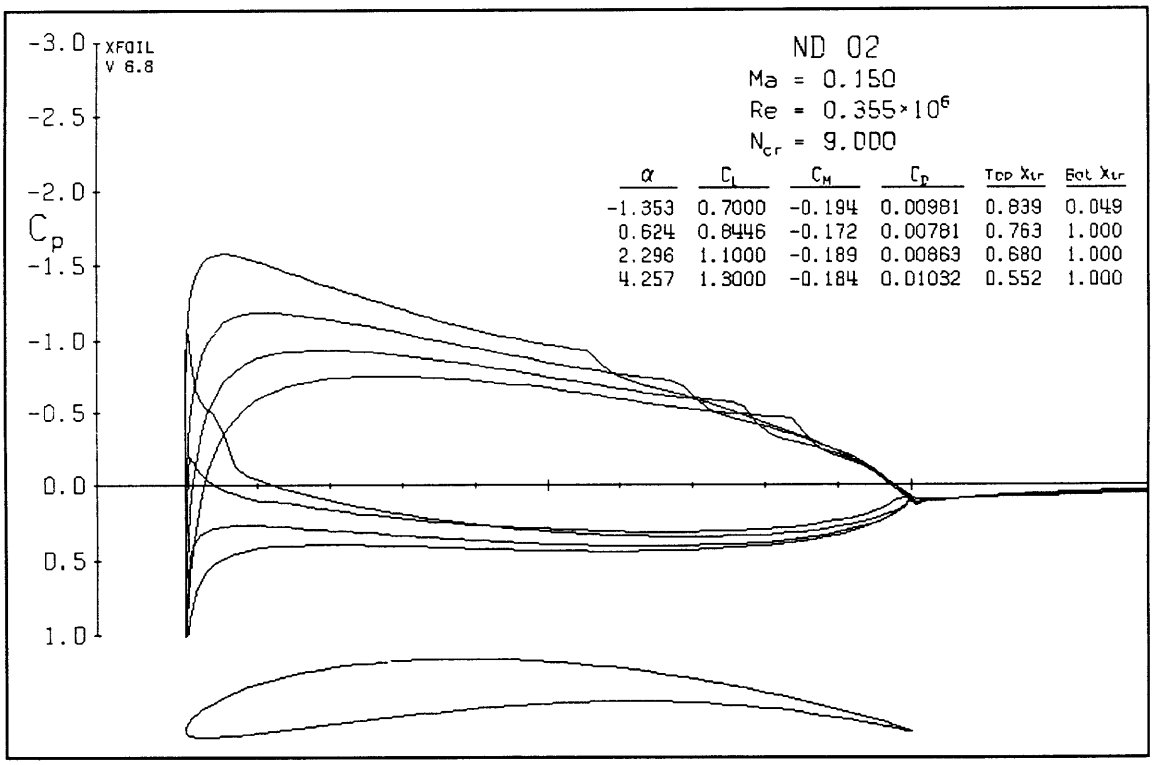

FIGURE 15(A): AIRFOIL PRESSURE DISTRIBUTIONS AT LOW ANGLES-OF-ATTACK

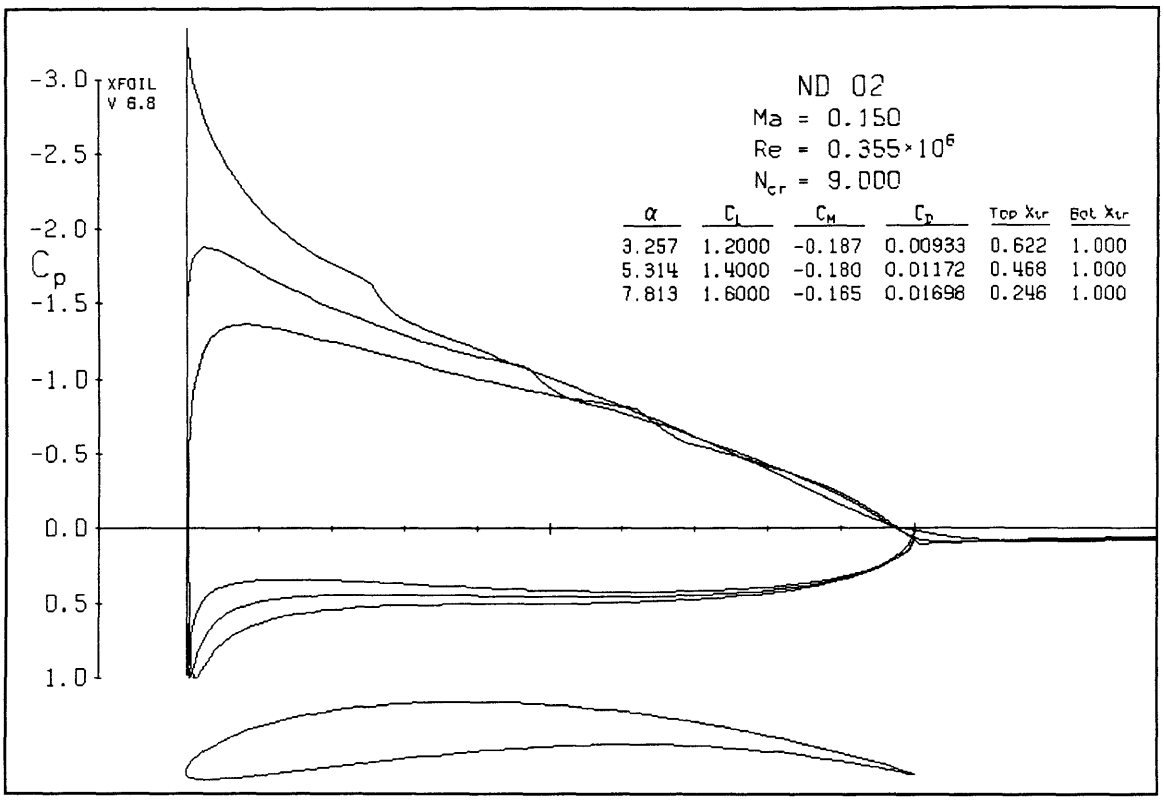

FIGURE 15(B): AIRFOIL PRESSURE DISTRIBUTIONS AT HIGH ANGLES-OF-ATTACK.

It can be seen from these plots that the airfoil is able to provide lift coefficients as high as 1.6, before stall occurs. It will be seen later that these high lift coefficients will be required of some sections of the wing during turns and when a lower speed is desired.

4.1.2 Wing and Tail Modeling and Configuration Selection

In order to determine the lift and stability characteristics of the vehicle, a modeling was done using the software program AVL. This program is an application of the Vortex Lattice Method, which models the characteristics of the vehicle by distributing "horse-shoe" vortex filaments across the aerodynamic surfaces. By varying the configuration, a design close to optimal was found. A more detailed discussion of the design procedure can be found in section 4.2.2.

The configuration modeling consisted of several parts. The flyer body was modeled as two flat plates, intersecting at right angles along the axis of the shell. These horizontal

and vertical plates represent the appropriate characteristics of the cylindrical body at low speeds.

The wings were modeled as four rectangular surfaces, accounting for the main portion of the wings and the telescoping extensions. These wings were moved to different positions along the body of the vehicle and swept back at various angles, to move the center of pressure and aerodynamic center of the configuration.

Finally, the tail surfaces were modeled as a downward-pointing v-tail. The use of a v-tail reduces the number of surfaces required to control the vehicle in both its longitudinal and its lateral motion. The dihedral angle of the tail was also varied to find the point where enough control was obtained for both modes of motion.

Figure 16 shows one of the configurations produced during the design iterations. All modeling surfaces can be seen. Also shown are the trailing vortices used to calculate aerodynamic forces.

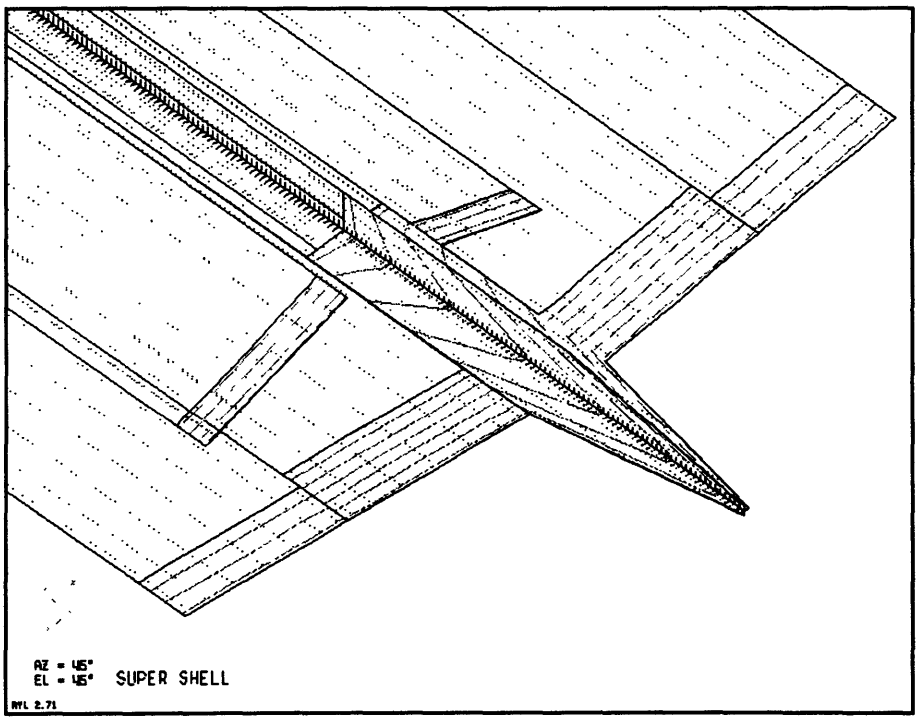

FIGURE 16: AVL SAMPLE FLIER MODELING.

4.1.3 Drag Estimation

The drag coefficient of the vehicle consists of two parts:

$$C_D = C_{Dprof} + C_{Dind} = C_{Df} + C_{Dp} + \frac{C_L^2}{\pi Ae}$$

where C_{dprof} is the profile drag, which includes both the drag due to friction (C_{Df}) and the drag due to pressure forces (C_{dp}). The induced drag (C_{Dind}) is caused by the tilting of the force vector due to the induced angle-of-attack produced by the trailing vortices.

The estimation of the profile drag is an approximate method in the initial stages of design. An estimate can be obtained from historical data, and later checked with wind-tunnel tests or more accurate Computational Fluid Dynamics (CFD) codes. An initial estimate of the drag coefficient was obtained using the methods described in references 9, 10 and 11.

The profile drag can be calculated as the sum of the drags of the components (with some factors for interference) as follows:

$$C_{Dprof} = \frac{\Sigma(C_f \times FF \times Q \times S_{wet})}{S_{ref}} \qquad \text{(reference 9)}$$

where C_f is the skin friction coefficient, FF is the form factor which accounts for the pressure drag contribution of each of the components, Q is the interference factor, S_{wet} is the wetted area of the component, and S_{ref} is the reference area for the drag coefficient (the wing area in this case).

The skin friction coefficient can be estimated as:

$$C_f = \frac{0.455}{(\log_{10} R)^{2.58}(1+0.144M^2)^{0.65}}$$

where R is the Reynolds number ($\rho VL/\mu$, L being the characteristic length).

The interference factors for wings and fuselage are approximately unity. For a V-tail the interference factor is approximately 1.04. The form factors are given by:

$$\text{Wing, Tail: } FF = \left[1 + \frac{0.6}{(x/c)_m}\left(\frac{t}{c}\right) + 100\left(\frac{t}{c}\right)^4\right]\left[1.34M^{0.18}(\cos\lambda)^{0.28}\right]$$

$$\text{Fuselage: } FF = \left(1 + \frac{60}{(l/d)^3} + \frac{(l/d)}{400}\right)$$

where t/c is the airfoil thickness to chord ratio, M is the Mach number, λ is the sweep angle, $(x/c)_m$ is the location of the maximum thickness in the airfoil, and l/d is the fineness ratio of the fuselage. The equation above for fuselage form factors can be used only for aerodynamic shapes. In the case of the flyer body, the flat base will produce a large pressure drag.

In order to determine the form factors for the flat-based flyer body, reference 10 was used. According to this source, the increase in profile drag due to flat base of a body can be estimated as:

$$\Delta C_{Dprof} = 0.029\left(\frac{d_B}{d}\right)^3 \frac{1}{\sqrt{C_f \frac{S_{wet}}{S_B}}}\left(\frac{S_B}{S_{wet}}\right)$$

where d_B is the diameter of the base, d is the maximum diameter, S_B is the surface area of the base, and ΔC_{Dprof} has been referenced to the wing surface area, as all the other coefficients.

Using all of these numbers, the following table shows the drag buildup for each of the components. Note that the quantity in parenthesis for the fuselage is for a tapered end to the fuselage:

TABLE 5: COMPONENT DRAG BUILDUP

Component	S_{wet} (m^2)	R	C_f	FF	Q	C_{Dprof}
Wing	0.1795	3.38E+05	0.00551	1.070	1	0.0118
Tail	0.0500	1.78E+05	0.00630	1.076	1.04	0.0039
Fuselage	0.0773	2.37E+06	0.00382	4.498	1	0.0301
(sharp end)	(0.1245)	(3.42E+06)	(0.00358)	(1.130)	(1)	(0.0056)
					TOTAL	***0.0458***
						(0.0213)

Figure 17 shows the decrease in drag coefficient as extra length of fuselage is added, to turn the flat-base projectile into a more aerodynamic shape. The added length ranges from zero to the length that makes the fuselage end in a point.

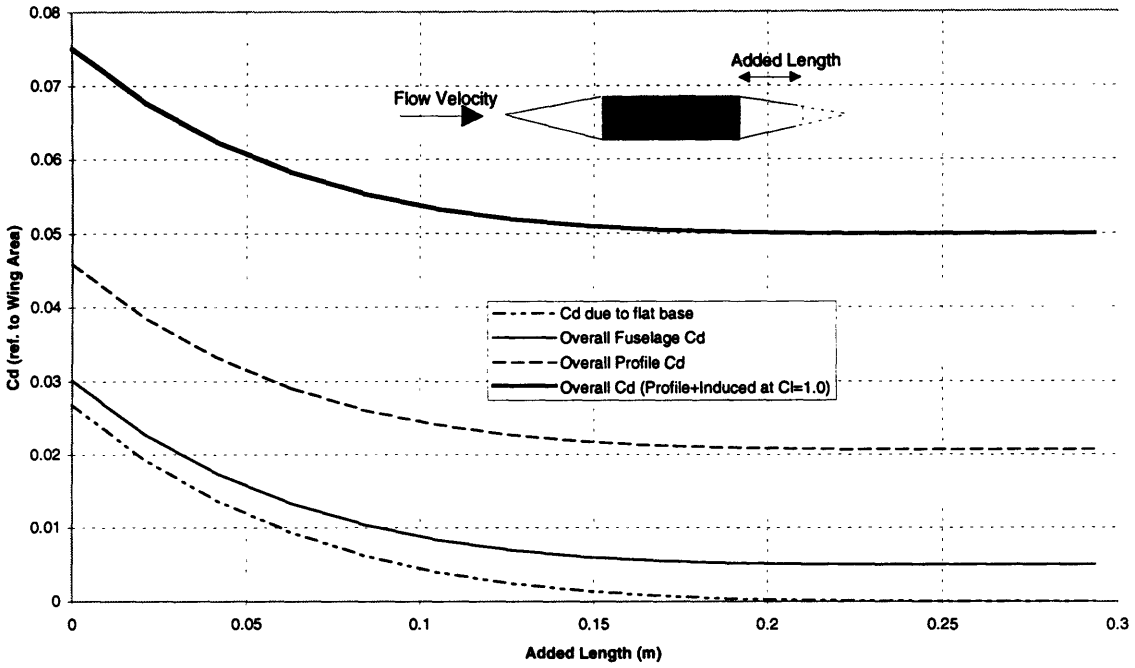

FIGURE 17: DRAG COEFFICIENT REDUCTION.

In can be seen in figure 17 that the contribution of the pressure drag in the flat-based body is very significant. There is an 100% increase in the overall profile drag from a pointy end to a flat base. Moreover it can be seen that with only half the length to a point (only 15 cm), the drag has reached a level close to its minimum.

This led to some design decisions, since if the shell was to be left with a flat base, the contribution of the pressure drag to the overall C_D would be significant. Specifically, from figure 17 it can be seen that the minimum and maximum overall drag coefficient are related by a factor:

$$\frac{C_{Dmax}}{C_{Dmin}} \cong \frac{0.075}{0.05} = 1.5$$

This factor is the same one that relates the L/D for the maximum and minimum drag coefficients. Similarly, the minimum and maximum profile drag coefficients are related by:

$$\frac{C_{Do\,max}}{C_{Do\,min}} \cong \frac{0.045}{0.02} = 2.25$$

Therefore, using the equation in section 3.2 for the velocity required for maximum loiter, a relationship can be obtained between the optimal velocities with minimum and maximum C_D:

$$V_{opt} \propto (C_{Do})^{-1/4} \quad \Rightarrow \quad \frac{V_{opt-max}}{V_{opt-min}} \cong \left(\frac{C_{Do\,max}}{C_{Do\,min}}\right)^{-1/4} = 0.8165$$

Hence, given the change in velocity and in descent angle, the loiter times will be related approximately by (assuming small descent angles):

$$\text{Time} \cong \frac{\text{Range}}{\text{Velocity}} \propto \frac{L/D}{V_{opt}} \quad \Rightarrow \quad \frac{\text{Loiter}_{CD-max}}{\text{Loiter}_{CD-min}} \cong \frac{V_{opt\text{-}min} D_{min}}{V_{opt\text{-}max} D_{max}} = \frac{1}{0.8165} \times \frac{1}{1.5} = 0.8$$

Therefore, we can see that there is a 20% reduction in the loiter time, assuming that the vehicle flies at the optimal speed. Given this reduction in loiter time performance, the use of a pointed or tapered back was suggested.

4.2 Aerodynamic Stability Analysis

Several important stability issues had to be taken into account in the design of the configuration: the vehicle had to be trimable, and the vehicle had to be stable in longitudinal and lateral motions. Each of these requirements led to variations in the sizes of the surfaces and their orientation. In addition, the stability of the flier depended on the location of its center-of-gravity. The calculation of the stability derivatives was done automatically by AVL, and the parametric plot shown in figure 13 was used to compare the performance of the possible stable configurations.

With the stability derivatives, a simulation of the vehicle dynamics can be performed. At the time of the final edition of this thesis, the simulation of the open-loop dynamic stability of the flier was being implemented, and could therefore not be included.

4.2.1 Center-of-Gravity Limits

Due to the iterative nature of the design process, the location of the center-of-gravity of the vehicle changed continuously. However, there are two limits to the location of the CG given by stability and control considerations:

- Aft Limit: The static stability of the vehicle can be achieved only when the center-of-gravity is located forward of the neutral point of the vehicle.

- Forward Limit: The location of the center-of-gravity has to be such as to give enough trimming and control authority to the tail surface, at reasonable tail incidence angles.

For an airplane to be statically stable, the moments about the CG must be zero. On a conventional configuration, the moments will be caused by the lift on the wing and tail, and the moment about the aerodynamic center of the wing, due to the airfoil camber is:

$$M_{CG} = (h - h_{nw})\bar{c}L_{wing} - (h_l - h)\bar{c}L_{tail} + M_{ac}$$

where the distances are measured from the leading edge of the mean aerodynamic chord (c-bar) as fraction's of the MAC itself. Hence "h" is the distance from the leading edge to the CG, h_{nw} is the distance from the leading edge to the aerodynamic center (ac) of the wing, and h_l is the distance to the ac of the tail.

If the neutral point is defined as the point in the aircraft about which the moment is constant, independent of angle-of-attack, then the distance h_n from the leading edge of the mean aerodynamic chord to the neutral point can be obtained by manipulating the equation above, to obtain (see reference 8):

$$h_n = \frac{h_{nw} + h_l \eta_t \frac{S_t}{S}\frac{a_t}{a_w}(1-\varepsilon_\alpha)}{1+\eta_t \frac{S_t}{S}\frac{a_t}{a_w}(1-\varepsilon_\alpha)}$$

where η_t is a measure of the efficiency of the tail, S_t is the surface area of the tail, a_t and a_w are the lift-curve slopes of tail and wing, respectively, and ε_α is the change in downwash angle with angle-of-attack.

All these quantities are harder to define in the present design, due to the unusual aircraft configuration, since the lift and moments provided by the flyer body itself add a contribution to the overall forces. But even with this, in non-dimensional form, the change in pitching moment coefficient with angle-of-attack will be:

$$C_{M\alpha} = (h - h_n) C_{L\alpha}$$

where $(h\text{-}h_n)$ is defined to be the static margin. For an airplane to be stable, the static margin must be positive, and in general between 5 and 10% is desired. In other words, the CG must be ahead of the neutral point by 5 to 10% of the mean aerodynamic chord. This determines the aft limit of the CG.

In order to determine the forward limit of the CG, the problem of controlling the aircraft must be considered. The magnitude of the control forces and moments to be applied for maneuvering increases as the CG moves forward. Hence, the limit will be determined by how much force the tail control surface can exert.

If the CG is located forward of the aerodynamic center of the wing, then the moment about the CG is:

$$M = M_{ac} + l_w L_{wing} + l_t L_{tail}$$

Therefore, the wing must exert a negative lift. As the CG moves forward, the distances l_w and l_t get closer together. As they approach each other, the lift provided by the tail must approach the lift provided by the wing. Therefore there is a limit to how far forward the CG can move, and still have enough tail surface to trim the aircraft. Neglecting the moment about the aerodynamic center of the wing (since it will be much smaller), the limit is given by:

$$l_w L_{wing} = l_t L_{tail} \Rightarrow (h + h_{nw})\bar{c} C_{Lwing} = (h + h_t)\bar{c} C_{Ltail} \frac{S_t}{S}$$

$$\Rightarrow h = \frac{h_t C_{Ltail} \frac{S_t}{S} - h_{nw} C_{Lwing}}{C_{Lwing} - C_{Ltail} \frac{S_t}{S}}$$

4.2.2 Design Methodology

Having the basic principles in terms of stability requirements, the software program AVL was used to calculate the stability behavior of the vehicle within various configurations. From figure 13, it was seen that in order to maximize performance, a high-surface area wing with low sweep angle and a high lift coefficient should be used.

Although the characteristics just mentioned would guarantee good performance, this loiter time might not be achievable if the flier is not stable. In order to ensure the stability of the vehicle, several configurations where developed. Initially, several parameters were varied to achieve stable configurations:

- Wing Sweep Angle: Ranging from 0 to 15 degrees.
- Wing Location / Span: In the stowed position, there is a limit for the endpoint of the wings, given by the volume constraints. Hence, by moving the pivoting point of the wing aft, the aerodynamic center of the wing moves back, as the span (and therefore the surface area) decreases.
- Overall Lift Coefficient: From 0.9 to 1.2.

For each of these configurations, the CG was calculated for the fixed structure (projectile, wings, tail and engine) and used as the reference point for the stability calculations. Tail size was fixed by volume constraints, but the dihedral angle could be varied. By changing the dihedral angle of the tail as well as its incidence angle, stable configurations were found. From these configurations, and making use of figure 13, the best final stable configuration was chosen that could be trimmed with a reasonable tail incidence angle (no more than 10 degrees).

Figures 18(a) and 18(b) show two views of the final configuration, as produced for the AVL calculations. This configuration was produced using the code using in appendix I.

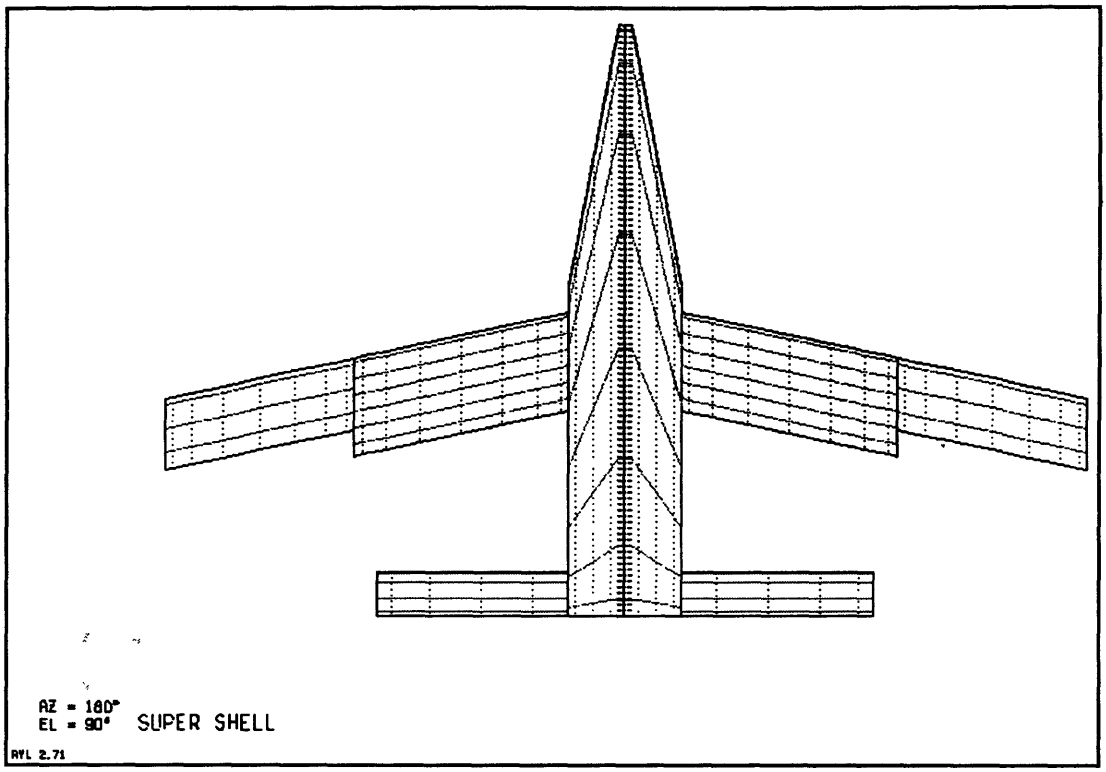

FIGURE 18(A): PLAN VIEW OF THE FINAL CONFIGURATION (FROM AVL).

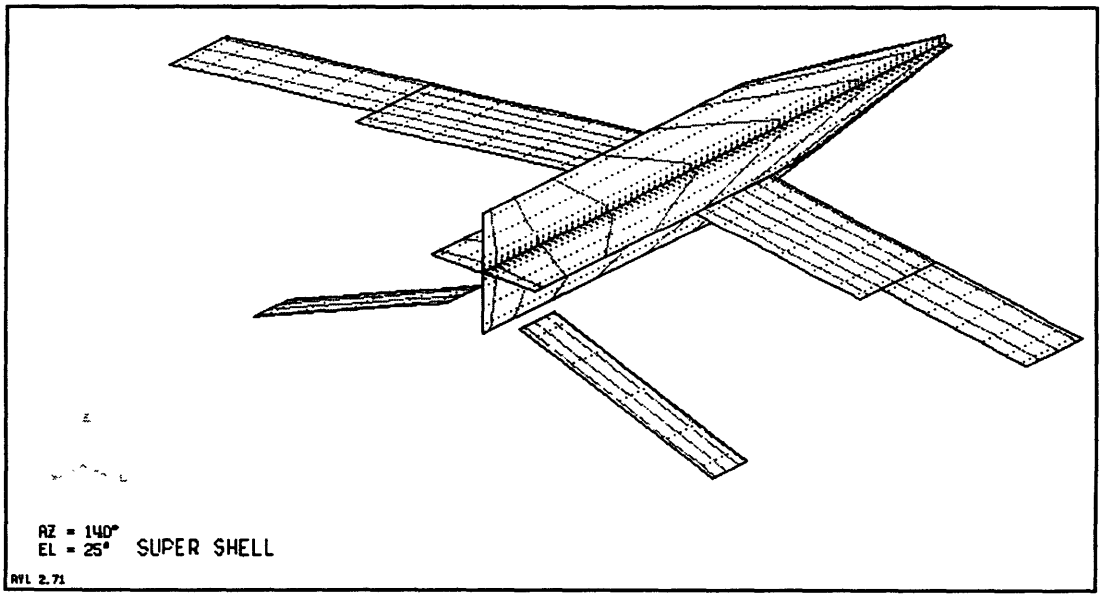

FIGURE 18(B): VIEW OF THE FINAL CONFIGURATION (FROM AVL).

Figure 19 shows the spanwise loading of the flier, in the Trefftz Plane.

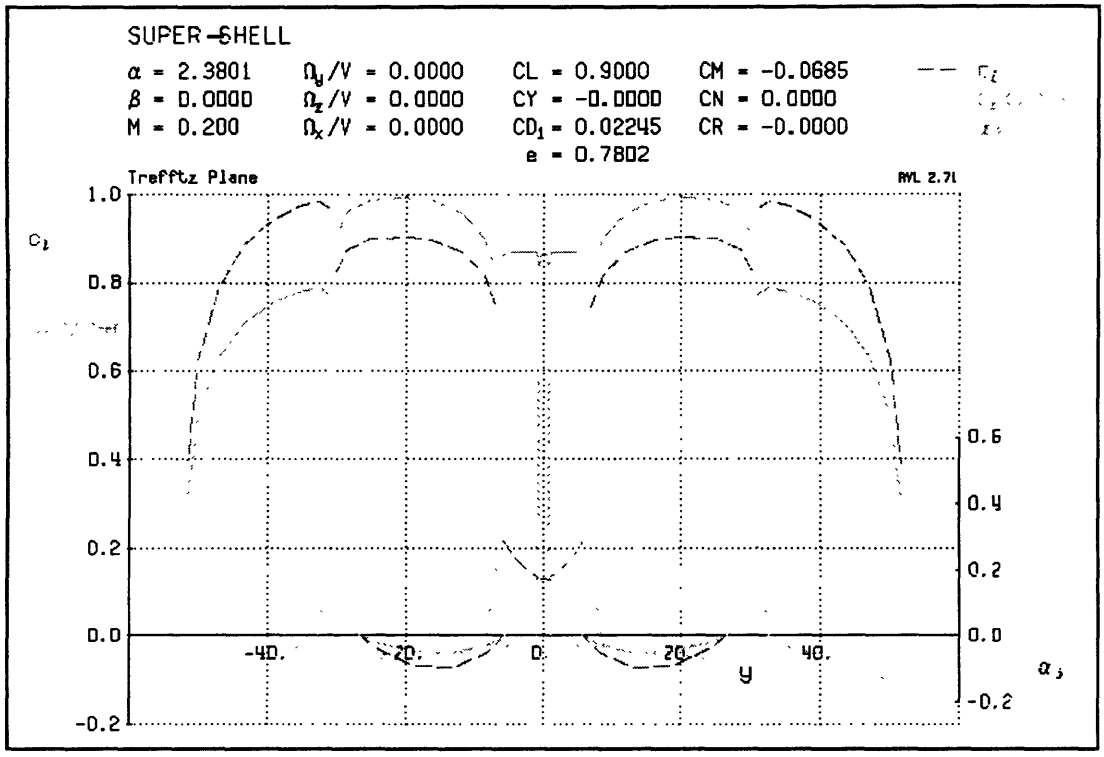

FIGURE 19: TREFFTZ PLANE LOADING.

It can be seen from Figure 19 that the local section lift coefficients do not go above 1 and therefore there will not be any stall problems.

The characteristics of the final configuration are the following:

- Wing Area: 957 cm^2.
- Sweep Angle: 12 degrees.
- Tail Dihedral Angle: 20 degrees.
- Tail Incidence Angle for Trim: 9 degrees.
- Lift Coefficient: 0.9.
- Static Margin: 8% stable.

Figures 20(a) and 20(b) show the 3-view model of the final configuration, with dimensions in centimeters, and a solid model, respectively.

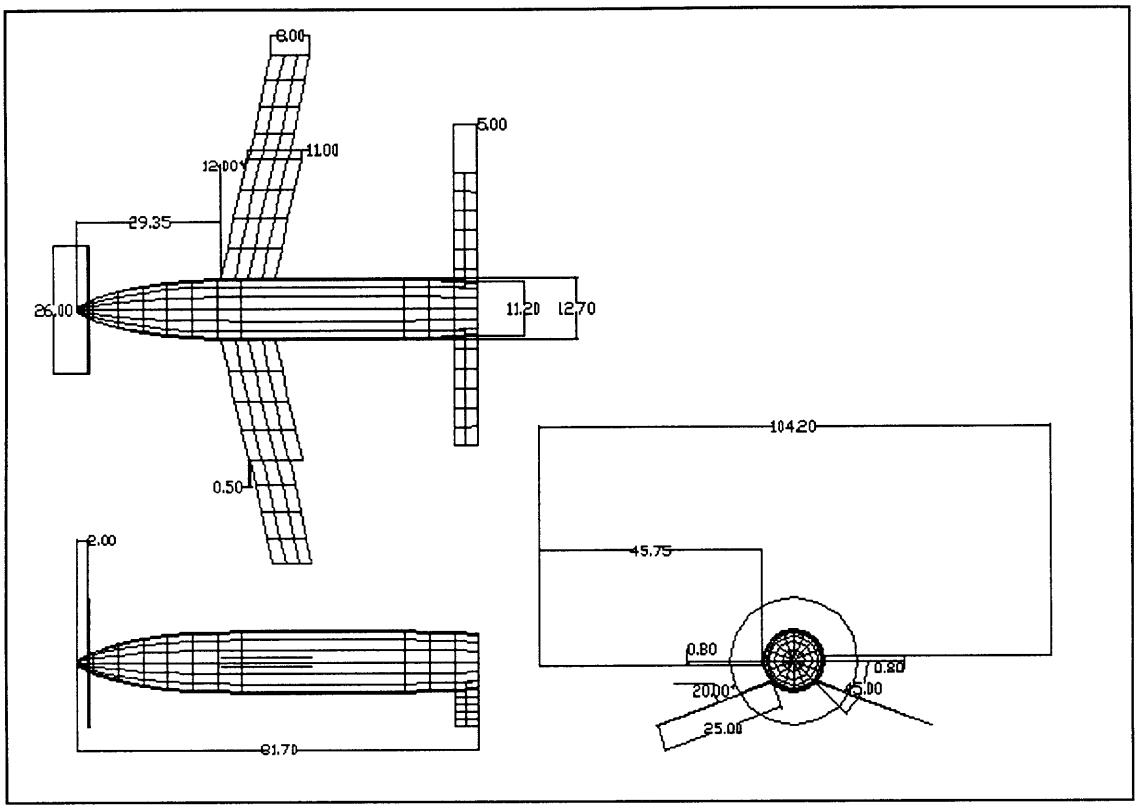

FIGURE 20(A): FINAL CONFIGURATION (BY TAN TRINH, ON AUTOCAD).

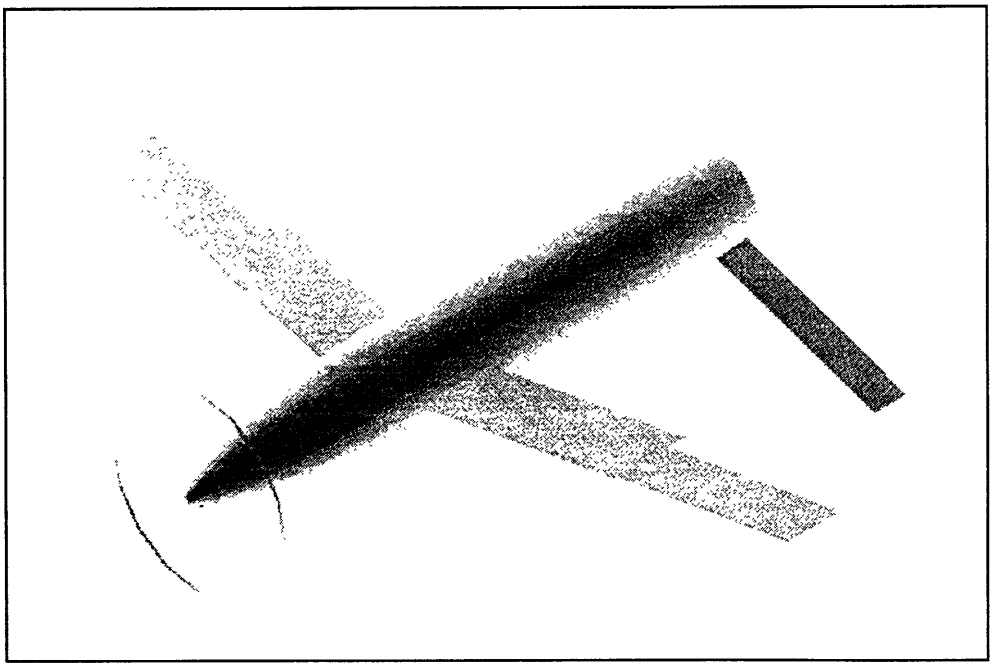

FIGURE 20(B): FINAL CONFIGURATION SOLID MODEL (BY TAN TRINH).

4.2.3 Stability Derivatives

The dynamic stability characteristics of an aircraft can be described in terms of stability derivatives. These are derivatives of forces and moments acting on an aircraft with respect to the angles and rotation rates. Although there are 36 derivatives, only 13 of them are meaningful once longitudinal and lateral-directional dynamics have been decoupled.

The following table shows desired values of this stability derivatives, together with the actual values obtained by AVL for the final vehicle configuration:

TABLE 6: STABILITY DERIVATIVE VALUES

Stability Derivative	Desired Value	Actual Value
$C_{L\alpha}$	$\approx 2\pi$	6.640
$C_{m\alpha}$	< 0	-0.562
$C_{Y\beta}$	< 0	-0.461
$C_{l\beta}$	≈ 0 (but < 0)	-0.003
$C_{n\beta}$	≥ 0	-0.011
C_{Yp}	Not important	0.165
C_{lp}	< 0	-0.510
C_{np}	< 0	-0.071
C_{Lq}	Not important	12.14
C_{mq}	< 0	-15.59
C_{Yr}	Not important	0.189
C_{lr}	> 0	0.156
C_{nr}	< 0	-0.039

From the table it can be seen that the aircraft is longitudinally stable, as the static margin ($C_{m\alpha}$ divided by $C_{L\alpha}$) is negative and close to the desired value of 10%. The damping terms, C_{lp}, C_{mq} and C_{nr} are negative as expected.

The only term that appears slightly unstable is the derivative of the yawing moment with respect to the sideslip angle ($C_{n\beta}$ = - 0.011). Due to the small magnitude of the instability, this problem could be solved by active control using the tail surfaces, or by increasing the dihedral angle of the tail.

4.3 Deployment Mechanism

Figure 21 shows three different views of the wing, including its pivoting mechanism for deployment.

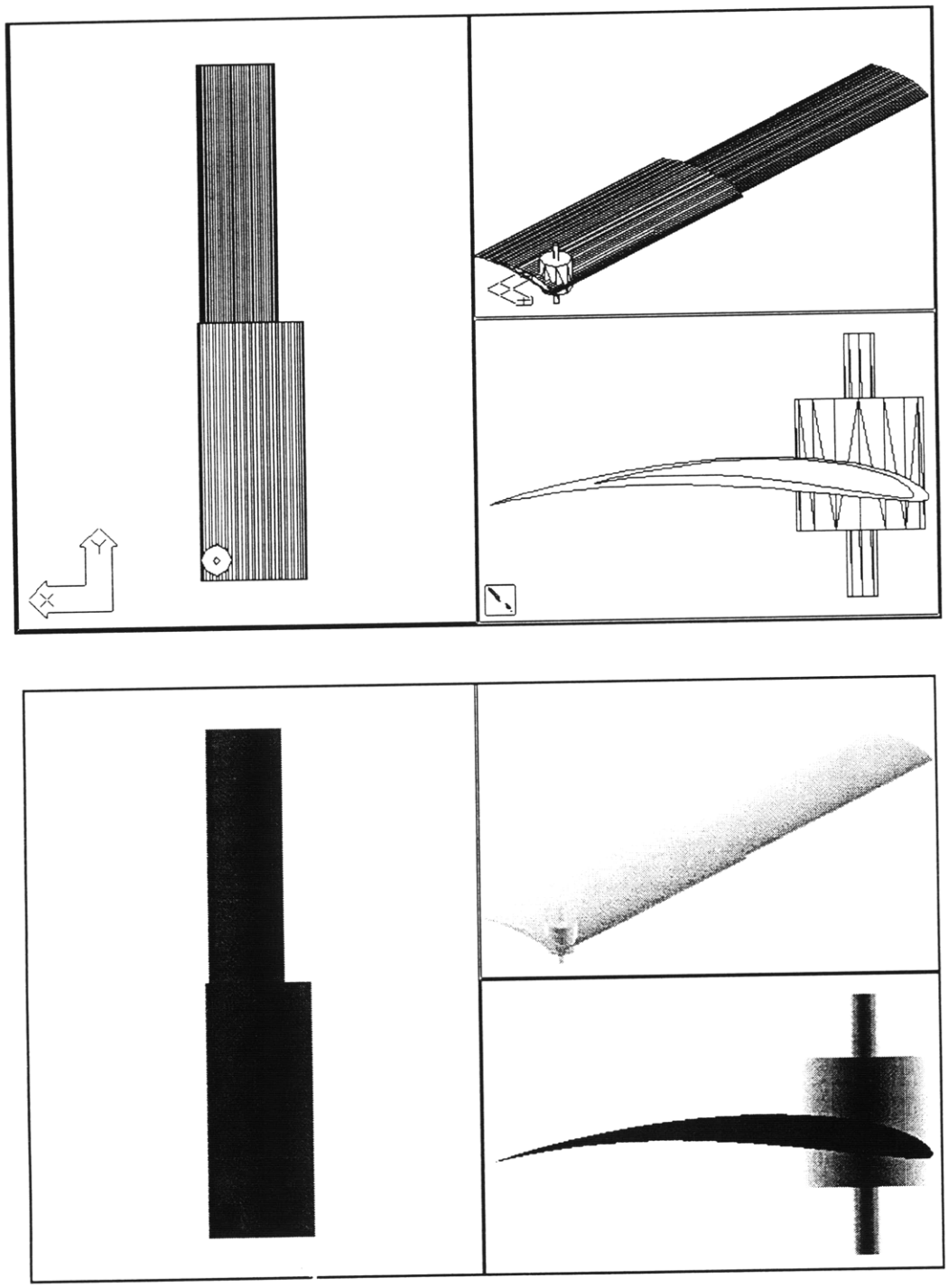

FIGURE 21: WING AND DEPLOYMENT MECHANISM.

The schematic block diagram (SBD) for the deployment mechanisms of the wing and the tail is shown in figure 22.

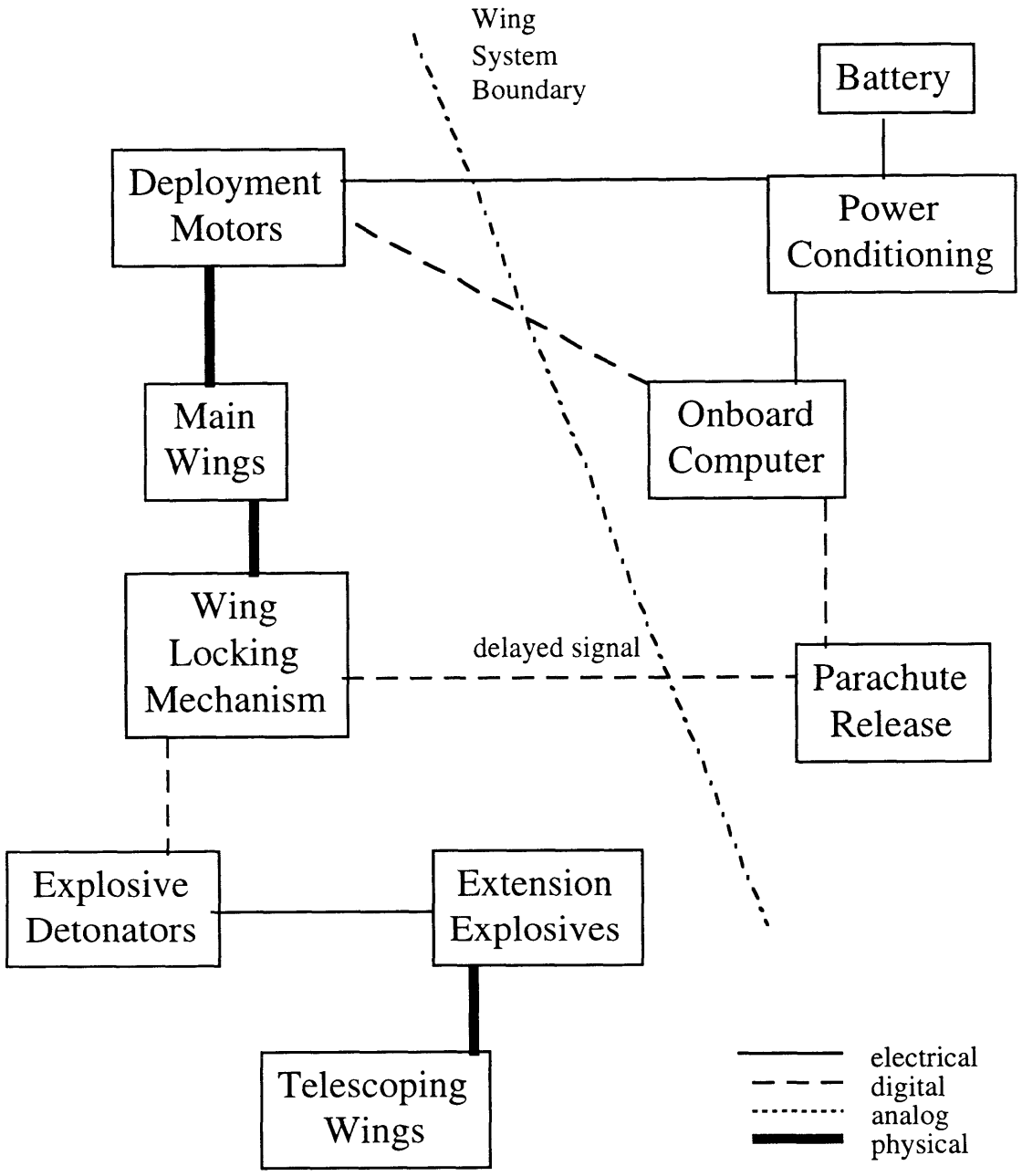

FIGURE 22: SCHEMATIC BLOCK DIAGRAM OF THE WING DEPLOYMENT MECHANISM.

When the onboard computer sends the deployment signal, the power conditioning unit sends the required power to the deployment motors. This motors rotate the main wings

to their extended position, and the wing locking mechanism locks the wing and sends a signal to the explosive detonators. The explosive detonators then emit a pulse which detonates the explosives that extend the telescoping wings.

Shortly after the wing locking mechanism sends the signal to the explosive detonators, it sends a signal to the parachute release mechanism through the onboard computer. At this point, the flier is in its flight configuration, and the parachute is released as the vehicle starts its gliding flight.

A similar but simpler deployment mechanism is used for the tail surfaces. These surfaces have the same actuator motors, but lack the explosives, since the tail surfaces do not extend telescopically.

4.4 Test Schedule

Once the preliminary aerodynamic design and stability analysis of the vehicle has been carried out, all the predictions have to be tested. An aggressive test schedule was developed for each of the subsystems, as well as for the integrated product. See reference 2, by Bernstein, for a more detailed description of the testing schedule for each of the subsystems and for the final integrated demonstrator vehicles.

From the point of view of aerodynamics, the vehicle is to be tested in two ways:

- High-g Testing: The vehicle will be tested to simulate actual launch conditions, making use of existing air or rail-guns at Army or Navy facilities. In this test, the vehicle would have all aerodynamic surfaces mounted as they would be in their stowed position in the operational vehicle. In this test, the flying vehicle will not be deployed, but the integrity of the wing structure and the functionality of the deployment mechanism will be checked.

- Air Drop Testing: The vehicle will be tested to simulate the flight of the vehicle, by being dropped from a general aviation aircraft in its stowed configuration. The vehicle will prove its stability and its ability to fly and receive control instructions for its aerodynamic control surfaces. Moreover, the test will show the operation of the deployment mechanism for all the aerodynamic surfaces (which will already have been tested on the ground).

Chapter 5 Recommendations and Conclusions

5.1 Aerodynamics

The preliminary aerodynamic design of the vehicle has been completed along with a top-level architecture of the entire operational system. Several possibilities appeared in the later stages of the design that could be interesting to consider: the use of inflatable wings; the extension of the effective wing area by deploying a flexible, cloth-like, extension; and the use of a pusher propeller for reduced drag.

With the use of inflatable wings, the span and surface area of the wing could be increased. By using a solidifying foam, the volume of the folded wing could be reduced significantly, therefore allowing for an increase in the fuel volume for the engine. On the other hand, a larger wing could be deployed from the same volume. Looking back at Figure 13, it can be seen that this increase in surface area would significantly improve the performance.

The use of a parafoil-like extension of the wing would increase the surface area of the wings, and therefore the lift coefficient at a given speed. Alternatively, the increase in wing area could produce the same vehicle lift coefficient with a lower airfoil section design lift coefficient, or with a lower speed. On the other hand, the induced drag would increase due to the reduction in the effective aspect ratio of the wings. This option could be submitted to further detail studies as a possible option.

Moving the propeller and the engine to the back of the vehicle would reduce drag. With a tapered end, or even with a flat base, using a pusher-propeller, would decrease the profile drag due to pressure, since the slow air in the wake would be accelerated by the motion of the propeller. This option has the problem of having to rearrange the internal layout, which would probably make it more difficult to find an optimal component arrangement.

5.2 Project Management

There were numerous lessons learned in this project from the point of view of management. Consequently, there are several recommendations to be made based on previous mistakes. These recommendations are related to scheduling, coordination, communication, documentation and team spirit.

As was described in section 2.6, scheduling the tasks of each and everyone of the team members is very important. Having weekly plans ensures that everyone knows what they are supposed to be doing, and allows for a global vision of the project.

Coordination of efforts avoids redundant work. Several times during the second semester of the project, team members realized that some calculations had been performed by two members at the same time. While this is a good routine for checks, it is not always necessary, as it reduces capacity.

The best way to achieve coordination is through communication. But communication is also useful to ensure that all documents are updated and there is an adequate interaction between the various subsystem groups.

Documenting calculations, drawings and diagrams constantly is vital. In performing calculations based on work done by other subsystem groups, it is important to have documentation available that fully describes the purpose and means of all calculations. Moreover documenting constantly avoids last-minute preparation of documents which not only causes stress, but also stops other advances in the project.

Finally, it is necessary to create in the team a good spirit and enthusiasm for what is being designed. If the project is seen as something better than just homework, a much better atmosphere is created for work and interaction between the team members.

References

1.- Anderson, John, Fundamentals of Aerodynamics, McGraw Hill, New York NY, 1991.

2.- Bernstein, Joshua, System Design for a Rapid Response Autonomous Aerial Surveillance Vehicle, Cambridge MA, 1997.

3.- Boppe, Charles, Class Notes for 16.870/1 Aerospace Product Design, MIT, 1996-97.

4.- Burba, Matthew, Systems Design and Communication Subsystem of an Innovative Projectile, Cambridge MA, 1997.

5.- Conklin, Ted, MIT/Draper Technology Development Partnership Project: Systems Analysis and On-Station Propulsion Subsystem Design, Cambridge MA, 1997.

6.- Drela, Mark, Class Notes for 16.110 Flight Vehicle Aerodynamics, MIT, 1996-97.

7.- Hallam, Cory, MIT/Draper Technology Development Partnership Project: Aerodeceleration, Structures, and Systems Design of a High-G, Rapid Response, Deployable Unmanned Aerial Vehicle, Cambridge MA, 1997.

8.- McCormick, B., Aerodynamics, Aeronautics & Flight Mechanics, John Wiley & Sons, New York NY, 1995.

9.- Raymer, Daniel, Aircraft Design: A Conceptual Approach, AIAA Educational Series, Washington DC, 1992.

10.- Hoerner, Sighard, Fluid-Dynamic Drag: Practical Information on Aerodynamic Drag and Hydrodynamic Resistance, New York NY, 1965.

11.- Covert, Eugene, Thrust and Drag: Its Prediction and Verification, AIAA Progress in Aeronautics and Astronautics Vol. 98, Washington DC, 1985.

12.- Chadwick, W.F., Sylvester, J.F., Dynamic Stability of 5-Inch/54 Rocket Assisted Projectiles (The Influence of Non-Linear Magnus Moment). NWL Report 2059. U.S. Naval Weapons Laboratory, Dahlgren, Virginia, USA, 1966.

13.- Etkin, B., Dynamics of Flight: Stability and Control, John Wiley & Sons, New York NY, 1982.

14.- Elwell, John, Charles Stark Draper Laboratories. Information obtained at the WASP Preliminary Design Review, MIT, May 16, 1997.

Appendix A MIT/Draper Technology Development Partnership Project Proposal

Draper Fiscal Year 97 IR&D Plan/Report

MIT / Draper Technology Development Partnership Project

Project Title

18 June 1996

Date Submitted

John Deyst & Charles Boppe

Principal Investigator(s)

Approved by Draper Technical Champion / P.O. Project Manager

MIT / Draper Technology Development Partnership Project

IR&D Project No.
MIT Investigators: John Deyst & Charles Boppe
Draper Contact: Byong Ahn

DESCRIPTION OF PROJECT

The MIT / Draper Technology Development Partnership project seeks to develop and demonstrate an innovative first-of-a-kind system judged to be important to the needs of the nation. While the technical capabilities and facilities of the organizations involved are critical in this process, another key factor for this project is the research performed to identify the national needs, identify opportunities, and select the best project with multiple ways to win. A market study will also be used to assess potential return-on-investment and structured risk mitigation plan will be developed in support of an "Adoption, Adaptation, and Invention Plan" and a "Forward, Reverse, and Re-Engineering Plan." A system technology demonstrator is planned for the second year's activity.

PROBLEM

In response to a rapidly changing world environment with shifting needs in both the defense and commercial sectors, there is a need to explore new opportunities that focus on multiple customer needs and are aligned with today's national priorities. It is important to recognize that dealing with *requirements* is the key to attacking this problem. This will require structuring the effort to merge key enabling technologies - both newly developed and those that now exist - to address a nationally important priority and demonstrate the resulting system within a 2-year period.

OBJECTIVES and SCHEDULE

Objectives

This project's objectives are aligned with two main themes. The first deals with the primary thrust that addresses the development of a first-of-a-kind system/product with related enabling technologies that addresses a nationally important need. Concept selection will be supported with a full competitive analysis and an identification of market potential. A strong customer focus will be inherent in this process. In achieving the objectives within the first theme - full use of both Draper and Institute facilities will be made.

A second theme focuses on a need to develop future entrepreneurs and innovative engineers. With creativity and innovation, the need to initiate, refine, and adapt a scheme that effectively sets up an environment where top-rated students can nurture new ideas becomes a significant challenge. Implementation of a somewhat structured plan and the use of consultants and special seminar speakers will play important roles in this process.

Milestone Schedule

Two Figures (#1 & #2) have been prepared to characterize the schedule and plan that will be used to link the proposed activities. A table of resulting objectives that addresses the two themes discussed in the preceding section follows.

Objective #	Description	Start	End
1	Priority / Opportunity Assessment	7/96	9/96
2	Market Assessment	9/96	11/96
3	Integrated Prgrm. & Risk Mgmt. Plan	11/96	1/97
4	Product Conceptual Design	1/97	5/97
5	Technology Demonstrator Design/Plan	3/97	5/97
6	Relevant Technology Development I	2/97	5/97
7	MIT / Draper Activity Coordination	5/97	9/97
8	Product Preliminary Design	9/97	12/97
9	Relevant Technology Development II	9/97	4/98
10	Tech. Demonstrator Construction	1/97	4/98
11	Technology Demonstrator	4/98	5/98
12	Final Report	4/98	6/98

APPROACH

The project plan shown in Figure #1 includes all the relevant end-to-end processes necessary to develop and demonstrate a system concept of national significance. In particular the project will define multiple system concepts, provide objective market assessments of each concept, select one system concept, develop critical technologies, design and develop a prototype, and demonstrate key system capabilities. Students and faculty from two departments and three graduate degree programs in the MIT School of Engineering will participate. Teams consisting of students, faculty and cognizant engineers from both Draper and Lincoln Laboratories, will be the primary organizational units through which the project will be executed. The project will include a five member student group from the Master of Engineering Program (MEng) in Aeronautics and Astronautics. It will also include five Master of Science (SM) students, appropriately chosen from either Aeronautics and Astronautics or Electrical Engineering. A few undergraduate students, supported through the Undergraduate Research Opportunity Program (UROP), will be participants as well. Faculty from both departments, and Draper and Lincoln

engineers will serve as both team members and academic advisors for the MEng, SM and UROP students.

The project plan spans a two year period from July 1996 through June 1998. July and August of 1996 will be a period of data gathering and capability assessment. During the first term of the 1996/97 academic year multiple concepts will be defined and analyzed, both in terms of feasibility and national importance. During the January Independent Activities Period (IAP) an intensive process of risk assessment, planning and documentation will be pursued; leading to a definitive plan and schedule for the remaining 1.5 year project period. From February 1997 through January 1998 the major system design activity will be pursued. From January through May of 1998 the system demonstration(s) will be developed culminating in a final design review. Finally, the month of June 1998 will be used to create an integrated final report.

The two groups of graduate students will play somewhat different roles in the project, according to their designated degree goals. The MEng program is design-oriented and focuses on system engineering. It requires students to successfully complete a significant design effort during the time period from January through May. For MEng students participating in this program, the project proposed here will be the focus of that design effort. Furthermore, since the MEng program is nominally completed in nine months, the program plan includes two groups of MEng student participants, one for the academic year 1996/97 and a second for 1997/98. Conversely, since the MS programs in both Aeronautics and Astronautics and Electrical Engineering are directed toward research, and typically span two or more years of effort, the proposed project plan assumes that the MS students will stay with the program for the full two years. Furthermore, these students and their faculty advisors will concentrate more on the critical technologies rather than the system aspects of the project. However, the Aerospace Product Design course, which is required for all MEng students, will be a requirement for all MS students participating in the program as well. The methods and tools developed in that course include a collection of integrative mechanisms which all participating students will need to ensure the project's success.

Figure #2 is another diagram of the proposed program plan, which provides another view or perspective of the planned phases and deliverables. As shown, the project will commence in the summer of 1996 with efforts to gather information on national priorities, identify Draper and Lincoln capabilities and facilities, and coordinate the complementary activity at Draper. During the fall semester 1996 all students will be enrolled in the Aerospace Product Design course which emphasizes the methods and tools for orderly and effective concept development. Also, in this same time period, a series of teams will be organized to define and study a series of possible system concepts. For each potential system concept a set of primary requirements and necessary technologies will be identified, along with a market assessment for the concept. At the end of the semester a single system concept will be chosen for development. During (IAP) a functional analysis and technology

assessment will be developed for the chosen system, leading to a thorough Requirements Review at the end of IAP. During the 1997 spring semester concentrated parallel efforts in conceptual design and technology development will be executed along with the development of a detailed demonstration plan. A concept design review will mark the end of the spring semester. MEng theses will also be available at this point in time. During the summer of 1997 the system design will be further developed and plans refined for the academic year 1997/98. A new group of MEng students will enter the program in the fall of 1997, at which point the project will be initiating the preliminary design of the system, along with further technology development. A Preliminary Design Review will be held at the end of the fall term, in preparation for construction of the system demonstrator. IAP and the spring term of 1998 will see an intense period of construction, integration and testing of the system demonstrator. Actual demonstration is planned for the end of the spring term, followed by a final design review and documentation in the form of both MEng and SM theses.

The concentrated team effort envisioned for the project will require coordination. Weekly meetings will be an integral part of the team development approach. MIT, Draper and Lincoln participants will be included, as appropriate, in these meetings. Particular care and attention will be given to the process of coordinating the parallel developments of the system and supporting technology.

PROGRESS

New Project Start

BIBLIOGRAPHY

Boppe, C. W.; "Aerospace Product Design: A New Graduate Subject For Practice-Oriented Degree Programs at MIT," Draft Paper Planned for AIAA 35th Aerospace Sciences Meeting.

MIT/Draper Technology Dvmt. Partnership
Process Elements & Relationships

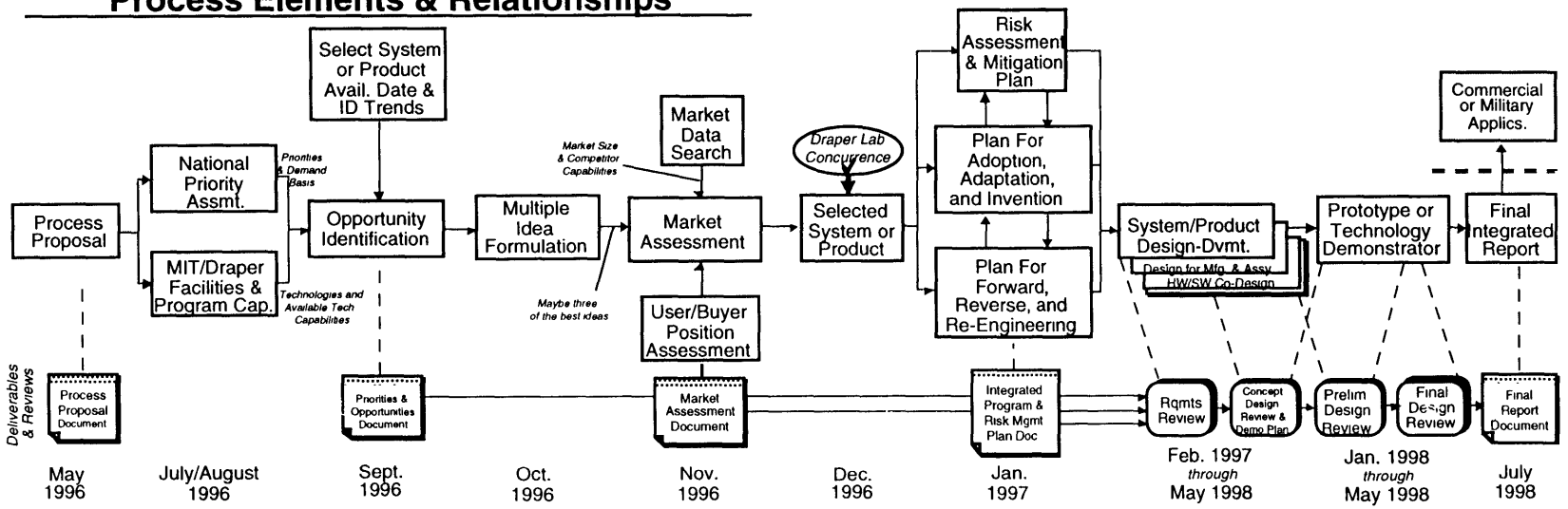

Figure #2

MIT/Draper Tech. Dvmt. Partnership
Proposed Time Blocks, Activities & Milestones

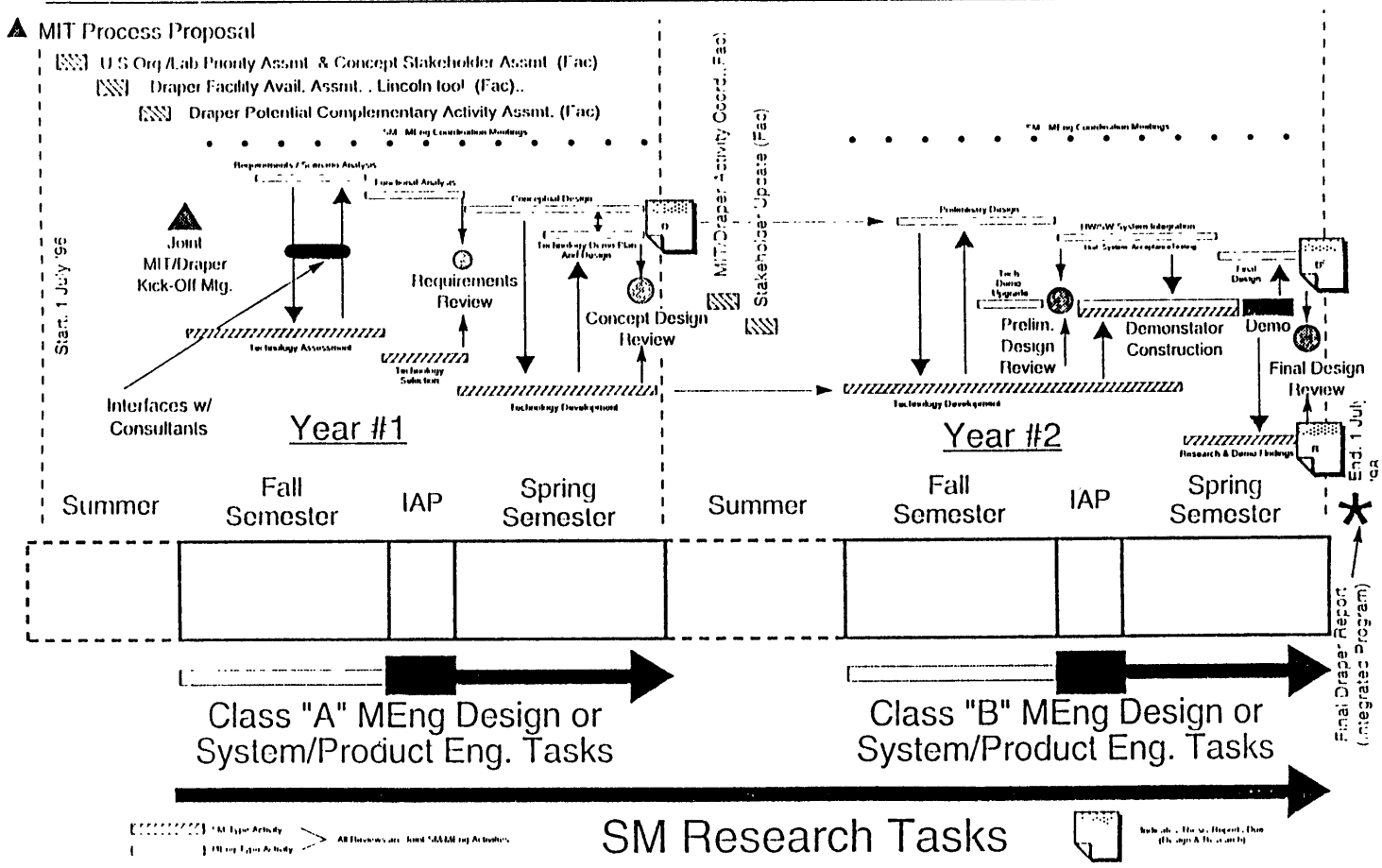

Needs Structure Candidate, 24 July '96

Source: National Critical Technologies List, Whitehouse... Mar. '95

Note: NCTL used to synthesize critical needs "bins"

U.S. National Security & Economic Prosperity

CRITICAL NEEDS BINS

1	2	3	4	5	6	7
Energy Efficiency & Independence	Environmental Quality	Information Access & Communication Effectiveness	Health Care & Agricultural Efficiency	Advanced Manufacturing	Improved Materials	Advanced Transportation
Sub - Bins						
• Adv. Building Efficiency	• Monitoring & Assessment	• Adv. Components	• Adv. Biotechnology	• Robotics & Automation	• Alloys, ceramics, composites, etc.	• Aircraft & Surface Vehicle Aerodyn.
• Adv. Prop. Systems	• Remediation & Restoration	• Data Comp. & Routing	• Medical Devices & Equipment	• Adv. Processes	• Infrastructure	• Adv. Avionics & Controls
• Storage, Distribution, Conditioning, and Transmission	• Pollution Avoidance & Control	• Computer Interop. & Parallel Processing	• Africultural Production Efficiency	• Semiconductor & microdevice mfg.	• Stealth	• Adv. Propulsion & Power Systems
• Advanced energy generation		• Information Mgmt.	• Food Supply Safety		• Superconductors	• Systems Integration
		• Intelligent Complex Adaptive Systems	• Adv. Human-Machine Interface		• Aircraft Structures	• Adv. Human Factors & Life Support
		• Sensors				
		• Software & Toolkits				

Appendix C Project Selection Matrix

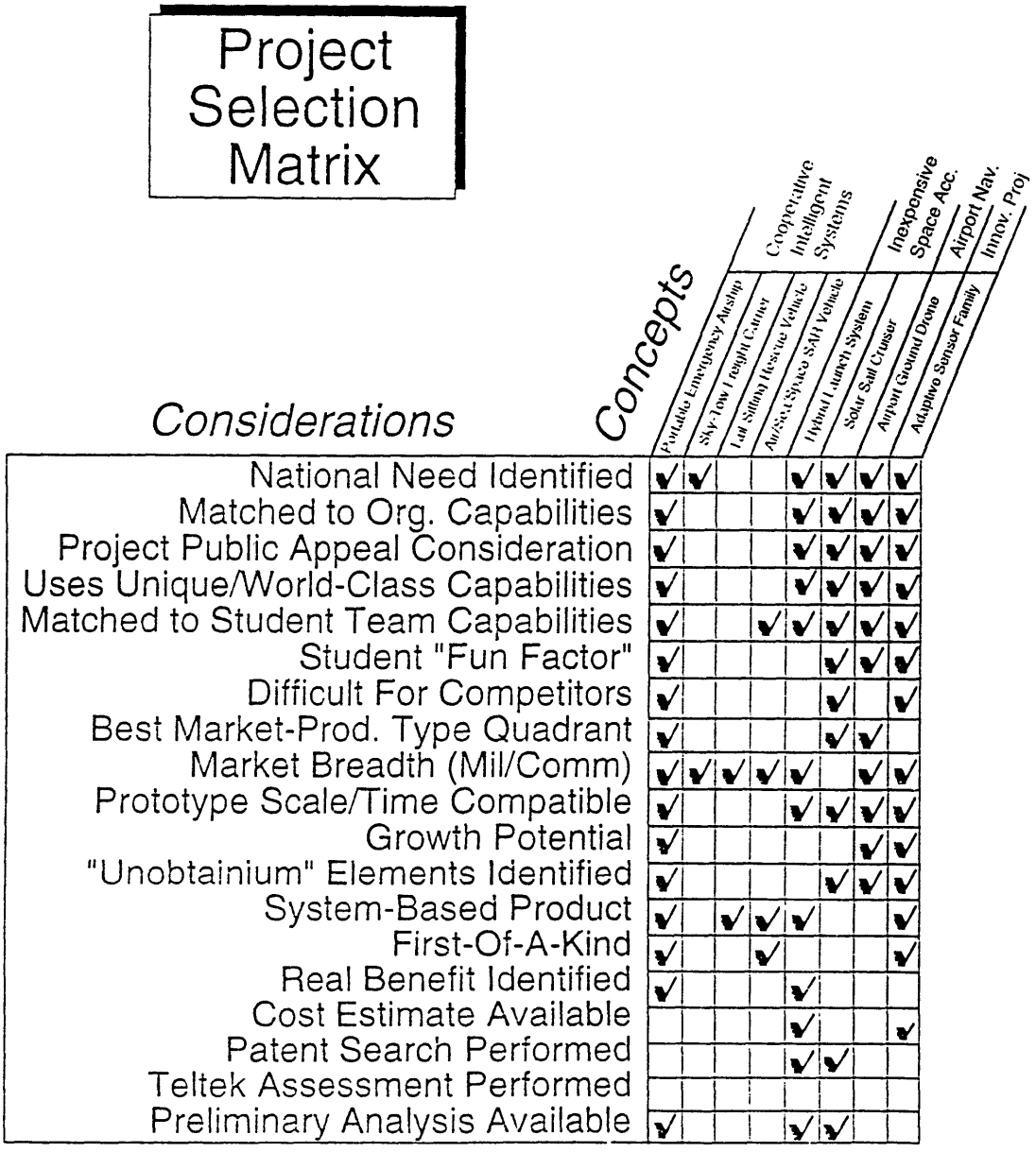

Appendix D Solar Sail Demonstrator Market Assessment

by Joshua Bernstein and David Iranzo-Greus

D.1 Motivation

Space exploration has been enjoying increased popularity recently both for commercial and scientific reasons. A major obstacle in space utilization, however, is propulsion. Space propulsion systems are often complex and expensive. While chemical rockets have proved to be reliable, there are missions where the fuel requirements for the rockets become prohibitive. Alternatives such as ion propulsion and nuclear rockets have been proposed, but each of these options face significant technological and political challenges. Other alternatives are needed.

Solar sail technology offers such an alternative. Initial spacecraft designs based on sails suggest that such a means of propulsion would be relatively inexpensive, and, for a variety of missions, offers advantages over other methods of travel (see references 1 and 2).

D.2 Background

The idea of a solar sail is not an entirely new one. The theory of solar sailing has been around for quite some time, but an actual solar sail vehicle has *never been built and deployed.* This failure of theory to result in hardware can be traced to a variety of setbacks, some technical, many political. At the present time, however, there appears to be considerable interest in the technology at NASA, and the space agency has expressed some interest in potentially assisting with this project, were it pursued further by the design team.

D.3 Introductory Description

The solar sail demonstrator is intended to be a small, simple spacecraft to confirm the principles of solar sailing and to prove the enabling technologies that must be brought together to successfully operate a solar sailing vessel. It is proposed that the vehicle be boosted to geosynchronous orbit, where it would deploy its sail. The vessel would then control itself autonomously, spiraling away from the Earth under the propulsive force provided by photons from the sun striking the sail. If the mission were properly timed, this spiraling trajectory would allow for a mission to the moon (see Figure D4).

As shown in Figure D1, the vehicle itself consists of three principal elements: the sail, the rigging, and the payload. Please note that this figure is simply a schematic, and may not necessarily represent the configuration of the final vehicle. The sail is constructed of a thin, light-weight, highly reflective material. Its purpose is to reflect photons that are streaming off the sun, and, in the process, provide a means of momentum transfer to the vehicle for propulsion. The sail is supported by a rigid structure, but the deployment of a mechanical structure of the necessary size would be extremely difficult (and is one of the reasons a sail has yet to be flown). Instead it is proposed that the sail's structure consist of a rigidizing inflatable structure. By its very nature, the inflatable structure would also provide a means for sail deployment.

The rigging is used to control the configuration of the sail, i.e., its angle relative to the sun. By changing the angle at which photons strike the sail, the ship can be maneuvered. For purposes of illustration, the rigging is depicted as a system of cables. On an actual vehicle, however, the rigging would most likely *not* be a mechanical system, but would instead be highly integrated with the sail itself. At present, three examples of such integrated systems have been discussed: solar cells, liquid crystals, and piezoelectric. If the sail were covered (at least partially) by solar cells, the vehicle could be controlled by varying the amount of power drawn from the cells over the sail's surface. By increasing or decreasing the amount of power produced by a given region of cells, the reflectivity of the sail in that region could be varied, changing the propulsive force on the sail. Similarly, by covering the sail with a thin layer of material which include liquid crystal, the sail's reflectivity could be modified in any given region. Finally, piezoelectric material could be included in the sail's construction. By providing an electric current to the piezoelectric material, it could be used to physically "deform" the sail's shape, and thereby provide control.

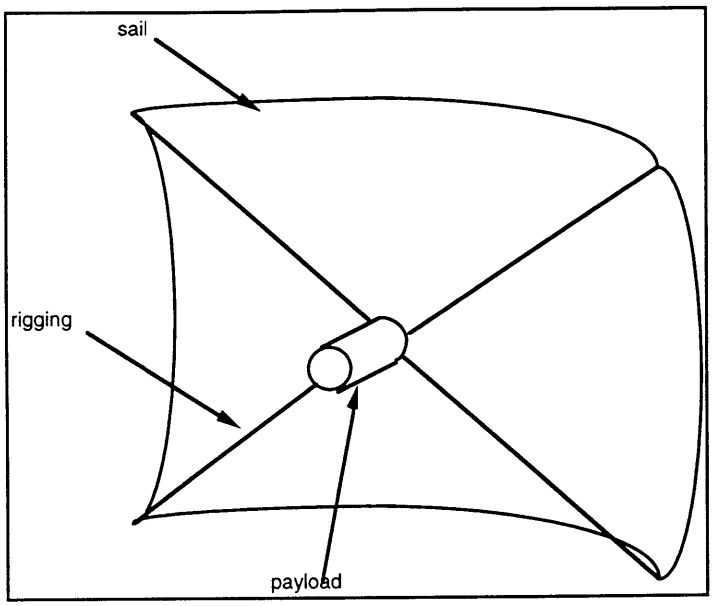

Figure D1: System Schematic

The final component of the vehicle is the payload, shown in greater detail in Figure D2. As previously stated, the intent of the demonstrator is to maintain a simple overall vehicle design, allowing for the use of a small sail. The payload, therefore, includes a sail control system (a means of controlling the systems discussed above); a power distribution system; guidance, navigation, and control; a sensor (such as a video camera); and communications equipment.

As previously noted, the demonstrator is intended to be an autonomous spacecraft. Rather than requiring a small army of ground controllers to monitor and control the spacecraft, this vehicle is intended to require no human intervention, except in the case of a severe problem. This feature of the design is in fact dictated by the use of the sail, which would be quite difficult to control effectively from the ground.

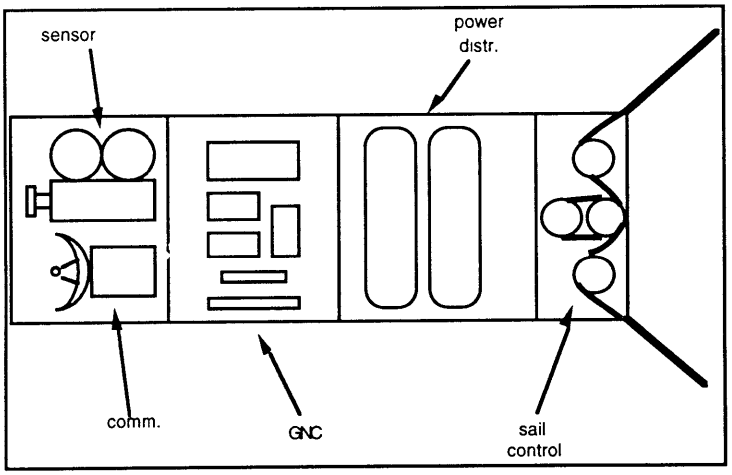

Figure D2: Payload Schematic

D.4 Benefits to Charles Stark Draper Laboratory

Draper would benefit from involving itself in this project. The Laboratory is already well respected in the fields of navigation, guidance, control, micromechanical devices, and equipment packaging. The development of a solar sail demonstrator would make use of all of these skills. While other companies are working on the structure of the sailing spacecraft, there appears to be a gap between such "mechanical"

design and the design of the necessary computer systems and their associated packaging for the vehicles. Draper, with its skill and experience in these fields, could readily step in to fill this gap.

While Draper would most likely not manufacture solar sails themselves, after working on the demonstrator, Draper would be firmly established as the leader in solar sail control. Draper Labs would then gain access into the space technology market, a market with a tremendous amount of growth potential. Once Draper has solidified its reputation with solar sail control systems, it is not unreasonable to imagine the Lab broadening its market share by applying its skills in other areas of spacecraft control.

The Laboratory has in fact been involved in several design efforts for micro-spacecraft, but none of these projects has resulting in flying a vehicle. This project would present Draper with the opportunity to do so, enhancing its market standing in the field of micro-spacecraft. Draper therefore stands to not only gain access to a newly emerging technology but to the growing market of spacecraft design and development.

D.5 Preliminary Analysis: The Basic Principles

A terrestrial sailboat uses the combination of wind and water for propulsion and steering. The solar sail equivalents are light (photons) and gravity, respectively.

Photons have momentum proportional to their wavelength. This momentum can be used to exert a force on a mirror: this is the basic principle of solar sailing (see Figure D3). Using Newton's Second Law, the solar pressure on a planar surface is:

$$P = \frac{2W\cos^2\alpha}{cR^2} = 9.126\times10^{-6}\cos^2\alpha \qquad \text{(at 1 Astronomical Unit)}$$

where P is the solar pressure in Pa, W is the power intensity (1368 W/m^2 at 1 AU from the Sun), c is the speed of light, R is the distance to the Sun in AU, and α is the angle between the surface normal and the line from the sail to the Sun [Ref. 2].

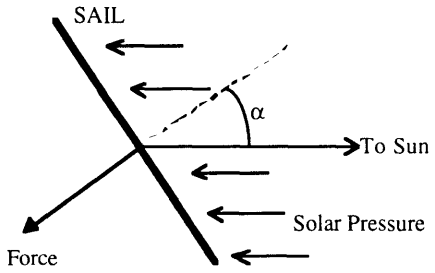

Figure D3: Solar Sailing Basics

The force of gravity is essential to guide a solar sail (otherwise, it would just be pushed away from the source of light). An advantage of solar sails is their ability to achieve trajectories out of the plane of the ecliptic (a very expensive maneuver with chemical rockets), simply by reorienting the sail.

D.6 Sail Design

The solar sail consists of a large lightweight mirror. The shape of the sail could be chosen from a variety of options: square, circular, annular, etc. Each design would require a different control system. The sail loading, σ, is defined as the total mass of the spacecraft divided by the area of the sail. With the current state of technology, a solar sail with a loading of 5 g/m^2 could be achieved (see Ref. 2 in Section D.11). The larger the sail loading, the longer the time required to reach a specific point. Hence, reducing the payload weight or increasing the sail size will reduce the travel time.

In the preliminary calculations (see Figure D4), the weight of the sail was assumed to be 8 grams per square meter, including the structure, based on the estimates in reference 1. In the vicinity of Earth, with a payload of 80 kg, the resulting acceleration is 0.5 mm/s^2. The thickness of the sail could be as low as 8 microns, which would produce a volume of only 0.04 cubic meters.

D.7 The Mission

In order to demonstrate the feasibility of solar sailing, the spacecraft would be launched as a secondary payload on a conventional expendable launcher or by the Space Shuttle. The large surface area of the sail would produce a fast decay in a low-Earth orbit due to atmospheric drag. Therefore, the spacecraft would be inserted into a geostationary orbit, where the deployment of the sail would take place.

From geostationary orbit (GEO), the sail would have an unobstructed view of the Sun almost permanently. The spacecraft would begin accelerating due to the solar pressure, rising to increasing orbital altitudes. After a few months of travel (depending on the size of the sail and the weight of the payload), the spacecraft could reach the Moon or even acquire escape velocity and travel out into the Solar system. Figure D4 shows an example of a possible mission.

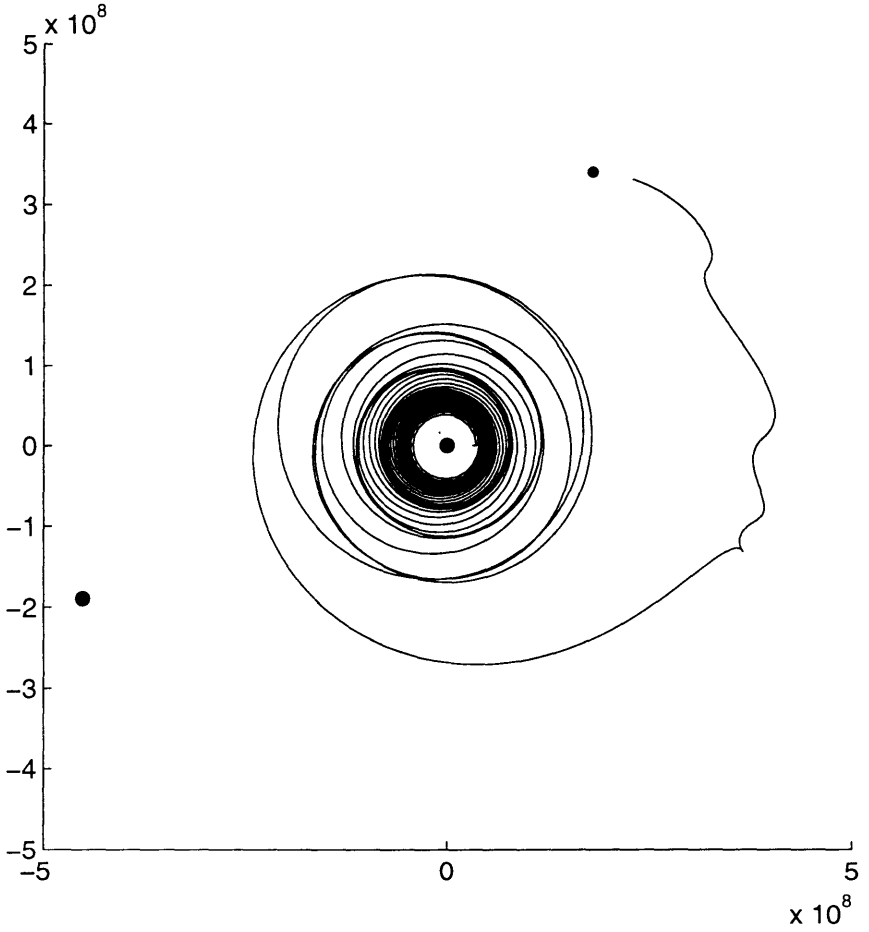

Figure D4: Numerical simulation of the trajectory of a Solar Sail Spacecraft from GEO to the Moon. Calculations based on a 70x70-meter sail (8 grams per square meter) and a payload of 80 kg.

D.8 The Technical Challenges

There are several technical challenges that would have to be met for the success of the project. These challenges include: design for cost (given the limited resources), deployment of a large space structure, control of the sail to achieve an optimum trajectory, and design of an autonomous spacecraft.

Given the high costs of launching a spacecraft and the limited funds available, an important driver for the project would be the design for cost. Using the experience of such programs as the NEAR (Near Earth Asteroid Rendezvous) Spacecraft from APL and other NASA New Millennium programs, and Draper experience in micro-spacecraft design, the solar sail could be built with a small budget. Where possible off-the-shelf components would be integrated into the spacecraft's design.

A major technical problem is the deployment of a large structure in the vacuum and zero-gravity conditions of space. Related to this deployment is the packaging of the structure so that it could be inserted into orbit by conventional means. An intensive study of the dynamics of flexible structures would be required, but recent experiments onboard the Space Shuttle have shown that flexible structures can be deployed.

In order to avoid the braking effects of solar pressure when traveling towards the Sun, the sail would have to rotate. In general, optimal trajectories could only be achieved by frequent rotations of the sail. The control of the large structure would represent a major challenge that would require imaginative solutions. These solutions could range from the use of microthrusters (which would provide enough torque given the large moment arms), to the construction of the sail as a series of vanes that would rotate separately. This problem also requires a significant software development effort to control the sail.

The design of an autonomous intelligent spacecraft would represent a first-of-a-kind project, since all current spacecraft are controlled from ground centers. The spacecraft would carry an onboard computer that would direct the control system of the sail, based on the reading from various sensors.

D.9 Ground Testing Alternative

While the team's preference is to conduct a space-based demonstration of the solar sail vessel, it is recognized that there are significant challenges. In the event that it becomes clear that the team will be unable to conduct a space-based test for technical or other reasons (difficulty in obtaining space on a launcher, for example), it would be possible to conduct a ground-based demonstration. This demonstration would verify the design and operation of a miniature inflation device for the inflatable structure, prove the packaging approach, and validate the overall integration of the spacecraft's systems. Such a ground test would then provide valuable data for future efforts on a space-based demonstration.

D.10 Market Assessment

Several potential markets have been identified by the team at this point. These sources are based on telephone interviews conducted by the team with representatives from NASA JPL, private industry, the World Space Foundation, the Planetary Society, and the University of Kent at Canterbury [see note 3].

As to be expected, the short term market for solar sails is dominated by NASA. Within the next five years, however, the National Oceanographic and Atmospheric Administration would like to place a satellite in the Sun-Earth Lagrangian point (L1) to provide additional warning time for solar storms. Since L1 is an unstable point and the satellite would require a long operating life, the only propulsion system that would appear practical is a solar sail. Over the next three to four years there is the potential for several additional vehicles that could make use of solar sail technology. Moving further ahead into the future, NASA is considering such a propulsion system for interplanetary cargo transport, in support of a manned mission to Mars, for example. Additionally, in the spirit of "faster, cheaper, better," solar sails can be an attractive alternative to chemical rockets for interplanetary space exploration, especially missions which require the vehicle to maneuver out of the ecliptic plane.

The design team has also attempted to identify other, less "traditional" markets. One proposed application would be for highly maneuverable satellites in geosynchronous orbit. By attaching a sail to such satellites, the spacecraft could maneuver an unlimited number of times, extending their service lives over similar satellites with chemical propulsion systems. Another potential application might be amusement parks. Several sails could be placed in high orbit above the Earth. Visitors could then be allowed to maneuver the sail in space (while the spacecraft's onboard computers prevented the visitor from sending the sail into the depths of space). The visitor would then be provided with a video sent back from the spacecraft, showing what he commanded the spacecraft to do.

It should be noted that since no solar sail has never actually been used, all of the benefits of this method of propulsion have yet to be explored. It is reasonable, therefore, to expect the market for solar sails to grow as the technology develops. By being the first to fly a demonstrator, MIT and Draper would be able to position themselves as leaders in this market.

A market assessment of this project would not be complete without also considering the field of miniature spacecraft. The idea of "microsats" is only just beginning to develop, but it is clear that such small spacecraft will have applications ranging from telecommunications constellations to interplanetary exploration [ref. 4]. Since the solar sail demonstrator would necessarily include a small satellite-type vehicle, Draper would gain valuable technical and market experience in this field as well. This

development work would also provide an excellent follow-on to work already done for the micro-satellite engineering lead project completed last June. While that project resulted in valuable design experience, it did not include the construction of "flyable" hardware. The solar sail demonstrator would build on the design experience of this past lead project, taking Draper to the next step of producing actual hardware components and integrating them into a spacecraft.

In conclusion, the solar sail represents a space technology which is ripe for development. By participating in such a project, MIT and Draper Laboratories would broaden their access to the developing space technology market, establishing themselves as leaders in the specific fields of solar sails and micro-spacecraft design and development.

D.11 Endnotes and References

1 - Friedman, Louis, *Starsailing, Solar Sails and Interstellar Travel*, John Wiley & Sons, New York NY, 1988.

2 - Wright, Jerome L., *Space Sailing*, Gordon and Breach Science Publishers, Philadelphia PA, 1992.

3 - This section is based on extensive telephone interviews with the following:
James Garry, University of Kent at Canterbury, November 6, 1996.
Emerson Labambard, World Space Federation, November 12, 1996.
Lou Friedman, The Planetary Society, November 12, 1996.
Costa Cassapakis, L'Garde, Incorporated, November 14 and 18, 1996.
Arthur Chmielewski, NASA Jet Propulsion Laboratory, Inflatable Structures Group, November 18, 1996. The statement of potential NASA funding was made by Arthur Chmielewski.
Guy Man, NASA Jet Propulsion Laboratory, Autonomous Spacecraft Group, November 19, 1996.
Charles Garner, NASA Jet Propulsion Laboratory, Solar Sail Group, December 5, 1996.
Bruce MacKinzie, Charles Stark Draper Laboratories, December 9, 1996.
Warren Fitzgerald, Charles Stark Draper Laboratories, December 9, 1996.
Steve Cropnik, Charles Stark Draper Laboratories, December 9, 1996.

4 - Robinson, Ernest Y., et. al. "Big Benefits from Tiny Technologies." Aerospace America, October, 1996. pp.38-43.

D.12 MATLAB Programs

```
%       Solar Sail Earth-Moon Trajectory model
%       by David Iranzo.

w = 2.664e-6;
Me = 5.974e24;
Mm = 7.3483e22;
G = 6.67259e-11;
dist = 3.844e8;  % Earth-Moon distance
mu = Me/(Me+Mm);
tol = 1e-2;

angul = 0*pi/180;
r0 = 3.6e7;
v0 = sqrt(G*Me/r0);
y0 = [-(1-mu)*dist+r0*cos(angul)  r0*sin(angul)
0 -v0*sin(angul) v0*cos(angul) 0];

h = y0(1:3)';
Y = h;
figure
plot3(0,0,0,'w:')
hold on
axis square
axis([-5e8 5e8 -5e8 5e8 -5e8 5e8]);
view(2)
line( ...
        'color','w',...
        'linestyle','.',...
        'markersize',20,...
        'erase','xor',...
        'xdata',0,'ydata',0,'zdata',0);
moon = line( ...
        'color','w',...
        'linestyle','.',...
        'markersize',15,...
        'erase','xor',...
        'xdata',[],'ydata',[],'zdata',[]);
sun = line( ...
        'color','w',...
        'linestyle','.',...
        'markersize',20,...
        'erase','xor',...
        'xdata',[],'ydata',[],'zdata',[]);
trail = line( ...
```

```
        'color','w',...
        'linestyle','-',...
        'erase','none',...
        'xdata',[],'ydata',[],'zdata',[]);
tail=line( ...
        'color','r', ...
        'linestyle','-', ...
        'erase','none', ...
        'xdata',[],'ydata',[],'zdata',[]);

until = 500;
for i=1:until,
        t0 = (i-1)*60000;
        tf = 60000*i;
        if i~=1,
                y0 = [y(ti,1) y(ti,2) y(ti,3)
y(ti,4) y(ti,5) y(ti,6)];
        end;
        [t,y] = ode23('trajfuns',t0,tf,y0,tol);
        k = y(:,(1:3));
        h = zeros(length(t),3);
        k(:,1) = k(:,1)+(1-mu)*dist;
        h(:,1)=(k(:,1).*cos(w*t))-
(k(:,2).*sin(w*t));
        h(:,2)=(k(:,1).*sin(w*t))+(k(:,2).*cos(w
*t));
      Y = [Y h'];

set(tail,'xdata',Y(1,1:length(Y)),'ydata',Y(2,1:len
gth(Y)),'zdata',Y(3,1:length(Y)))
        set(trail,'xdata',dist*cos(w*t0),'ydata',dis
t*sin(w*t0),'zdata',0)
        set(moon,'xdata',dist*cos(w*t0),'ydata',d
ist*sin(w*t0),'zdata',0)
        set(sun,'xdata',4.9e8*cos(pi/2+t0*2e-
7),'ydata',4.9e8*sin(pi/2+t0*2e-7),'zdata',0)
      drawnow;
        ti = length(t);
end;
tf
-------------------------------------------------------
%       Solar Sail Earth-Moon Trajectory model
%       by David Iranzo-Greus.

function yp = trajfuns(t,y)
        global mu dist area;
        Me = 5.974e24;
        Mm = 7.3483e22;
        Re = 6.37812e6;
        Rm = 1.738e6;
        G = 6.67259e-11;
        w = 2.664e-6;
        dist = 3.844e8;
        k = G*(Me+Mm);
        mu = Me/(Me+Mm);
        x1 = -(1-mu)*dist;
        y1 = 0;
        z1 = 0;
        x2 = mu*dist;
        y2 = 0;
        z2 = 0;
        r1 = sqrt((x1-y(1))^2+(y1-y(2))^2+(z1-
y(3))^2);
        r2 = sqrt((x2-y(1))^2+(y2-y(2))^2+(z2-
y(3))^2);
        area = 70^2;
        mass = 0.008*area + 80;
        zeta = pi/2+t*(2e-7);
        sunx = cos(zeta);
        suny = sin(zeta);
        sunz = 0;

        yp(1) = y(4);
        yp(2) = y(5);
        yp(3) = y(6);
        yp(4) = 2*w*y(5)+w^2*y(1)-
k*(mu*(y(1)-x1)/r1^3+(1-mu)*(y(1)-
x2)/r2^3)+thrustsa(y(1),y(2),y(3),y(4),y(5),y(6),s
unx)/mass;
        yp(5) = -2*w*y(4)+w^2*y(2)-
k*(mu*y(2)/r1^3+(1-
mu)*y(2)/r2^3)+thrustsa(y(1),y(2),y(3),y(5),y(4),
y(6),suny)/mass;
        yp(6) = -k*(mu*y(3)/r1^3+(1-
mu)*y(3)/r2^3)+thrustsa(y(1),y(2),y(3),y(6),y(4),
y(5),sunz)/mass;
-------------------------------------------------------
%       Solar Sail Solar Pressure Force Model
function th =
        thrustsa(x,y,z,velo1,velo2,velo3,sunfac)

        global zeta mu dist area;
        vproject =
        velo1/sqrt(velo1^2+velo2^2+velo3^2);
        th = -9.126e-6*area*sunfac;
        if vproject==0,
                th = 0;
        else
                if (th/vproject)<0,
                        th=0;
                end;
        end;
```

Appendix E Low-Cost Instrumented Surveillance Projectile (LISP): System Requirements

MIT / Draper Technology Development Partnership

Low-cost Instrumented Surveillance Projectile (LISP)

System Requirements
(Status: 2 January 1997)

• General System Functional Goals:

The non-lethal LISP system goal is to provide local theater commanders with rapid localized reconnaissance information that can be used in a timely manner as an aide to ensure mission objectives are secured. Launched from the sea or from land (see operational scenario), 5-inch or 155mm projectile launchers will be the basic interface for LISP operations. Ideally, LISP's surveillance objectives should be selectable just before launch, while LISP is en route, and during the system's flight data collection and/or targeting mode. Since LISPs are expendable - low cost will be an important design driver. While the primary functional objective is surveillance, LISP's secondary goal is to provide a temporary network of airborne relay stations that can be used for linked line-of-sight communications.

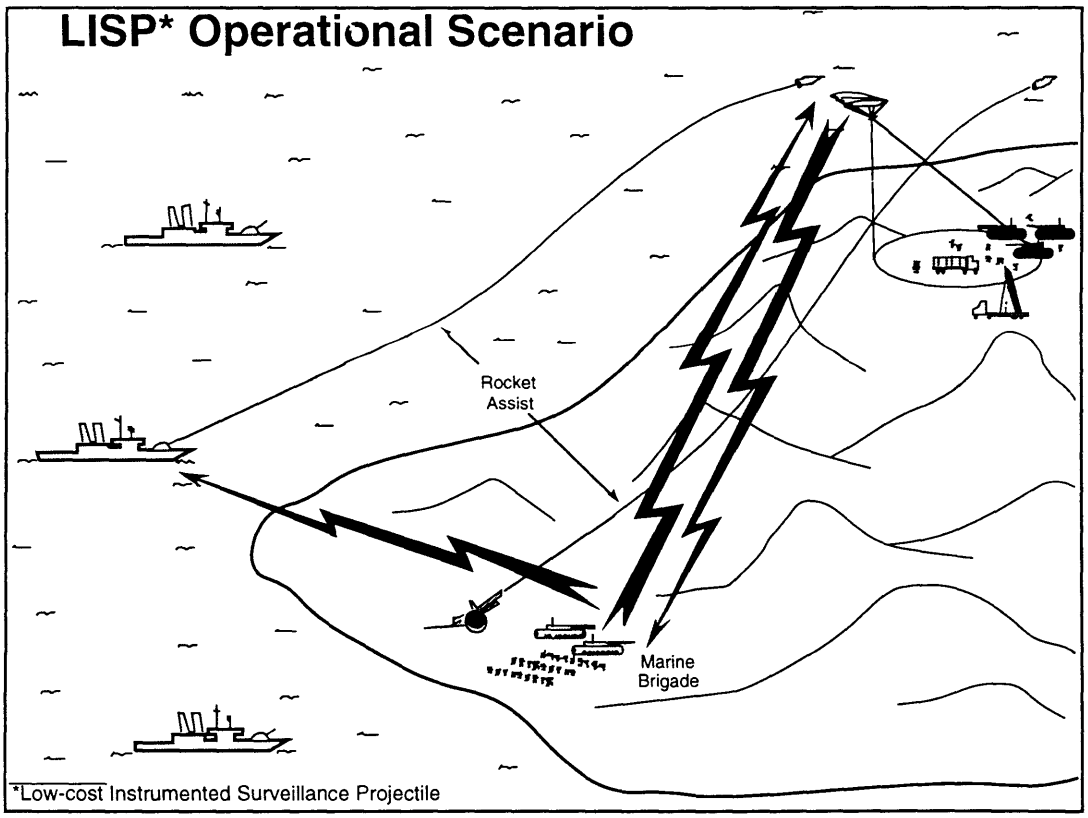

• Range:

70-200 miles from launcher using rocket-assisted projectiles.

• Time aloft after projectile delivery / operating time:

1 to 8-hours and this will depend to some extent on trades made between system performance, complexity, and cost. Operational time: 2-hours.

• Desired surveillance area:

To be determined as the typical "Area of Action" or operational area for a self-sustained Marine Brigade.

• Projectile diameter / length:

5-inch or 155mm diameters. Length will be consistent with existing projectiles in this class.

• Location accuracy:

Several meters.

• Sensor type:

Primary focus should be on an imaging camera.

• Self destruct mechanism:

Self destruct will ensure that no piece of the destroyed projectile will exceed the characteristics of an 8-oz can of cat food. For military operations - the flyer will also be designed to self destruct at the end of its useful mission.

• Acquisition cost target:

Conventional 5-inch and 155mm munitions cost approximately $800. Rocket-assisted projectiles in this class can cost $10,000. The expendable LISP (projectile, flyer, and sensor package) cost should be within the $20,000-$30,000 range in production.

• Information timing:

Near-real-time.

• Level of autonomy:

To be determined via system trades.

• Existing physical, political, or organizational constraints:

LISP must be inexpensive to ensure its use in local theater operations.... organic. Projectiles in this class spin at 250 Hz - so a slip obturator (launch shroud) of some type might be required to ensure "near-0" launch spin for LISP

• Environment:

Launch "g"s baseline - 10,000. However, "g"s will increase if trades suggest that the LISP system will result in an integrated projectile with weight less than that of conventional munitions.

• Shelf life:

Approximately 20-years with provisions for replacing batteries and expendables for flyer and communications at pre-determined intervals.

• Existing surveillance MOEs:

Not aware of any at this time. Check with potential customers once design project is underway.

• Covertness level:

The flyer sensor package is expected to be quite small. So an effort should be made to ensure that large flyer components like wings or rotating components like propellers and rotors are of suitable materials to ensure that low RADAR signatures are maintained. Visual and acoustic signatures must also be low.

• Reliability expectations:

90% availability. That is to say - one out of 10 LISPs might not perform as expected.

• Extensibility:

The primary extension of the LISP concept is to provide a temporary LOS communication network for relaying data and messages. Additional sensor applications, beyond static imaging, for all-weather operations (RADAR?) and chemical/biological sampling should be considered. Acoustic, IR, and motion sensors are also of interest. LISP variants should be adaptable to address civil and commercial needs providing that the system can be adapted to smaller launchers and possibly smaller projectile sizes.

• Prep. and launch time:

2 to 3-minutes

• Safety issues:

LISP will be stored in magazines along with conventional munitions. As such, it will have the same or better characteristics as munitions when exposed to mishandling, fire, or detonations.

• Special demonstration considerations:

LISP will be field tested at the Navy's Test Facility in Dahlgren, Virginia. For the field test, a 70+ mile range will not be required. In addition, it would be desirable to retrieve the test article and as such - no self-destruct mechanism will be assessed during the planned system demonstration period.

Some additional information

• Picatinny Arsenal has tested a $5000 hockey-puck sized imaging camera that can withstand 21,000 "g"s. This Xybion system includes a 50-mb data transmitter and base station for receiving the image.

• Draper's Judy Miller can provide UAV scenario trajectories for our use. In addition, Don Gustavson has the ability to simulate any projectile trajectory.

• Draper's Jack Stevie and Bob Polutchko have information on Draper's Parafoil designs.

• Draper's Dick Phillips has background information on triangulating to obtain range using GPS during a position fly-by.

• There is data available for a very small Wankel Engine that might have application to LISP.

• Draper's Paul Motyka and John Dowdle have information on gun barrel environments.

Appendix F N^2 Diagram: Subsystem Interfaces

by Cory Hallam

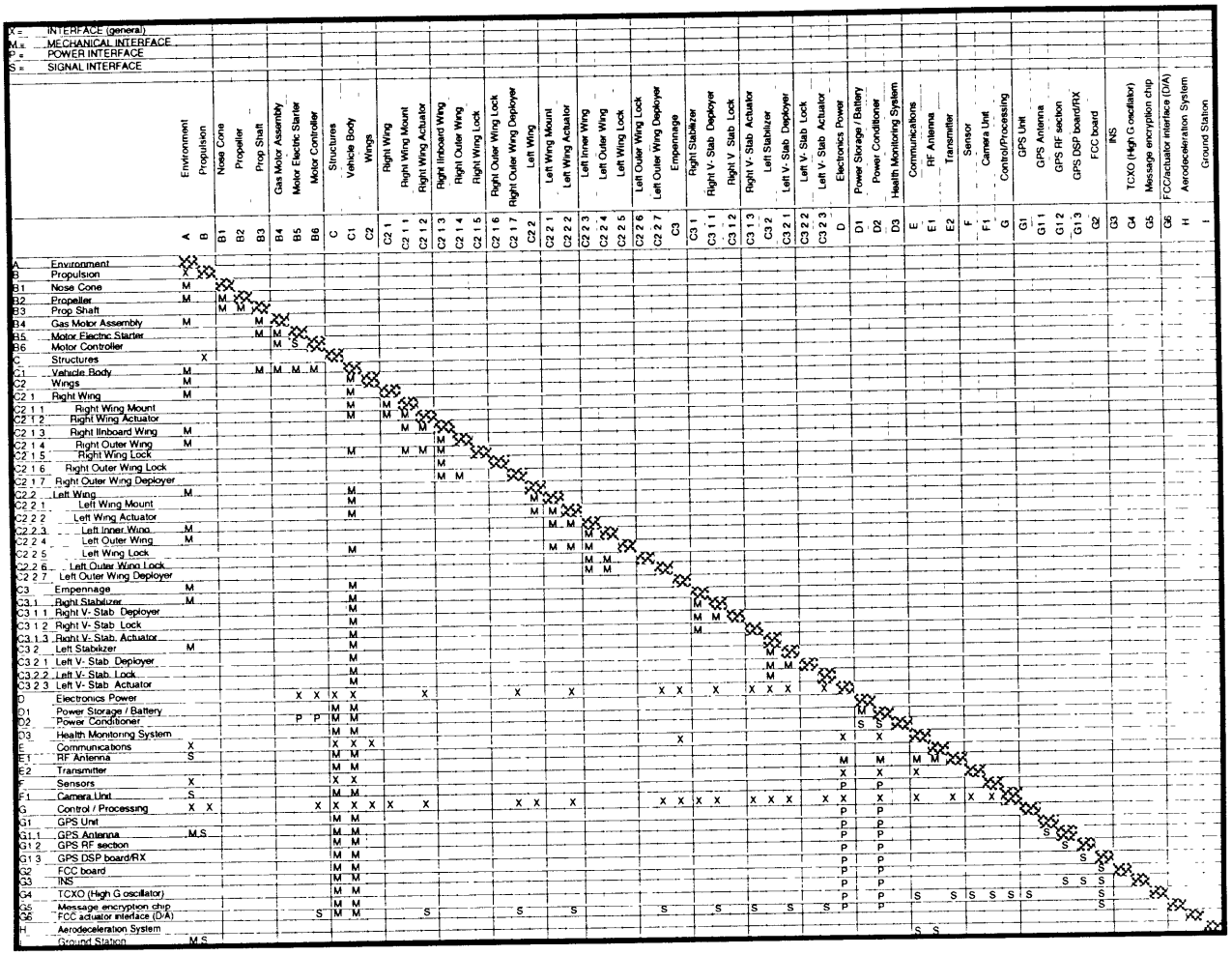

Appendix G Team Tasks and Schedule

by Joshua Bernstein

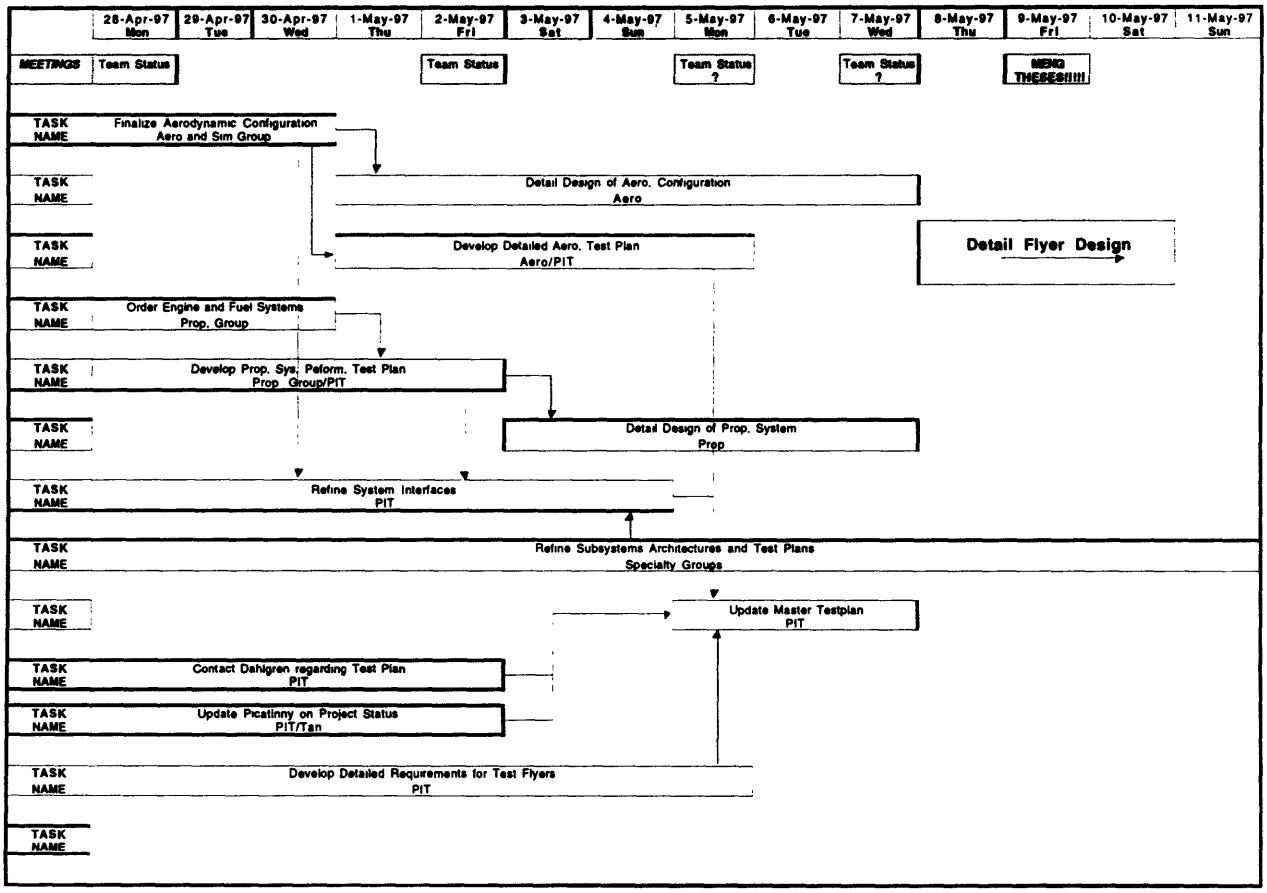

Appendix H Concept Downselect Tables

Composition by Joshua Bernstein, calculations by all team members.

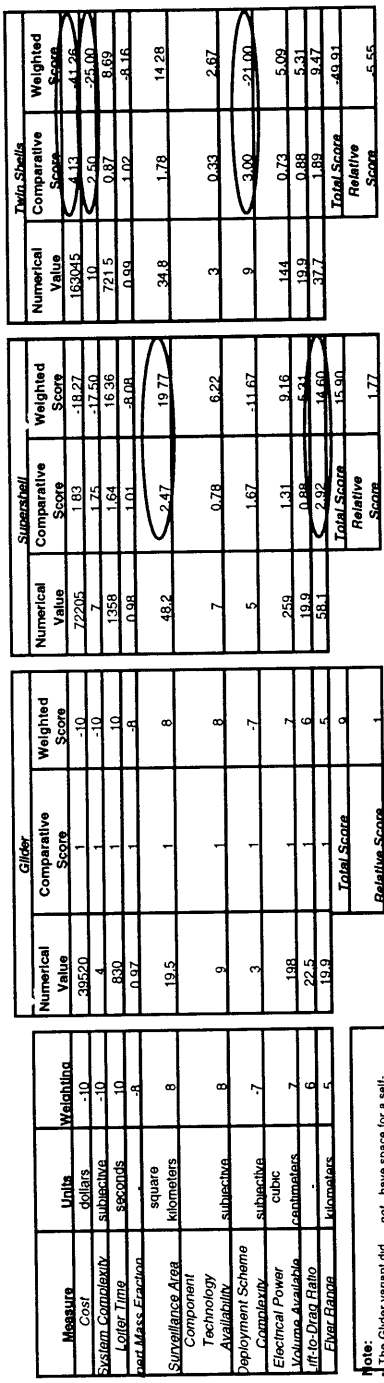

Measure	Units	Weighting
Cost	dollars	-10
System Complexity	subjective	-10
Loiter Time	seconds	10
part Mass Fraction	-	-8
Surveillance Area	square kilometers	8
Component Technology Availability	subjective	8
Deployment Scheme Complexity	subjective	-7
Electrical Power	cubic centimeters	7
Volume Available	-	6
Lift-to-Drag Ratio	kilometers	5
Flyer Range		

Glider			
Numerical Value	Comparative Score	Weighted Score	
39520	1	-10	
4	1	-10	
830	1	10	
0.97	1	-8	
19.5	1	8	
9	1	8	
3	1	-7	
198	1	7	
22.5	1	6	
19.9	1	5	
	Total Score	9	
	Relative Score	1	

Supershell		
Numerical Value	Comparative Score	Weighted Score
72205	1.83	-18.27
7	1.75	-17.50
1358	1.64	16.36
0.98	1.01	-8.08
48.2	2.47	19.77
7	0.78	6.22
5	1.67	-11.67
259	1.31	9.16
19.9	0.88	5.31
58.1	2.92	14.60
	Total Score	15.90
	Relative Score	1.77

Twin Shells		
Numerical Value	Comparative Score	Weighted Score
163045	4.13	41.26
10	2.50	-25.00
721.5	0.87	8.69
0.99	1.02	-8.16
34.8	1.78	14.28
3	0.33	2.67
9	3.00	21.00
144	0.73	5.09
19.9	0.88	5.31
37.7	1.69	9.47
	Total Score	49.91
	Relative Score	5.55

Note:

- The Glider variant did *not* have space for a self-destruct mechanism, so such a device was left out. This omission means that the design does *NOT meet all of the requirements for the system*

Appendix I Software Input Codes

```
% ballisticdrag.m
% Calculation of ballistic drag coefficient
% by C. Hallam and D. Iranzo, 1997

function Cd=ballisticdrag(V,altitude)

n=1;
gamma=1.4;
R=287;
To=288.16;
Temp=(1-.0065/To*altitude)*To;
Mach=V/sqrt(gamma*R*Temp);

CDB=[.01 .7 .8 .9 1 1.05 1.1 1.5 1.75 2 2.5 3 3.5 4
4.5 5 100; .1215 .1215 .1215 .1450 .325 .375 .38
.385 .335 .305 .285 .25 .25 .25 .25 .25 .25];

while Mach>CDB(1,n),
        n=n+1;
end

Cd=CDB(2,n-1)+(CDB(2,n)-CDB(2,n-1))*((Mach-
CDB(1,n-1))/(CDB(1,n)-CDB(1,n-1)));

=====================================
% aero.m
% Calculation of WASP trajectories
% by D. Iranzo and C. Hallam, 1997

m=5:10:55;  % Varying masses

for step=1:6,
        [t,y]=ode23('trajfunb',0,125,[0,sqrt(20e6/m(ste
p))*cos(45*pi/180),0,sqrt(20e6/m(step))*sin(45*pi/180
),m(step)],1e-5);
        figure(1)
        axis([0,25,0,8])
        plot(y(:,1)/1000,y(:,3)/1000)
        hold on
        figure(2)
        axis([0,140,0,1200])
        plot(y(:,1)/1000,sqrt(y(:,2).^2+y(:,4).^2))
        hold on
        figure(3)
        axis([0,35,0,8])
        plot(t/60,y(:,3)/1000)
        hold on
        cou=1;
        while y(cou,3)<y(cou+1,3),
                cou=cou+1;
        end;
        apexran(step)=y(cou,1);
        apexalt(step)=y(cou,3);
        apexvel(step)=sqrt(y(cou,2)^2+y(cou,4)^2);
        vmax(step)=max(sqrt(y(:,2).^2+y(:,4).^2));
        altmax(step)=max(y(:,3)/1000);
        while y(cou,3)>0,
                cou=cou+1;
        end;
        totran(step)=y(cou,1);
end;
figure(1)
grid on
title('Projectile Trajectory (m = 25 kg)')
xlabel('Range (km)')
ylabel('Altitude (km)')
figure(2)
title('Projectile Velocity (m = 25 kg)')
xlabel('range')
ylabel('velocity (m/s)')
grid on
figure(3)
title('Altitude-Time Profile (m = 25 kg)')
xlabel('Time (min)')
ylabel('Altitude (km)')
grid on
figure(1)
gtext('Ballistic');          gtext('Parachute');
gtext('Powered Flight');  gtext('Glide');

=====================================
% trajfunb.m
% Equations of motion of WASP
% by D. Iranzo and C. Hallam, 1997

function yp=bull(t,y)

rho=1.225*((288.16-(288.16-
216.66)*y(3)/11100)/288.16)^4.256;

if t<125,
        Cd=ballisticdrag(sqrt(y(2)^2+y(4)^2),y(3));
        S=0.013;

        if ((y(4)<0) & (y(3)<3000)),
                Cd=0.9;
                S=3;
        end

        yp(1)=y(2);
        yp(2)=-
(rho*S*Cd/(2*y(5)))*y(2)*sqrt(y(2)^2+y(4)^2);
        yp(3)=y(4);
        yp(4)=-9.8-
(rho*S*Cd/(2*y(5)))*y(4)*sqrt(y(2)^2+y(4)^2);
        yp(5)=0;
```

```
end;

if t>125,
        Cd=.031408;
        S=.138;
        power=0.85*0.42*746;
        Cl=1.2;
        prop=0;

        if t>225,
                if t<(225+60*10),
                        prop=1;
                end;
        end;

        yp(1)=y(2);
        yp(2)=-
(rho*S*Cd/(2*y(5)))*y(2)*sqrt(y(2)^2+y(4)^2)-
(rho*S*Cl/(2*y(5)))*y(4)*sqrt(y(2)^2+y(4)^2)+prop*p
ower/(sqrt(y(2)^2+y(4)^2)*y(5))*y(2)/sqrt(y(2)^2+y(4)^
2);
        yp(3)=y(4);
        yp(4)=-9.8-
(rho*S*Cd/(2*y(5)))*y(4)*sqrt(y(2)^2+y(4)^2)+(rho*S
*Cl/(2*y(5)))*y(2)*sqrt(y(2)^2+y(4)^2)+prop*power/(s
qrt(y(2)^2+y(4)^2)*y(5))*y(4)/sqrt(y(2)^2+y(4)^2);
        yp(5)=-0.0071/60;
end;

=====================================
% loit.m
% Calculation of Loiter time performance
% by David Iranzo, 1997

global S Clp c1 c2 c3 Cd ang;
m=15;
S=0.072:0.005:0.102;
Clp=0.9:0.1:1.2;
ang=0:3*pi/180:15*pi/180;

for c1=1:length(S),
        for c2=1:length(Clp),
                for c3=1:length(ang),
        [t,y]=ode23('loitfun',0,1000,[0,sqrt(2*m*9.8/(
1.1126*S(c1)*Clp(c2))),1000,0,m],1e-5);
                        c4=length(y(:,3));
                        while y(c4,3) < 100,
                                c4=c4-1;
                        end;
                        if c2==1,
                        firstcl(c1,c3)=interp1([y(c4,3)
y(c4+1,3)],[t(c4) t(c4+1)],100);
                        end;
                        if c2==2,
                secondcl(c1,c3)=interp1([y(c4,3)
y(c4+1,3)],[t(c4) t(c4+1)],100);
                        end;
                        if c2==3,
                thirdcl(c1,c3)=interp1([y(c4,3)
y(c4+1,3)],[t(c4) t(c4+1)],100);
                        end;
                        if c2==4,
                fourthcl(c1,c3)=interp1([y(c4,3)
y(c4+1,3)],[t(c4) t(c4+1)],100);
                        end;
                        velo=[velo;S(c1) Clp(c2)
ang(c3) Cd mean((3.6/1.6)*sqrt(y(:,2).^2+y(:,4).^2))
std((3.6/1.6)*sqrt(y(:,2).^2+y(:,4).^2)) t(c4)];
                end;
        end;
end;

hold on
for b1=1:length(ang),
        plot(S+0.1*(b1-1),firstcl(:,b1));
        plot(S+0.1*(b1-1)+0.1,secondcl(:,b1),':');
        plot(S+0.1*(b1-1)+0.2,thirdcl(:,b1),'-.');
        plot(S+0.1*(b1-1)+0.3,fourthcl(:,b1),'--');
end;
for b2=1:length(S),
        plot(S(b2):0.1:S(b2)+0.1*(b1-1),firstcl(b2,:));
        plot(S(b2)+0.1:0.1:S(b2)+0.1*(b1-
1)+0.1,secondcl(b2,:),':');
        plot(S(b2)+0.2:0.1:S(b2)+0.1*(b1-
1)+0.2,thirdcl(b2,:),'-.');
        plot(S(b2)+0.3:0.1:S(b2)+0.1*(b1-
1)+0.3,fourthcl(b2,:),'--');
end;

set(gca,'XColor',get(gcf,'Color'))
ylabel('Loiter Time (sec)');
gtext('Cl-perp')
gtext('0.9');       gtext('1.0');       gtext('1.1');
gtext('1.2');       gtext('S (m^2)'); gtext('0.072');
gtext('0.077');     gtext('0.082');     gtext('0.087');
gtext('0.092');     gtext('0.097');     gtext('0.102');
gtext('Sweep');     gtext('0');         gtext('3');
gtext('6');         gtext('9');         gtext('12');
gtext('15')

=====================================
% loitfun.m
% Equations of motion of the flier
% by David Iranzo, 1997

function yp=bull(t,y)

global S Clp ang c1 c2 c3 Cd;
Cd=0;
rho=1.225*((288.16-(288.16-
216.66)*y(3)/11100)/288.16)^4.256;

b=(S(c1)/0.095)*cos(ang(c3));
Cd=0.015+Clp(c2)^2/(0.9*pi*(b^2/S(c1)));
```

```
power=0.85*0.42*746;
prop=0;

if t<(60*10),
        prop=1;
end;

yp(1)=y(2);
yp(2)=-
(rho*S(c1)*Cd/(2*y(5)))*y(2)*sqrt(y(2)^2+y(4)^2)-
(rho*S(c1)*Clp(c2)/(2*y(5)))*(cos(ang(c3)))^2*y(4)*sqr
t(y(2)^2+y(4)^2)+prop*power/(sqrt(y(2)^2+y(4)^2)*y(5
))*y(2)/sqrt(y(2)^2+y(4)^2);
yp(3)=y(4);
yp(4)=-9.8-
(rho*S(c1)*Cd/(2*y(5)))*y(4)*sqrt(y(2)^2+y(4)^2)+(rh
o*S(c1)*Clp(c2)/(2*y(5)))*(cos(ang(c3)))^2*y(2)*sqrt(y
(2)^2+y(4)^2)+prop*power/(sqrt(y(2)^2+y(4)^2)*y(5))*
y(4)/sqrt(y(2)^2+y(4)^2);
yp(5)=-0*0.0071/60;
```

==========

Airfoil Coordinates: ND02

```
  1.000000 -0.000164
  0.985302  0.004635
  0.967858  0.010160
  0.946045  0.016716
  0.919800  0.024067
  0.891245  0.031424
  0.861733  0.038515
  0.831814  0.045290
  0.801706  0.051739
  0.771509  0.057837
  0.741274  0.063567
  0.711015  0.068905
  0.680733  0.073838
  0.650433  0.078355
  0.620119  0.082440
  0.589791  0.086080
  0.559452  0.089261
  0.529101  0.091976
  0.498753  0.094217
  0.468416  0.095965
  0.438104  0.097212
  0.407847  0.097946
  0.377674  0.098138
  0.347616  0.097764
  0.317712  0.096792
  0.288012  0.095185
  0.258565  0.092894
  0.229425  0.089869
  0.200674  0.086062
  0.172439  0.081425
  0.144912  0.075900
  0.118355  0.069427
  0.093131  0.061962
  0.069737  0.053511
  0.048854  0.044220
  0.031298  0.034464
  0.017794  0.024883
  0.008639  0.016299
  0.003380  0.009439
  0.000910  0.004499
  0.000054  0.000991
  0.000164 -0.001507
  0.001133 -0.003453
  0.002924 -0.005131
  0.005770 -0.006599
  0.010253 -0.007699
  0.019416 -0.008495
  0.034653 -0.008395
  0.056234 -0.007126
  0.084121 -0.004677
  0.113843 -0.001534
  0.144904  0.002054
  0.176407  0.005781
  0.208120  0.009564
  0.239701  0.013301
  0.271146  0.016942
  0.302472  0.020444
  0.333690  0.023767
  0.364806  0.026876
  0.395826  0.029730
  0.426761  0.032296
  0.457614  0.034543
  0.488389  0.036437
  0.519090  0.037951
  0.549727  0.039059
  0.580306  0.039737
  0.610838  0.039969
  0.641325  0.039738
  0.671771  0.039034
  0.702171  0.037852
  0.732520  0.036179
  0.762797  0.034020
  0.792969  0.031354
  0.823032  0.028156
  0.853013  0.024404
  0.883060  0.020053
  0.913725  0.015045
  0.943079  0.009769
  0.966596  0.005312
  0.984815  0.001716
  1.000000 -0.001387
```

==========

```
! AVL Flier Definition Code
!static margin 8%
!trimmed @ 9 degrees tail deflection
!S(wing) = 957 cm^2
!Sweep = 12 degrees
!Super Shell Design
!by David Iranzo and Vlad Gavrilets
```

```
!************************************
Super Shell
!Mach
 0.2
!IYsym   IZsym   Zsym
 0       0       0.0
!Sref    Cref    Bref
957      10      118.7
!Xref    Yref    Zref
-27      0.0     -0.1
!
SURFACE
Main Wing
!Nchordwise  Cspace
6            3.0
YDUPLICATE
0.0
SECTION
!Xle    Yle    Zle    Chord   Ainc  Nspanwise  Sspace
-34.23  6.35   0      11      0     8          1.0
AFILE
airfoil
SECTION
!Xle    Yle    Zle    Chord   Ainc  Nspanwise  Sspace
-29.06  30.7   0      11      0     8          1.0
AFILE
airfoil
!
SURFACE
Telescope
!Nchordwise  Cspace
3            3.0
YDUPLICATE
0.0
SECTION
!Xle    Yle    Zle    Chord   Ainc  Nspanwise  Sspace
-29.06  30.7   0.     8       0.    8          1.0
AFILE
airfoil
SECTION
!Xle    Yle    Zle    Chord   Ainc  Nspanwise  Sspace
-24.51  52.1   0.     8       0.    8          1.0
AFILE
airfoil
!
SURFACE
FuselageH
!Nchordwise  Cspace
8            1.0
YDUPLICATE
0.0
SECTION
!Xle    Yle    Zle    Chord   Ainc  Nspanwise  Sspace
-66.7   0      0      66.7    0.    4          1.0
SECTION
!Xle    Yle    Zle    Chord   Ainc  Nspanwise  Sspace
-66.7   0.75   0.     66.7    0.    4          1.0
SECTION
!Xle    Yle    Zle    Chord   Ainc  Nspanwise  Sspace
-37.35  6.35   0.     37.35   0.    4          1.0
!
SURFACE
FuselageV
!Nchordwise  Cspace
8            1.0
SECTION
!Xle    Yle    Zle    Chord   Ainc  Nspanwise  Sspace
-37.35  0      -6.35  37.35   0.    4          1.0
SECTION
!Xle    Yle    Zle    Chord   Ainc  Nspanwise  Sspace
-66.7   0      -0.75  66.7    0.    4          1.0
SECTION
!Xle    Yle    Zle    Chord   Ainc  Nspanwise  Sspace
-66.7   0      0      66.7    0.    4          1.0
SECTION
!Xle    Yle    Zle    Chord   Ainc  Nspanwise  Sspace
-66.7   0      0.75   66.7    0.    4          1.0
SECTION
!Xle    Yle    Zle    Chord   Ainc  Nspanwise  Sspace
-37.35  0      6.35   37.35   0.    4          1.0
!
SURFACE
Tail
!Nchordwise  Cspace
4            1.0
YDUPLICATE
0.0
HINGE
0.0  1.0  -1.0
SECTION
!Xle    Yle    Zle    Chord   Ainc  Nspanwise  Sspace
-5      4.49   -4.49  5       0.    6          1.0
AFILE
airfoil
SECTION
!Xle    Yle    Zle    Chord   Ainc  Nspanwise  Sspace
-5      27.98  -13.04 5       0.    6          1.0
AFILE
airfoil
```